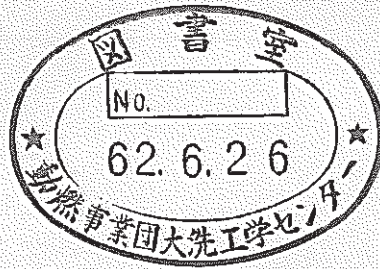


LARGE — SCALE TEST ON SODIUM LEAK AND FIRE (V)

—Simulation Test of a Sodium Leak Accident within
the Monju Secondary Building, Run —D2 —



May 1987

OARAI ENGINEERING CENTER
POWER REACTOR AND NUCLEAR FUEL DEVELOPMENT CORPORATION

複製又はこの資料の入手については、下記にお問い合わせください。

〒311-13 茨城県東茨城郡大洗町成田町4002

動力炉・核燃料開発事業団

大洗工学センター システム開発推進部・技術管理室

Enquires about copyright and reproduction should be addressed to: Technology Management Section O-arai Engineering Center, Power Reactor and Nuclear Fuel Development Corporation 4002 Narita-cho, O-arai-machi, Higashi-Ibaraki, Ibaraki-ken, 311-13, Japan

動力炉・核燃料開発事業団 (Power Reactor and Nuclear Fuel Development Corporation)

大規模ナトリウム漏洩燃焼試験 (V)

-二次系ナトリウム漏洩事故の事象推移に関する総合模擬試験, Run-D2-

宮原信哉*, 姫野嘉昭*

要 旨

「もんじゅ」の原子炉補助建屋を模擬したコンクリート製二階建セルSOLFA-1を用い、二次系Na漏洩事故の事象推移に関する総合模擬試験を行った。試験では、「もんじゅ」二次主冷却系配管の保温構造を模擬した模擬Na配管、床ライナ、連通管及び燃焼抑制板と床ライナで構成された貯留槽を試験セル内に実機と類似に配置し、温度505℃、総重量約3 tonのナトリウムを模擬Na配管から実機と同じ圧力(約3.8 Kg/cm²G)で漏洩させることによって、配管からのナトリウム漏洩に始まり貯留槽でのナトリウム燃焼の自然鎮火によって事故が終息するまでの事象推移を調べた。その結果、次の結論を得た。

- (1) 模擬Na配管から漏洩したNaは、現在「もんじゅ」設計で想定されている事象推移と同様に床ライナから連通管を経て貯留槽に円滑にドレンされ、燃焼抑制板によってその燃焼が抑制されることにより事故が終息した。
- (2) 配管からのNa漏洩形態は下向きの滝状(コラム状)漏洩であり、保温構造体の崩壊による上向きのスプレー状漏洩は生じなかった。
- (3) 模擬Na配管から漏洩したNaは、床ライナ上及び連通管内を円滑に流れて貯留槽にドレンされ、燃焼生成物やNaの凍結による流路の閉塞は起こらなかった。
- (4) 貯留槽内にドレンされたNaの燃焼は、燃焼抑制板による燃焼抑制効果によって自然鎮火した。
- (5) Na燃焼の熱的影響によるコンクリート建物とNa漏洩対策設備の破損や著しい変形等は生じなかった。また、雰囲気に出したコンクリート表面の浸食や破損も認められなかった。

* 大洗工学センター安全工学部プラント安全工学室

May. 1987

LARGE-SCALE TEST ON SODIUM LEAK AND FIRE (V)

- Simulation Test of a Sodium Leak Accident within
the Monju Secondary Building, Run-D2 -

S. Miyahara*

and Y. Himeno *

Abstract

A large-scale test of a secondary sodium leak accident has been conducted to demonstrate the feasibility of the Monju fire mitigation systems. The two-story high concrete cell, SOLFA-1, simulating the Monju secondary building was used. A reduced-scale model of the Monju IHTS pipe including its

* Plant Safety Section, Safety Engineering Division, OEC.

This text was prepared from ZN9410 86-113 , Oct.1986.

thermal insulation jackets, a floor liner, a sodium drain pipe, and a smothering tank (consisting of a fire suppression board and a liner) were installed in the test cell to simulate the fire mitigation systems.

In the test, about three tons of sodium at 505°C was leaked from the pipe at a pressure of 3.8 kg/cm² G, then a whole accident sequence starting from a sodium leak to self-extinguishment of the fire within the smothering tank was studied.

From the test results, the following conclusions were drawn.

- a) The whole sodium leak and fire accident sequence proceeded as postulated in the Monju design.
- b) The sodium leaked from the pipe in a downward columnar flow not in an upward spray, because the thermal insulation jackets performed satisfactorily.
- c) The spilled sodium on the liner was led smoothly toward the smothering tank via the drain tank.
- d) Sodium fire was successfully self-extinguished in the smothering tank.
- e) Breaks in and remarkable transformation of the fire mitigation systems were not observed. No appreciable damage was observed on the surfaces of the bare concrete walls or the bare concrete ceiling.

Contents

Abstract	II
Contents	IV
List of Tables	VI
List of Figures	VII
List of Photographs	IX
Introduction	1
1. Purpose	3
2. Test Rig and Instrumentation	6
2.1 Outline of the Test Rig	6
2.2 Simulated Sodium Pipe	8
2.3 Floor Liner	11
2.4 Sodium Drain Pipe	12
2.5 Fire Suppression Board and Smothering Tank	13
3. Test Conditions and Methods	15
4. Test Results and Discussion	19
4.1 General Development of Phenomena Associated with Sodium Leak in Secondary System	19
4.2 Development of Phenomena within the Upper Cell	20
(1) Sodium Leak from Simulated Sodium Pipe	20
(2) Fluidity of Leaked Sodium on the Floor Liner	22
(3) Heat Transfer Characteristics in the Upper Cell	24
(4) Aerosol Behavior	27

4.3	Development of Phenomena within the Lower Cell	28
(1)	Leaked Sodium Drain Performance through Sodium Drain Pipe	28
(2)	Effects of Fire Suppression Board	29
(3)	Heat Transfer Characteristics in Lower cell	30
(4)	Aerosol Behavior	34
4.4	Visual Observation and Washing of Sodium after the Test	35
(1)	Visual Observation and Inspection of Various Test Cell Parts	35
(2)	Reaction of Concrete with the Aerosol	37
(3)	Washing of Sodium and Distribution of Residue within the Test Cell	38
(4)	Inspection of Simulated Sodium Pipe Thermal Insulation jackets	39
(5)	Inspection of the Floor Liner, the Sodium Drain pipe, and the Smothering Tank	39
4.5	Post-Test Destructive Inspection of the Concrete of the Upper Cell	40
	Conclusions	43
	Acknowledgements	45
	References	45

L i s t o f T a b l e s

Table 1	:	Compositions of Structural Concrete used in SOLFA-1 and in Monju.....	47
Table 2	:	Test Conditions of Run-D2	48
Table 3	:	Test Record of Run-D2.....	49
Table 4	:	Enthalpy Change in Upper Cell.....	50
Table 5	:	Distribution of Residual Sodium in Test Rig after the Test	51
Table 6	:	Specific Weight, Compressive Strength and Young's Modulus of Upper Cell Concrete after the Test	52

List of Figures

Fig. 1	: Subject Examples in Monju Secondary System	53
Fig. 2	: Arrangement of Test Rig for Run-D2	54
Fig. 3	: Bird's-eye View of SOLFA-1 for Run-D2	55
Fig. 4	: Instrumentations and Sensors Installed in Test Rig for Run-D2	56
Fig. 5	: Concept of Monju Secondary Sodium Piping with Thermal Insulation Cover.....	57
Fig. 6	: Cut View of Simulated Sodium Pipe for Run-D2	58
Fig. 7	: Geometric Configuration of the Upper Cell of SOLFA-1	59
Fig. 8	: Location of Thermocouples on Floor Liner of the Upper Cell of SOLFA-1	60
Fig. 9	: Location of Thermocouples in the Lower Cell of SOLFA-1	61
Fig. 10	: Changes of Oxygen Injection Rate and of Oxygen Concentration during the Test (Upper Cell)	62
Fig. 11	: Flow Rate of Feed Sodium into Simulated Sodium Pipe	63
Fig. 12	: Temperature Distribution Changes in Vertical Cross Section of Upper Cell Atmosphere during Sodium Spill.....	64
Fig. 13	: Flow Pattern of Gas and of Spilled Sodium in Vertical Cross Section of Upper Cell Atmosphere during Sodium Spill	65
Fig. 14	: Temperature Distribution of Sodium on Floor Liner and Its Change during Sodium Spill	66
Fig. 15	: Temperature Changes of Liner and of Sodium on the Liner during the Test (Upper Cell)	67
Fig. 16	: Temperature Distribution Change in the Upper Cell of SOLFA-1 During the Test ..	68
Fig. 17	: Heat Generating Rate and Sodium Combustion Rate during the Test (Upper Cell) ..	69
Fig. 18	: Distribution of Combustion Heat Transferred to the Various Portions of the Upper Cell	70
Fig. 19	: Concentration Changes of Aerosol during the Test (Upper Cell)	71
Fig. 20	: Temperature Changes of Sodium Drain Pipe and of Sodium at Inlet of the Pipe during the Test	72

Fig. 2 1 :	Temperature Changes in Bucket and in Smothering Tank during Sodium Spill.....	7 3
Fig. 2 2 :	Flow Rate of Drain Sodium into Smothering Tank	7 4
Fig. 2 3 :	Oxygen Concentration Changes of Cell Atmosphere and of Gas Phase in Smothering Tank during the Test	7 5
Fig. 2 4 :	Temperature Changes of Sodium in Bucket and in Smothering Tank during the Test	7 5
Fig. 2 5 :	Temperature Distribution Change in the Lower Cell of SOLFA-1 during the Test	7 6
Fig. 2 6 :	Heat Generating Rate and Sodium Combustion Rate in the Smothering Tank	7 7
Fig. 2 7 :	Heat Flux to Floor Concrete in Lower Cell during the Test	7 8
Fig. 2 8 :	Concentration Changes of Aerosol during the Test (Lower Cell)	7 9
Fig. 2 9 :	Amount of Aerosol in SOLFA-1 after the Test	8 0
Fig. 3 0 :	Post-Test Sodium Distribution in Test Rig	8 1
Fig. 3 1 :	Post-Test Aerosol Distribution in Test Rig	8 2
Fig. 3 2 :	Temperature Changes of Upper Cell Concrete during the Test	8 3
Fig. 3 3 :	Compressive Strength of the Various Portions in Upper Cell Concrete after the Test	8 4
Fig. 3 4 :	Relation between Specific weight and Compressive Strength of Upper Cell Concrete ..	8 5
Fig. 3 5 :	Relation between Compressive Strength and Young's Modulus of Upper Cell Concrete ..	8 6
Fig. 3 6 :	Relation between Weight Loss and Compressive Strength of Upper Cell Concrete	8 7
Fig. 3 7 :	Temperature Changes of Lower Cell Concrete during the Test	8 8

List of Photographs

Photo. 1	: Simulated Sodium Pipe installed in the Upper Cell of SOLFA-1 (Pre-Test)	89
Photo. 2	: Arrangement of Drain Pipe and Smothering Tank	89
Photo. 3	: Sodium Leak at the Beginning of the Test	90
Photo. 4	: Post-Test View of the Upper Cell of SOLFA-1.....	90
Photo. 5	: Post-Test View of Inlet of Drain Pipe	91
Photo. 6	: Post-Test View of Sodium and Its Reaction Products in Smothering Tank	91
	(A part of fire suppression board is removed for Visual Inspection)	
Photo. 7	: Post-Test View of wall Concrete Surface in Upper Cell	92
Photo. 8	: Post-Test View of Simulated Sodium Pipe.....	92
Photo. 9	: Disassembling of Simulated Sodium Pipe after the Test	93
Photo. 10	: Post-Test View of Connecting Pipe in Simulated Sodium Pipe	93
Photo. 11	: Non-desructive Inspection of Weld Line of Liner in Upper Cell after the Test.....	94
Photo. 12	: Non-desructive Inspection of Weld Line of Liner in Lower Cell after the Test.....	94
Photo. 13	: Concrete Samples for mesuring the Compressive Strength and the Young's Modulus..	95

Introduction

When the secondary coolant sodium leaks in the auxiliary building of the fast breeder reactor Monju, it may burn generating heat due to the reaction with the oxygen and water vapor in the air and impairing the structural integrity of the building. Monju is therefore provided with sodium fire control systems such as the thermal insulation jackets around sodium pipe, floor liner, sodium drain pipes, and a smothering tank to protect the reactor building against a postulated sodium leak accident from a leak hole whose diameter is equivalent to $1/4 Dt$ (D , pipe diameter; t , pipe thickness).

Parts of these sodium fire control systems have already been tested, and their function have been demonstrated by the basic tests of Runs-A1, B1, B2, and B4⁽¹⁾⁽²⁾, the small-scale simulation test of Run-B3⁽³⁾, and a water simulation test using a mock-up IHTS pipe⁽⁴⁾ conducted from fiscal 1983 to 1984. In fiscal 1985, the following five comprehensive tests below were completed using the large-scale sodium leak and fire test facility, SAPFIRE:

- 1) A sodium pool fire test in air (Run-D1), ⁽⁵⁾
- 2) Sodium spray fire test in water vapor containing air (Run-F1) ⁽⁶⁾
- 3) A large-scale sodium spray fire test in air (Run-E1) ⁽⁷⁾

- 4) A realistic sodium leak-test with simulated sodium pipe (Run-E2) ⁽⁸⁾, and
- 5) A simulation test of a sodium leak accident within the Monju secondary building (Run-D2).

This paper presents the results of Run-D2.

1. Purpose

The auxiliary building of Monju is designed so that, even if any sodium leak accident occurs, the sodium leaking from the piping will first drop on the steel floor liner then drain through the sodium drain pipe into the smothering tank as shown in Fig. 1. The smothering tank is located at the bottom of the building, and it suppresses the sodium fire. The regulatory authorities asked us to confirm the items described below to verify that the above sodium fire control systems in the building can work as designed in the event of the postulated sodium leak accident.

Whole Accident Sequence

Based on a small-scale simulation test (Run-B3)⁽³⁾, we confirmed that the accident sequence proceeded as expected in the actual plant design. However, it is necessary to determine unexpected phenomena occur or not from an engineering viewpoint due to scale effect.

Sodium leakage flow pattern from the pipe

In Run-B3, where sodium temperature was the same as that during operation of the actual plant, the sodium feed pressure was $0.2 \text{ kg/cm}^2 \text{ G}$, lower than that in the actual plant. Nevertheless, the test clarified that no failure occurs in the

thermal insulation jackets due to the reaction with sodium. It was also found that sodium leakage flow pattern was a downward columnar flow. In the previous water simulation test with the water pressure at the reactor operating conditions, no failure of the thermal insulation jackets occurred and the leakage flow pattern was also in a downward columnar flow. But the question was asked whether similar results can be obtained if sodium at the same temperature and pressure as in the actual plant are used (i.e., whether or not the sodium leakage from the piping will directly contact with concrete surfaces of the ceiling and walls.

Fluidity of Leaking Sodium

Fluidity of the leakage sodium on the floor liner and through the sodium drain pipe has already been demonstrated in the basic tests; Run-B1, Run-B2, Run-B3, and Run-B4, where it was found that the deposition of combustion products and the freezing of sodium does not obstruct the flow. However, a question arose as to whether the same result could be obtained when the leakage sodium flow rate and its flow passage area increased.

Effect of the Fire Suppression Board

From the results of Run-B1 and Run-B3, we confirmed that the sodium fire can be suppressed by reducing the opening area of the fire suppression board. But can the same effect be obtained with the same kind of structure installed in the

actual plant?

Structural Integrity of the Concrete Building and
the Sodium Fire Control Systems

Will the structural integrity of the concrete building and the sodium fire control systems be impaired by the sodium fire accident? Furthermore, since no liner is provided on the ceilings and walls of the rooms in the reactor auxiliary building, their concrete surfaces are exposed to the room atmosphere. Consequently, a question arises whether any erosion or chemical reaction of the concrete occurs due to the sodium aerosol deposition during a sodium fire.

To answer the above, we conducted the present simulation test Run-D2.

2. Test Rig and Instrumentation

2.1 Outline of Test Rig

As shown in Fig. 2, the test rig used in Run-2 consists of SOLFA-1 and its peripheral components including a sodium heater, a sodium drain tank, and an aerosol scrubber.

The sodium heater can heat about 4 tons of sodium (maximum) to the desired temperature and supply the sodium into SOLFA-1 by pressurizing its cover gas (nitrogen). The aerosol scrubber traps the sodium aerosol generated during the test using a water scrubber and a HEPA filter.

SOLFA-1 is a two-story concrete cell simulating the auxiliary building of Monju. Its second floor simulates the IHTS rooms, and its first floor simulates the sodium drain room where a smothering tank consisting of a fire suppression board is installed (the second floor will be called the upper cell and the first floor the lower cell). Figure 3 shows a bird's-eye view of SOLFA-1.

The concrete wall, floor, and ceiling of SOLFA-1 is made of reinforced concrete to facilitate their repair after the test. Therefore, the test cell does not exactly simulate the actual plant in construction. Concrete composition of the cell is considered to govern the phenomena relating to the thermal influences of the accident, so we used Graywacke produced from Habara, Fukui Prefecture and land sand from Mikuni, the same prefecture, which were to be used in Monju as the aggregate of

the concrete. Table 1 compares the compositions of the concrete to be used in Monju to that used in SOLFA-1.

A simulated sodium pipe from which sodium is to be leaked and a floor liner are provided within the upper cell of SOLFA-1. The ceiling and wall concrete surfaces of the upper cell are directly exposed to the air as in most rooms of the auxiliary building of Monju. On the side walls of the upper cell are the air intake and discharge ducts and the penetrations for instrumentation. These are, for releasing over-pressure of atmospheric gas and for the instrumentation during the test. An oxygen injection pipe is provided just below the ceiling to supply the oxygen needed to sustain the sodium combustion throughout the test.

In the lower cell on the first floor of SOLFA-1, a smothering tank consisting of a fire suppression board and a floor liner and the sodium drain pipe that comes from the upper cell for draining the sodium are installed. On the walls, as in the upper cell, there are the air intake and discharge ducts to ventilate the cell and the penetrations for instrumentation. On the ceiling and inner wall surfaces, as in the actual plant, the thermal radiation shields and thermal insulators are attached to prevent a temperature increase due to heat transfer from the fire suppression board.

Next, the instrumentation of SOLFA-1 will be described. Figure 4 shows the instruments and their installation locations. The temperature and the flow rate of sodium being supplied to the simulated sodium pipe during the test are

measured by thermocouples installed in the sodium heater and in the sodium feed pipe and by an electromagnetic sodium flow meter installed in the sodium feed pipe, respectively. Flow rate of oxygen being supplied to the upper cell is measured by an orifice flow meter, and flow rate of the ventilated air in the lower cell by an air flow meter. Furthermore, an electric transducer type pressure gauge is used to monitor the cell atmospheric pressure during the test. This is to avoid too high pressure build-up because SOLFA-1 is made of concrete with low pressure resisting structure. In the upper and lower cells, the temperatures at various parts are measured by thermocouples. The concentration of sodium aerosol and oxygen in the cell atmosphere are also measured. A filter-type sampler which samples the cell atmosphere and collects the aerosol on a sintered metallic filter is used for this purpose. The aerosol concentration is determined from the weight of collected aerosol and the volume of gas sampled. Oxygen concentration is measured by a magnetic oxygen concentration meter and a gas chromatograph. To observe and record the phenomena occurring in the cell during the test, an industrial TV camera, a 35mm camera, and an infrared TV camera are set up.

2.2 Simulated Sodium Pipe

The simulated sodium pipe represents a straight portion of the secondary main cooling piping system of Monju including its thermal insulation jackets (Fig.5) at a reduced scale of about 1/2.6 in length. Figure 6 shows its general sectional view. The thermal insulation jackets that had been used in Run-B3 and in

the water simulation test of a sodium leak followed the 1983 design, while the ones used in the sodium leak test (Run-E2)⁽⁵⁾ conducted in fiscal 1985 and in Run-D2 reported here conformed to the 1985 design. These two designs are basically identical except for some rationalization in their small parts. In the 1985 tests, the clamp part of the thermal insulation jackets was also simulated to evaluate a sodium leak more realistically.

The pipe is stainless steel 304, 216.3mm in diameter and 1,600mm long. A sodium leak hole is on its top as shown in Fig. 6. As the simulated sodium pipe has a reduced scale of about 1/2.6 in length, the sodium leak hole was scaled down to about $1/(2.6)^2$ of the area $1/4 Dt$ (13.3cm^2) of the secondary main cooling piping system of the actual plant. On the external surface of the pipe were attached round bars to simulate the sheath heaters for preheating the actual plant piping. The simulated sodium pipe was preheated during the test by the sheath heaters attached to the internal surface of the pipe. Furthermore, a clamp was installed near one end of the pipe to support it. This clamp was not used to support the simulated sodium pipe but was attached only to represent the shape and installation method of the actual clamp. (The pipe was supported at both ends by two hooks from the ceiling).

The thermal insulation cover consists of an inner jacket (stainless steel 304, 0.8mm thick), a thermal insulating material (rock wool (trade name, Rock Fine), 70mm thick) and an outer jacket (carbon steel, 0.4mm thick). The same thickness

as in the actual plant was adopted for the inner and outer jackets as in Run-B3. This was to evaluate the past individual test results from an overall viewpoint, as it had already been confirmed by the water simulation test that both the inner and outer jackets were strong enough to stand the flow pressure of the leaked sodium within the design standard. Furthermore, their integrity under the accident conditions had already been confirmed by Run-B3.

The inner jacket was made in vertically split halves and fixed to the flanges located on the axis of the sides of the pipe by means of bolts and nuts. The circumferential joint is located at two positions (i.e., the clamp part and the simulated heater penetration). In the former, the flange on the circumference was fixed to the clamp. In the latter, the two vertically split straps covering the joint were fixed to the pipe in the same manner as the inner plate was fixed to the pipe (bolts and nuts).

Multiple ring-shaped spacer bands (8mm high) were installed between the inner jacket and the outer surface of the pipe at intervals of 195mm in the axial direction of the pipe to provide the annular portion there between. This is because in the actual plant, the atmospheric gas at this part is led to the sodium leak detector. The sampling tube and the connecting tube of the clamp were also simulated and provided.

The outer jacket was manufactured to be wound around the thermal insulating material and fixed to the pipe with ends folded in the circumferential direction of the pipe and simply

in layers in the axial direction. The boat-shaped outer jackets in the shape of vertically split halves were made to cover the clamp and were fixed to it at the top and bottom with both ends folded.

The thermal insulation cover has an opening at the bottom of its center as a penetration for the simulated heater in the axial direction of the piping. This opening in the inner jacket was designed to be easily deformed and expanded by the flow pressure of leaking sodium, while the opening in the outer jacket had a larger diameter than that of the heater. Both ends of the thermal insulation cover were completely sealed at the sides by welding and packing to prevent the sodium leak from penetrating unnecessary parts during the test.

Photo.1 shows the simulated sodium pipe in the upper cell.

Thermocouples were used as the measuring sensors during the test. Since results of Run-B3 already confirmed that no chemical reaction occurs between the thermal insulation material and sodium, no sensor was installed in the thermal insulator in this test. One was, however, provided on the inner surface of the pipe to control its preheating and one at the opening for the simulated heater in the external surface of the outer jacket to measure the leaked sodium temperature.

2.3 Floor Liner

A floor liner, a 6mm thick steel plate (carbon steel) lined with U-shaped steel beams, was laid in both the upper

and the lower cells, as shown in Fig. 3. This is called a catch pan which is to be used as the liner of the secondary building of Monju. The U-shaped steel beams vertical movement is restricted by the anchor bolts and holding brackets fixed to the concrete, but they can move laterally to absorb the thermal expansion of the floor liner when it heats up during sodium leakage.

Retaining walls are provided (375mm high in the upper cell and 600mm high in the lower cell) to prevent the leaked sodium from overflowing and collecting the floor liner. In the upper cell, the floor has a 1/100 gradient toward the inlet of sodium drain.

Perlite boards are provided between the floor liner and the concrete for thermal insulation. All this work was executed in the same way as planned in the Monju.

Only thermocouples were used for measurements during the test. A total of 28 thermocouples were installed in the upper cell to measure the sodium temperatures at the surface and back of the liner and at the U-shaped beams, a total of seven in the lower cell to measure the temperature at the back of the liner and the U-shaped beams. Figure 7 shows their positions relative to the simulated sodium pipe, and Figs. 8 and 9 their locations on the floor liner.

2.4 Sodium Drain Pipe

The sodium drain pipe made of carbon steel (318.5mm diameter) forms the floor liner opening in the upper cell toward the lower

cell. Another carbon steel pipe (216.3mm diameter) in the lower cell stands on the smothering tank. These two are being connected by welding using a reducer. The total distance from the floor liner opening in the upper cell to the smothering tank shown in Fig. 3 is about 4.1m.

Only thermocouples were used as the measuring sensor during the test. They were installed at the floor liner opening in the upper cell to measure the sodium temperature at the inlet of the sodium drain pipe, and on the external surface of the sodium drain pipe in the lower cell to measure the temperature of the pipe.

2.5 Fire Suppression Board and Smothering Tank

The fire suppression board in the smothering tank consists of 15 carbon steel plates (thickness 4.5mm) with sides of 900mm x 1100mm and 900mm x 1800mm. As shown in Fig. 3, these are laid on horizontal beams and form a smothering tank 500mm deep with the floor liner.

A bucket is provided below the bottom opening of the sodium drain pipe, as shown in Photo.2. It is to seal the bottom opening of the pipe by the sodium inflow during the test and preventing the acceleration of sodium fire within the smothering tank by the funnel effects of air through the sodium drain pipe. Furthermore, a gas escape hole (carbon steel, 150mm long, and 114.3mm in diameter) was provided at a fire suppression board opposite the bucket to release the expanded gas from the smothering tank during the inflow of sodium. The opening area ratio of the fire suppression board

including this gas escape hole is less than 1% as in the actual plant.

Thermocouples were used as sensors during the test; one was provided within the bucket, 12 at two points in the vertical direction in the smothering tank, and two at the fire suppression plates level with these points. Figure 9 shows the location of thermocouples on the fire suppression plates and within the smothering tank.

3. Test Conditions and Methods

Table 2 shows the test conditions of Run-D2. In determining them, the following two test purposes were the major factors:

- 1) The form of sodium leak from the pipe.
- 2) The effectiveness of the fire suppression board.

The leaked sodium temperature and the sodium leak pressure in the simulated pipe during the test were determined from the former, and the total volume of leaked sodium from the latter. The leaked sodium temperature and the sodium leak pressure were determined to make the conditions of the sodium leak from the simulated sodium pipe equal to those in the actual plant. The same sodium conditions as in the secondary main cooling piping system of the actual plant were adopted, since the simulated sodium piping was scaled down in length to about $1/2.6$ that of the actual plant and the sodium leak hole was also reduced in area to about $1/(2.6)^2$ of the actual plant piping ($1/4 Dt$). The total volume of leaked sodium was determined so that the space per unit surface area of sodium collected within the smothering tank might be equal to that in the actual plant since the combustion of the sodium within the smothering tank is affected by the volume of oxygen existing in the tank. We had learned in Run-B3 that about 10% of the total volume of leaked sodium remained in the upper cell, so this volume was added to the total leaked

sodium volume chosen.

During the test, oxygen gas was supplied to the upper cell while the lower cell was ventilated. This was to prevent the suppression of sodium fire halfway during the test by the shortage of oxygen in the upper cell and to prevent the oxygen from running short and making it impossible to confirm the effectiveness of the fire suppression board in the lower cell.

Oxygen was injected into the upper cell at a flow rate so that the oxygen concentration in the atmosphere during the test might not exceed that in normal air (21%). This flow rate was precalculated by means of the analysis code used in evaluating the safety of and the application for Monju. Since the upper cell simulated the secondary main cooling system piping room of the actual plant and this room shares the atmosphere with adjacent or connecting rooms through their openings, the total oxygen injection volume in the test was determined so as not to exceed the volume of oxygen existing in these rooms multiplied by the space volume ratio of the accident room (the upper cell of SOLFA-1) to the intermediate heat transport system room of the actual plant. Figure 10 shows the changes of oxygen injection rate and oxygen concentration in the upper cell during the test.

The ventilation rate in the lower cell was selected to simulate the oxygen concentration in the secondary dump tank room of the actual plant where the smothering tank is provided, considering the result of a preliminary evaluation in which the oxygen concentration in the tank room would

remain almost constant (21%) even when sodium was collected there in an emergency, and the value was determined in the same way as in the upper cell.

Next, the test method will be described. In the test, the sodium in the sodium heater and the simulated sodium pipe were heated to the desired temperature in advance and the aerosol scrubber was started. The cover gas of the sodium heater was then pressurized to increase the sodium outflow pressure at the leak hole of the simulated sodium pipe, and the sodium supply piping valve was opened to leak sodium and start the test. Table 3 shows the test process. After the test started, ventilation of the lower cell was begun when the leaked sodium seemed to enter the lower cell. Oxygen was then injected into the upper cell after the pressure within the cell was stabilized. The oxygen injection rate was changed after the predetermined volume of sodium leaked and was stopped about 40 minutes after the start of the test. Thereafter, the observation of the development of phenomena within the upper and lower cells was continued, and the sodium collected in the lower cell was drained to the drain tank after the temperature of sodium within the smothering tank dropped below the sodium ignition temperature.

In the post-test sodium disposal and examination, the residual sodium in the test cell was first disposed of and the distribution conditions of the residual sodium and sodium aerosol were surveyed. The post-test soundness of the floor liner, the sodium drain pipe, and the fire suppression board

was examined. The ceiling and wall concrete in the upper cell was examined to see if it had any trace of reaction with sodium and sodium aerosol. The thermal insulator jackets of the simulated sodium pipe was only disassembled to observe the conditions as it had already been examined in every detail in Run-B3. Furthermore, the concrete panels of the ceiling, walls, and floor of the upper cell were disassembled and some cores (samples) were taken to measure the post-test strength.

4. Test Results and Discussion

4.1 General Development of Phenomena Associated with Sodium Leak in the Secondary System

The observation results for the entire test after sodium began to leak from the simulated sodium pipe will first be described. Sodium began to leak from the opening of the thermal insulation jacket for the simulated heater several seconds after the start of sodium supply to the simulated sodium pipe. Soon the sodium was seen leaking downward through the circumference of the outer jacket and the joint of the clamp and moving upward along the joint of the outer jacket. Throughout the sodium leak, there was no corrosion or rupture of the outer jacket that allowed sodium to leak upwardly through any anticipated part of the thermal insulation jackets. Sodium continued to leak downward in a columnar shape. Photo.3 shows these leak conditions.

The sodium leaking from the simulated sodium pipe dropped onto the floor liner without contacting the surrounding walls and flowed smoothly on the liner along its gradient toward the sodium drain pipe. Reaching the inlet of the drain pipe, the sodium was quickly drained into the smothering tank in the lower cell without blocking the drain-pipe.

In the smothering tank, the drained sodium did not flow over the fire suppression board as observed in test Run-B3 where the small diameter of the gas escape pipe had restricted the

gas release. The tank could fully discharge the expanded gas and reliably accommodate the sodium leaking from the upper cell. Subsequently, the sodium fire was extinguished by the fire suppression board, restraining the fire of the collected sodium. The temperature of the collected sodium dropped with the passage of time through heat releases.

In the observations by an industrial TV camera and an infrared TV camera, the general phenomena of sodium leak developed as expected in the actual plant, producing no phenomena differing from those observed in Run-B3, a small-scale test. We therefore think it unnecessary to make any essential change in the accident sequence postulated for the present Monju design.

4.2 Development of Phenomena within the Upper Cell

(1) Sodium Leak from Simulated Sodium Pipe

Figure 11 shows changes in the leaking sodium flow rate during the test. As can be seen from this figure, the leaking sodium flow rate during the test was nearly constant about 240 l/min (about 3.22 kg/sec), and the predetermined sodium volume could be leaked in 874 seconds. In evaluating the safety of the actual plant, the sodium flow rate in a sodium leak accident was calculated assuming that there is no pressure loss in the thermal insulation jackets (i.e., assuming that the pressure loss coefficient = 1.0) to make the calculation result more conservative. For comparison, we calculated the actual pressure loss coefficient based on

the results of the sodium flow pressure and sodium leak flow rate in this test. The following equation was used for the calculation:

$$\Delta P = \zeta \frac{\rho}{2} v^2 = \zeta \frac{\gamma}{2g} \left(\frac{w}{\gamma A} \right)^2 \dots\dots\dots (1)$$

where

- ΔP Pressure difference between the sodium in the pipe and the atmosphere (= $3.8 \times 10^4 \text{ kg/m}^2 \text{ G}$)
- ζ Pressure loss coefficient of the thermal insulation jackets
- ρ Density of leaked sodium ($\text{kg} \cdot \text{sec}^2 / \text{m}^4$)
- v Sodium flow velocity at the sodium leak hole (m/sec)
- γ Specific weight of leaked sodium = 830.6 kg/m^3
- g Acceleration of gravity = 9.807 m/s^2
- w Sodium leak flow rate = 3.22 kg/s
- A Sodium leak hole area = $2.247 \times 10^{-2} \text{ m}^2$

The pressure loss coefficient was determined as $\zeta = 3.015$ from the actually measured ρ , v , and Eq. (1).

This value almost agrees with the value obtained from the water leak simulation test (2.852 to 2.843) and the value from Run-E2 (3.33). We can thus say that the actual plant safety evaluation estimates the leaked sodium flow rate about twice as conservatively as the actual one.

Next the behavior of the upper cell atmosphere when sodium

leaked and of the sodium leaking from the simulated sodium pipe will be described. Figure 12 shows the temperature distribution changes with the passage of time in the vertical cross section of the upper cell along the line passing through the central section of the simulated sodium pipe. As this figure shows, when sodium begins to leak from the simulated sodium pipe, the temperature of gas just below the simulated sodium pipe starts to rise and continues to do so with the passage of time. The distribution of this high-temperature region tells us that a conic leaked sodium region is formed in the space below the simulated sodium pipe. No such hot spot is formed above the pipe, however, and it can be seen that the sodium leakage from the pipe, as mentioned in section 4.1, is in a downward columnar flow, not an upward spray-shaped leak. The change of the atmospheric temperature during the sodium leak is such that the gas temperature near the sodium leaking down from the simulated sodium pipe first rises. This temperature distribution then moves upward to the ceiling above the pipe. It next moves along the ceiling toward the wall opposite the side where the piping is located and goes down along the wall.

It became clear from the above that sodium leaked from the simulated sodium pipe in a downward columnar shape, and this caused a convection of the atmosphere as shown in Fig. 13. We think these convection patterns may be instructive when a more precise analysis code taking account of the atmospheric convection is developed.

(2) Fluidity of Leaked Sodium on Floor Liner

Figure 14 shows the temperature distribution of sodium on the floor liner and its change, and Fig. 15 shows the temperature changes of the liner and of sodium on the liner at typical positions with the passage to time. From Fig. 14, the fluidity of leaked sodium on the floor liner is demonstrated by the fact that the sodium leaking from the simulated sodium pipe drops onto the liner just below, then spreads over it and gradually flows toward the inlet of the sodium drain pipe. Figure 15 shows that when the sodium drops, the liner temperature begins rising. When the sodium leak is completed, it has already reached 600°C or above which is higher than the supply sodium temperature (505°C). In Run-B2, sodium at 505°C was caused to flow from one end of the liner, and the liner temperature was measured. In this case, the liner temperature remained at the leaking sodium temperature while sodium was flowing. Furthermore, in Run-B3 in which the leaked falling distance was shorter than in this test, the liner temperature exceeded the supply temperature during the leak, but not so much as in this test. These observations indicate that the extent of the columnar combustion of the falling sodium and of the sodium temperature rise due to combustion of scattered sodium drops depends on the falling distance of the leaking sodium, which governs the liner temperature rise during the sodium leakage. After the sodium leak was stopped, the liner temperature continued to rise and reached about 680°C because the sodium pool left on the floor liner burnt.

The maximum temperature was reached at every part of the

floor liner when the oxygen injection into the upper cell was stopped. Considering that the oxygen concentration, which was already shown in Fig. 10, dropped later and then rose again, we think that if the oxygen injection had been continued, the liner temperature would have become even higher than that. The maximum temperature tended to be higher at points closer to the inlet of the sodium drain pipe. This was, we think, because a large sodium pool was formed closer to the inlet, allowing its fire to last longer.

(3) Heat Transfer Characteristics in the Upper Cell

Figure 16 shows the temperature distribution change in the upper cell during the test. The figure demonstrates that it was the temperature of the liner and of sodium on the liner mentioned in (2) above that were remarkably high among the maximum temperature at various parts. The temperature of the atmosphere reached about 400°C, but the temperature of the concrete ceiling, walls, and floor remained at 150°C or below.

The heat generating rate produced by the combustion in the upper cell was calculated based on the test data shown in Fig. 16 in order to compare it with that of the sodium pool combustion in Run-B1 tests and that of the column and pool mixed combustions in Run-B3. The method of calculating the heat generating rate produced by combustion is the same as in previously reported Run-B3. The difference of enthalpy between the supplied sodium and the sodium drained through the sodium drain pipe is deducted from the total rise of enthalpies of the atmospheric gas, the floor liner and

concrete, and the ceiling and wall concrete. The equation is as follows:

$$Q = Q_{Na, out} - Q_{Na, in} + Q_{ceil} + Q_{wall} + Q_{floor} + Q_{gas} \quad \dots (2)$$

where

$Q_{Na, out}$	
$- Q_{Na, in}$	Difference of enthalpy between sodium drained from the upper cell through the sodium drain pipe and sodium supplied to the simulated sodium pipe (Kcal/h).
Q_{ceil}	The enthalpy change of the the ceiling concrete of the upper cell (Kcal/h)
Q_{wall}	The enthalpy change of the wall concrete of the upper cell (Kcal/h).
Q_{floor}	The enthalpy change of the floor liner and floor concrete of the upper cell (Kcal/h).
Q_{gas}	The enthalpy change of the atmospheric gas of the upper cell (Kcal/h)

The result shown in Fig. 17 was obtained after the equation as solved using test data to determine the amount of combustion heat Q . This figure also shows the amount of combustion heat per unit floor liner area and the sodium combustion rate assuming that the combustion product is Na_2O_2 .

In Fig. 17, the heat generating rate in the early stage of sodium leak decreased with the reduction of the oxygen

concentration in the cell, but increased again to a maximum of 2.2×10^6 Kcal/h after the oxygen injection began. This is about 135 kw/m^2 per unit floor liner area and only 1.35 times as large as the typical heat generating rate of sodium pool combustion (100 kw/m^2). It was also smaller than the result from Run-B3 (165 kw/m^2). When the combustion product is assumed to be Na_2O_2 , the present sodium combustion rate (about 850 kg/h) corresponds to only about 7.3% of the sodium leak flow rate 3.22 kg/sec (11592 kg/h). From these results it was learned that the combined fire following a sodium leak from the simulated sodium pipe is not violent but rather moderate like a sodium pool combustion.

After the sodium leak, the heat generating rate remained at 70 to 90 kw/m^2 until the oxygen injection stopped, while sodium pool combustion continued on the floor liner. The rate decreased after the oxygen injection was stopped, reduced to zero, and the fire extinguished about an hour after the start of the test.

We then determined the fraction of the combustion heat transferred to various parts of the upper cell using Eq. (2). The results are shown in Fig. 18, from which it can be seen that more than 90% of the total combustion heat was transferred to the ceiling, walls, and floor of the upper cell (more than 70% to the ceiling and walls alone), and only a little was transferred to the sodium drained to the sodium drain pipe and to the atmospheric gas.

In Run-B3, 64% of the combustion heat was consumed in heating the sodium drained to the sodium drain pipe and the floor liner, which largely differs from the present test result. We think the reason is that in Run-B3, the floor area was small relative to the leaked sodium volume, the cell ventilation was stopped immediately after the completion of sodium leak by filling the test cell with nitrogen, so the temperature was not much affected by the sodium pool combustion. In the present test, however, the floor area was relatively large and enough oxygen existed both during and after the sodium leak, so the sodium pool combustion significantly affected the temperature rises of the cell structures. When we reviewed the results during one hour from the start of the test considering the enthalpy changes listed in Table 4, especially those after the sodium leak was stopped, we found that more than 50% of the combustion heat was consumed in heating the walls, which causes us to think that heat transfer from the combusting sodium pool on the floor has exercised a large influence.

(4) Aerosol Behavior

Figure 19 shows the concentration changes in the aerosol in the atmosphere of the upper cell during the test. The aerosol concentration rose with the start of sodium leak from the simulated sodium pipe and reached a maximum of about 23 g-Na/m^3 when the sodium leak was stopped. Thereafter it decreased with the decrease of the sodium combustion rate shown in Fig. 17 to about 1 g-Na/m^3

or less one hour after the start of the test. The concentration temporarily rose about 2.5 hours after the start of the test, probably due to the resuspension of aerosol deposits by the cell ventilation.

4.3 Development of Phenomena in the Lower Cell

(1) Leaked sodium drain performance through sodium drain pipe

As mentioned in Section 4.1, the sodium leaking in the upper cell drained smoothly into the smothering tank in the lower cell through the sodium drain pipe. Figure 20 shows the temperature changes in the sodium drain pipe and the sodium flowing into the pipe during the test. This figure tells us that the temperature of the sodium drain pipe rises as soon as sodium begins to flow into it and remains above 500°C while sodium is flowing there. This indicates that the sodium drain pipe was not blocked by frozen sodium. We calculated the flow rate of drained sodium from the vertical temperature distribution in the smothering tank shown in Fig. 21. The result is shown in Fig. 22. We found from this figure that at an early period of sodium leak, the leaked sodium was partially drained while it spread over the floor liner of the upper cell, so the flow rate of drained sodium was lower than the flow rate of sodium leaking from the simulated sodium pipe (240 l/min = 4 l/sec) but became nearly equal to it about 150 seconds the test started. Therefore, we do not think there would be any excessive leaked sodium remaining on the floor liner of the upper cell in a sodium leak accident.

(2) Effect of Fire Suppression Board

The fire suppression board's ability to suppress the burning of collected sodium was evaluated by surveying the oxygen concentration changes inside and outside the smothering tank and the collected sodium temperature changes. Figure 23 shows the oxygen concentration changes inside and outside the smothering tank. The figure shows that for the drained sodium entering the smothering tank, the oxygen inside was consumed through its reaction with sodium and reduced to zero 30 minutes later. Its concentration was kept at less than 4% until the test ended. The oxygen concentration outside the tank, on the other hand, dropped once due to a temporary and violent combustion through the reaction with sodium after it entered the tank, but then increased due to cell ventilation and remained at a constant 21% thereafter. This indicates that the fire suppression board successfully prevented the air from entering the smothering tank and effectively suppressed the fire.

The collected sodium temperature, as shown in Fig. 24, reached a maximum of about 400°C when the sodium flow into the tank was stopped but then dropped with the passage of time to about 240°C, below the lower limit combustion temperature, when the test ended. The temperature history of sodium from leaking from the simulated sodium pipe to flowing into the smothering tank is an increase from 505°C to 680°C. (on the floor liner of the upper cell), an increase to 700°C (at the inlet of the sodium drain pipe), a decrease to 560°C (at the

outlet of the pipe), and a decrease to 400°C (in the smothering tank). We found that no fire occurred downstream from the inlet of the sodium drain pipe and that the sodium temperature was constantly decreasing due to heat loss to the surroundings. The collected sodium cooling performance, which is closely related to the sodium fire suppression ability of the fire suppression board, will be mentioned in section (3).

(3) Heat Transfer Characteristics in Lower Cell

Figure 25 shows the temperature changes in the lower cell during the test. The collected sodium temperature and the liner temperature mentioned in (2) were the highest among the maximum temperatures at various parts. The two were similar in value. These temperatures gradually decreased due to heat loss to the atmosphere above the collected sodium within the smothering tank, the atmosphere within the cell, and the thermal radiation shield.

The temperature at each concrete part rose only a little, indicating that the thermal insulators behind the thermal radiation shield on the ceiling and walls and the perlite boards under the liner on the floor were effective.

Next, the sodium combustion heat within the smothering tank was determined based on this test data. The combustion heat were calculated in the same way as for that of the upper cell; the difference of enthalpy between the sodium flowing into the lower cell and the collected sodium pool was deducted from the total rise of enthalpies in the atmospheric gas;

ceiling, wall, and floor structural materials; the sodium drain pipe; and the fire suppression board. The following equation was used:

$$Q' = Q_{\text{ceiling}} + Q_{\text{floor}} + Q_{\text{gas}} + Q_{\text{pipe}} + Q_{\text{board}} - Q_{\text{Na, in}} - Q_{\text{pool}} \dots\dots\dots (3)$$

- Q_{ceiling} The enthalpy change of the ceiling structural material of the lower cell (Kcal/h).
- Q_{wall} The enthalpy change of the wall structural material of the lower cell (Kcal/h).
- Q_{floor} The enthalpy change of the floor structural material of the lower cell (Kcal/h).
- Q_{gas} The enthalpy change of the atmospheric gas in the lower cell (Kcal/h).
- Q_{pipe} The enthalpy change of the sodium drain pipe in the lower cell (Kcal/h).
- Q_{board} The enthalpy change of the fire suppression board in the lower cell (Kcal/h)
- $Q_{\text{Na, in}}$ The enthalpy change of sodium flowing into the lower cell (Kcal/h).
- Q_{pool} The enthalpy change of sodium pool in the lower cell (Kcal/h).

Equation (3) was solved using the test data to determine the heat generating rate Q' . The result is shown in Fig. 26. As mentioned in the paragraph on the effect of the fire

suppression board in (2) described, when the drained sodium began to flow into the smothering tank, the heat generating rate reached about 50 kw/m^2 due to the combustion through the reaction of the oxygen in the lower cell and the smothering tank with the inflow sodium. This was, however, only about 1/2 of the averaged heat generating rate of the sodium pool combustion (100 kw/m^2). After the inflow of the drained sodium into the smothering tank ended, the heat generating rate was kept at nearly zero by the fire suppression board.

The collected sodium cooling performance, which is closely related to the effectiveness of the fire suppression board, can be evaluated by comparing the thermal conduction from the collected sodium to the floor concrete with the heat generating rate of collected sodium combustion. We determined the heat flux Q_{flux} from the sodium collected in the smothering tank to the floor concrete using the following equation and compared it with the above heat generating rate Q' :

$$Q_{\text{flux}} = Q' + Q_{\text{Na, in}} + Q_{\text{pool}} - Q_{\text{conv1}} - Q_{\text{rad1}} - Q_{\text{conv}} - Q_{\text{rad2}} \dots\dots\dots (4)$$

where

- Q' The heat generating rate of collected sodium determined by equation (3) (Kcal/h).
- $Q_{\text{Na, in}}$ The enthalpy of sodium flowing into the smothering tank (Kcal/h).

- Q_{pool} Enthalpy change of sodium pool within the smothering tank (Kcal/h)
- Q_{conv1} The heat flux from the surface of sodium pool to the atmosphere within the smothering tank through natural convection (Kcal/h).
- Q_{rad1} The heat flux from the surface of sodium pool to the fire suppression board through thermal radiation (Kcal/h).
- Q_{conv2} The heat flux from the fire suppression board to the atmosphere within the lower cell through natural convection (Kcal/h).
- Q_{rad2} The heat flux from the fire suppression board to the thermal radiation shield of the ceiling and walls (Kcal/h).

The heat-transfer coefficient of natural convection was used to derive the following equation for the natural convection of a heated horizontal flat plate:

$$Nu = 0.14 (Gr \cdot Pr)^{1/3}$$

where

Nu: Nusselt Number

Gr: Grashof Number

Pr: Prandtl Number

Equation (4) was solved using the test data and the heat generating rate Q' determined by the equation (3) to obtain

the heat flux Q_{flux} . The result is shown in Fig. 27. The heat flux to the floor reached a peak of about 10 kw/m^2 at an early period of the drained sodium flowing into the smothering tank. It decreased with time to about 3 kw/m^2 , about 1/3 the initial value, about one and a half hours later. The figure contains the result of Run-B3 for comparison. In Run-B3, the thermal insulating material under the floor liner was not perlite board but perlite concrete, and a fixed-type floor liner structure to be adopted in the cell liner of the actual plant's primary system was used. Nonetheless, the test results agree well with those at the initial stage of this test. This, we think, indicates that the heat flux from the sodium collected on the floor concrete tends to be almost constant irrespective to the form of the floor liner and the type of perlite. Furthermore, when the heat generating rate of collected sodium shown in Fig. 26 is compared with the heat flux from the sodium collected on the floor shown in Fig. 27, they are found to have shown almost the same value 2 hours from the start of the test. From this, we can conclude that the generated heat of the collected sodium combustion is consumed by the thermal conduction toward the floor concrete. There is, however, another heat transport path through the fire suppression board, which makes it certain that the collected sodium will be cooled with time and frozen in the smothering tank after several hours.

(4) Aerosol Behavior

Figure 28 shows the concentration changes of aerosol in the atmosphere of the lower cell. The concentration reached a maximum of about 5 g-Na/m^3 at an early stage because when the drained sodium flowed into the tank, aerosol containing expanded gas was discharged from the tank. Later, the concentration was kept under about 1 g-Na/m^3 because the combustion of collected sodium is suppressed by the fire suppression board and the cell was ventilated.

4.4 Visual Observation and Washing of Sodium after the Test

(1) Visual Observation and Inspection of Various Test Cell Parts

Test Run-D2 was completed by draining sodium from the lower cell, but in this test we continued to monitor the temperatures of various parts of SOLFA-1 until dropped nearly to room temperature. Subsequently, carbon dioxide gas was injected into the upper and lower cells to chemically stabilize the residual sodium and sodium aerosol. After confirming that they were stabilized, we opened the doors of the cells to observe and take photographs of the internal conditions.

Photo.4 shows the internal conditions of the upper cell. We observed that the outer jacket and the thermal insulating material of the simulated sodium pipe significantly deformed. We also found that sodium aerosol thinly coated the bare concrete side walls and ceiling surfaces. Most of the residual substances on the floor liner were sodium compounds consisting

mainly of sodium oxide and hydroxide. Since the volume of these residues, which were measured later when the sodium was removed on the floor liner, was only about 7% of the total sodium supply, we found that almost all the leaked sodium had been drained into the smothering tank through the sodium drain pipe.

Photo.5 shows the inlet of the sodium drain pipe connected to one end of the floor liner of the upper cell. The sodium drain pipe is reduced in diameter from 318.5 mm to 216.3 mm about 1234 mm away from the inlet; this step is seen in the photograph. As in test Run-B3 results, no solid material that hinders the flow of sodium within the pipe was found, except a small amount of residue remaining around the inlet including this step.

Finally, in the test, when the sodium temperature in the smothering tank in the lower cell dropped to about 200°C in the latter half of the test (i.e., 6 hours 36 minutes from the start of the test), the sodium was drained to the sodium impurities settlement tank seen in Fig. 2. About 80% of the 2,729.7 kg of sodium in the smothering tank was drained to the sodium impurities settlement tank at that time, with the rest remaining in the smothering tank. Photo.6 shows the sodium, and sodium compounds remaining in the smothering tank. The photograph was taken after the fire suppression board was partially removed. As was made clear later at the sodium disposal stage, the residues in the photograph consisted mainly of oxides around the outlet of the sodium drain pipe, which

changed into sodium at places farther from the sodium drain pipe. Such a difference of chemical composition of the residues by location suggests that in an early stage of the sodium leak test, relatively pure sodium flowed from the upper cell into the smothering tank through the sodium drain pipe, while in the later stage the combustion products produced on the floor liner of the upper cell flowed into the tank. The development in this test can also explain such a chemical composition distribution. Table 5 shows the distribution of residual sodium after the completion of the test.

(2) Reaction of Concrete with the Aerosol Deposited on its Surface

In this test, the side walls and ceiling concrete of the upper cell are directly exposed to the cell atmosphere. One of the largest concerns was whether sodium aerosol deposited on the bare concrete surfaces would react chemically with it. The concrete surface on which the aerosol had been deposited was therefore visually observed to see whether such a reaction had occurred.

In the inspection, the thin layer of deposition on the concrete surface was washed away by water. No roughness increase due to the reaction could be observed, except for some corrosion of concrete at the lower part of the north wall where leaked sodium rebounded and attached directly. We can conclude from this that no reaction would occur between concrete and aerosol deposits at temperatures of 200°C or below as in this test. Figure 29 shows the volume of sodium

aerosol deposited on each part.

(3) Washing of Sodium and Distribution of Residues within the Test Cell

When washing and disposing of sodium, we collected the residual sodium and combustion products in the upper and lower cells by shovels and put into drum cans. Next, the remaining material was washed away by water to inspect the floor liner in the upper cell and the floor liner of the smothering tank in the lower cell. This work was done while the weight distribution of the residues and sodium aerosol deposits was measured at each part of the test cell. In measuring the aerosol deposits weight, the deposits on typical square areas with 30cm sides on the ceiling, floor, and walls sampled, dissolved in water, and their sodium weight was measured by atomic absorption analysis.

Figure 30 shows the distribution of residual sodium and aerosol deposits thus measured. The percentages in the figure are based on taking the total leaked sodium as 100%. Nearly all the leaked sodium (about 92%) was collected in the smothering tank, and a very small amount (about 7%) remained on the floor liner of the upper cell. The ratio of sodium aerosol to the total leaked sodium was only 0.3%, including aerosol in the upper and lower cells and that collected by the aerosol scrubber. This indicates that the sodium fire control systems used in this test, that is, the fire control systems of Monju, were effective.

Figures 29 and 31 show the measured distribution of

aerosol deposits alone. Much aerosol (about 55% of the total) is found in the upper cell because of the sodium pool combustion on its floor liner during the test, while there is a relatively little (about 15%) in the lower cell because the fire suppression board worked effectively.

(4) Inspection of Simulated Sodium Pipe Thermal

Insulation jackets

Before the sodium was washed away, the simulated sodium pipe test body was removed from the upper cell for inspection.

Photo.8 was taken during the inspection. The outer jacket and the thermal insulating material were significantly deformed by the high temperature of sodium combustion. The survey of the leaked sodium flow rate had previously indicated that this deformation occurred as the temperature of the outer jacket surface increased due to the combustion of residual sodium after the sodium leak was stopped. It did not occur while the sodium was leaking because during the sodium leakage, the temperature of both the outer jacket and the thermal insulating material did not exceed that of the leaking sodium due to the sodium flow's cooling effect.

Photos.9 and 10 show the simulated sodium pipe being disassembled. No damage was found on either the inner jacket or its joint, nor was any abnormality seen in the connecting pipe of the clamp.

(5) Inspection of Floor Liner, Sodium Drain Pipe, and

Smothering Tank

The floor liner and the bottom liner of the smothering tank must prevent the propagation of an accident. They must therefore completely isolate the leaked sodium from the building concrete by absorbing large thermal shocks from the leaked sodium without being cracked. Our past tests have already proven that the thermal shocks in a sodium leak accident can only cause a plastic deformation of the liners and cannot cause cracks in their weld parts. However, this has never been confirmed by any large-scale test. We therefore conducted a dye penetration test (nondestructive test) on the floor liner, the sodium drain pipe, and the bottom liner of the smothering tank.

We tested all the weld lines of the floor liner and the bottom liner of the smothering tank and the inner surfaces of the sodium drain pipe cut in round slices at 30-cm intervals. Photos. 11 and 12 show the conditions of the floor liner of the upper cell and the bottom liner of the smothering tank revealed during the nondestructive test.

No cracks were found in any part.

4.5 Post-Test Destructive Inspection of the Concrete of the Upper Cell

In this test, the upper bare concrete surfaces of the wall and ceiling were directly exposed to the high-temperature atmosphere of sodium combustion. Their temperature (12 mm from the surface) reached 114°C to 133°C about 50 minutes after the test started, as shown in Fig. 32. Accordingly, after

completing a series of post-test inspections, we disassembled the upper cell, cut core samples from the concrete panels, and conducted some destructive tests including a comprehensive strength test and a Young's Modulus test. Photo.13 shows the core samples.

Table 6 shows the specific weight of the core samples, their compressive strength test and Young's Modulus, the specific weight of the concrete panel when it was fabricated, and its compressive strength test results. Figure 33 shows the relations between the positions where the cores were cut out and the compressive strength of those positions when the concrete panels were assembled. Figure 34 shows the relations between the specific weight and compressive strength of the upper cell concrete when the cores were cut out. Figure 35 shows the relations between the compressive strength and Young's Modulus of the upper cell concrete. Figure 36 shows the relations between the weight loss of the concrete and its compressive strength, calculated from the specific weight of the concrete panel when it was fabricated.

These test results have clarified the following:

- (1) In comparison to the pre-test concrete properties (i.e., specific weight 2,301 to 2,311 kg/m^3 , age 28 days, and compressive strength 318 to 335 kgf/cm^2), the specific weight changed from 2220 to 2340 kg/m^3 and the compressive strength from 250 to 421 kgf/cm^2 .
- (2) After the test, there was a closer correlation between

the specific weight and the compressive strength, the latter tending to decrease as the former decreased as shown in Fig. 33. This seems to be attributed to the heating during the sodium fire.

(3) The compressive strength and Young's Modulus also showed a high correlation as shown in Fig. 35. Its trend was linear type similar to that shown by the Japan Construction Society's Standard. In general, Young's Modulus of the concrete subjected to high temperature decreases and the compressive strength lowers. Our test results generally agree with the above Society's Standard in which a remarkable reduction of Young's Modulus occurs when concrete is exposed to a high temperature. Since such phenomena were not seen, the heat received by the concrete panels during the sodium fire was not high enough to impair their function.

Although we have not yet destructively tested the concrete panels in the lower cell, we can suppose they have remained sound, since they were not bare as were those in the upper cell, and their internal temperature did not rise as seen in Fig. 37.

Conclusions

We conducted large-scale simulation test of a secondary sodium leak accident to demonstrate the whole accident sequence using the two-storied concrete cell SOLFA-1 which simulated the Monju secondary building. A simulated sodium pipe was installed in the upper cell to simulate the whole accident sequence. In the test, the sodium leaking from the simulated sodium pipe dropped onto the floor liner, drained through the sodium drain pipe into the smothering tank in the lower cell, and was extinguished by the fire suppression board.

About 3 tons of sodium at 505°C was used. The sodium leaked from the simulated sodium pipe was under the same pressure as in the actual plant (3.8 kg/cm² G). As a result, the following conclusions have been drawn:

Whole accident sequence

The sodium leaking from the simulated sodium pipe was smoothly drained from the floor liner to the smothering tank through the sodium drain pipe. The fire of the collected sodium was suppressed by the fire suppression board to end the accident. This process was the same as postulated for the Monju design. No remarkable difference from the process, which had also been observed in the previous small-scale Run-B3, occurred as a result of increasing the test scale.

Sodium leakage from pipe

Neither corrosion nor high-temperature destruction of the inner and outer jackets was caused by the chemical reaction between sodium and the thermal insulation material or, by sodium combustion. Collapse of the thermal insulation jackets under the pressurized sodium leak was not observed. The sodium leaked from the pipe is a downward columnar flow, and not an upward spray leak.

Fluidity of leaked sodium

The sodium leaking from the simulated sodium pipe flowed smoothly over the floor liner and was drained through the sodium drain pipe into the smothering tank. No combustion products or frozen sodium blocked the sodium flow.

Effects of the fire suppression board

Air entrance into the smothering tank was completely prevented by a fire suppression board in the same way as used in an actual plant. The combustion of the collected sodium was suppressed. The collected sodium naturally cooled through heat losses to the surrounding to below the combustion limit temperature.

Structural integrity of the concrete building and the sodium fire control systems

The inspection after the test confirmed that no destruction or remarkable deformation of the concrete building

of the sodium fire control systems occurred. Nor was any corrosion or destruction of the concrete surfaces exposed to the sodium atmosphere observed.

Acknowledgements

We express our gratitude to people of the machinery section, the Reactor Construction & Operation Project, for their advice about planning this test. Mr. K. Sasaki, Mr. T. Yamada, Mr. T. Fukuchi, Mr. K. Kawada, Mr. T. Morii, and Mr. Y. Katogi of the Plant Safety Engineering Section, Oarai Engineering Center gave us their technical cooperation in carrying out this test. The authors would like to express their gratitude to Mr. T. Kitahara, director of the Safety Engineering Division, for his encouragement and advice from a broad viewpoint.

References

- (1) R. Kawabe, Y. Himeno, et al., "Basic Test on Sodium Fire Protection Systems," PNC Report, SN941 84-124, Aug. 1984.
- (2) R. Kawabe, Y. Himeno et al., "Basic Test on Sodium Fire Protection Systems (II) - Flow and Combustion of Low-Temperature Sodium on Simulated Floor Liner," PNC Report, SN9412 85-104, July 1985.
- (3) Y. Himeno, S. Miyahara, et al., "Basic Test on Sodium Fire Protection Systems (III), Simulation Test Run-B3 of a Design Basis Sodium Leak from the Monju IHTS," PNC Report,

SN941 85-130, Sept. 1985.

- (4) Y. Himeno, M. Usami, et al., "Basic Test on Sodium Fire Protection Systems (IV) - Water Simulation Test of a Leak from IHTS Pipe" PNC Report, SN941 86-088, Aug. 1986.
- (5) S. Miyahara, K. Sasaki, et al., "A Large-Scale Test on Sodium Leak and Fire (I) - A Sodium Pool Fire Test in Air, Run-D1," PNC Report, to be printed.
- (6) Y. Himeno, K. Kawada, et al., "A Large-Scale Test on Sodium Leak and Fire (I) - A Spray Fire Test in Water Vapor Containing Air, Run-F1," PNC Report, to be printed.
- (7) T. Morii, T. Fukuchi, et al., "A large-Scale Test on Sodium Leak and Fire (III) - A Large Scale Test of Sodium Spray Fire in Air, Run-E1," PNC Report, to be printed.
- (8) T. Morii, T. Fukuchi, et al., "A Large-Scale Test on Sodium Leak and Fire (IV) - A Realistic Sodium Leak-Test with Simulated Pipe, Run-E1," PNC Report, to be printed.

Table 1 Compositions of Structural Concrete used in SOLFA-1 and in MONJU

		SOLFA-1	MONJU
Materials	Cement	Flyash B	Flyash B
	Aggregate	Graywacke	Graywacke
	Retarder	—	Pz. No. 8
	AE Water Reducing Agent	Pz. No. 5L	303A
Maximum Size of Coarse Aggregate (mm)		25	25
Design Strength (kgf/cm ²)		240	240
Bulk Density (kg/m ³)		2150	2150
Water Cement Ratio (%)		49.6	55
Sand Percentage (%)		40.3	43
Slump (cm)		8±2.5	12±1.5
Air Content (%)		3±1	4±1

PSS-SFE-343

Table 2 Test Conditions of Run-D2

Sodium Fedded	: 2974.1 kg
Sodium Temperature	: 505 °C, Hot-Leg Temperature of Monju IHTS
Sodium Pressure	: 3.8 kg/cm² G, Hot-Leg Sodium Pressure of Monju IHTS
Simulated Sodium Pipe	: 1/2.6 (linear scale) of Monju ITHS Pipe
Cross Area of Leak Hole	: 1/(2.6)² of a 1/4 Dt Leak Hole Posturated for Monju IHTS Pipe
Initial Temperature of Simulated Sodium Pipe	: 505 °C
Oxygen Injection Rate into Upper Cell	: 2.2 m³/min (during Sodium Spill) 0.2 m³/min (after the end of Sodium Spill)
Air Flow Rate into Lower Cell	: 1.4 m³/min
Temperature of Feed Air	: 16.0 °C
Relative Humidity of Feed Air	: 52.0 %

PSS-SFE-344

Table 3 Test Record of Run-D2

Time	Record	Time after Initiation of Sodium Feed
10:13	Start-up of Aerosol Scrubber	
14:05	Pressurization of Cover Gas in Sodium Heater	
14:43	Start-up of Data Acquisition System	
14:44	Start of Sodium Feed	0
14:45	Start of Ventilation in Lower Cell (1.3m ³ / min)	1min 30sec
14:49	Start of Oxygen Injection into Upper Cell (2.2m ³ / min)	5min 01sec
15:01	End of Sodium Feed	14min 35sec
15:03	Change of Oxygen Injection Rate (0.2m ³ / min)	17min 22sec
15:25	End of Oxygen Injection	39min 47sec
21:20	Drain of Sodium in Smothering Tank	6hr 36min
6:31	Turn-off of Data Acquisition System	15hr 48min

PSS-SFE-345

Table 4 Enthalpy Change in Upper Cell

	Enthalpy Change (kcal)	
	up to the end of Sodium spill	up to 1 hour
Sodium, $Q_{Na,out} - Q_{Na,in}$	1.82×10^4	1.82×10^4
Ceiling Concrete, Q_{ceil}	7.17×10^4	1.90×10^5
Wall Concretes, Q_{wall}	1.70×10^5	5.87×10^5
Floor liner and Floor Concrete, Q_{floor}	1.27×10^5	3.10×10^5
Gas, Q_{gas}	5.84×10^3	1.21×10^4
Total, $Q_{Na,out} - Q_{Na,in} + Q_{ceil} + Q_{wall} + Q_{floor} + Q_{gas}$	3.87×10^5	1.11×10^6

PSS-SFE-346

Table 5 Distribution of Residual Sodium in Test Rig after the Test

	Compartment	Place		Distribution					
				Weight (kg)		Ratio (%)			
Sodium	Upper cell	Floor liner		217.0	232.9	2961.0	7.3	7.9	99.7
		Simulated sodium pipe		10.5			0.4		
		Sodium drain pipe		5.4			0.2		
	Lower cell	Smothering tank	Reaction products	422.9	613.4		20.6		
			Sodium	190.5					
Dump tank	—		2114.7		71.2				
Aerosol	Upper cell	Ceilling		2479 g	5.5	10.1	0.2		
		Wall	East	740 g					
			South	757 g					
			West	687 g					
	North		872 g						
	Lower cell	Fire suppression board (upper surface)		1514 g	1.6		0.1		
		Ceilling		4 g					
		Wall	East	11 g					
			South	7 g					
			West	9 g					
North			9 g						
Scrubber (Water pool)			3.0		0.1				

PNC-TN9410 87-086

Table 6 Specific Weight, Compressive Strength and Young's Modulus of Upper Cell Concrete after the Test

Panel No.	Sample No.	Specific Weight (kg/m ³)			Compressive Strength (kgf/cm ²)			Young's Modulus (X10 ⁵ kgf/cm ²)	
		Post-test Data	Mean Value of Post-test Data	Pre-test Data	Post-test Data	Mean Value of Post-test Data	Pre-test Data	Post-test Data	Mean Value
3W2	1	2312	2291	2311	359	364	322	3.47	3.28
	2	2286			384			3.24	
	3	2276			349			3.13	
3W3	1	2275	2275	2302	356	348	328	3.08	3.14
	2	2268			329			3.13	
	3	2283			359			3.22	
3W4	1	2272	2283	2311	330	329	333	2.84	2.87
	2	2304			320			2.85	
	3	2273			337			2.91	
3W5	1	2241	2248	2309	284	279	335	3.14	2.81
	2	2261			275			2.67	
	3	2243			279			2.61	
3W6	1	2283	2290	2302	339	360	323	3.06	3.05
	2	2285			396			3.17	
	3	2296			345			2.91	
3W7	1	2310	2304	2311	339	320	322	3.24	3.17
	2	2319			322			3.30	
	3	2283			298			2.98	
3W8	1	2336	2325	2302	365	350	323	3.16	3.03
	2	2316			364			2.94	
	3	2323			320			2.98	
3S1	1	2227	2255	2302	279	299	328	2.77	2.76
	2	2273			297			2.64	
	3	2265			322			2.86	
3S2	1	2333	2340	2301	398	421	318	3.24	3.36
	2	2334			434			3.24	
	3	2353			432			3.61	
3S3A	1	2232	2222	2311	332	317	322	2.71	2.55
	2	2243			312			2.57	
	3	2191			307			2.37	
3S3B	1	2226	2278	2311	377	390	322	3.35	3.20
	2	2306			402			3.09	
	3	2265			390			3.18	
4C1	1	2209	2220	2302	250	250	328	2.57	2.57
	2	2265			252			2.64	
	3	2185			248			2.51	
4C2	1	2289	2312	2311	360	369	333	2.93	2.96
	2	2317			372			2.99	
	3	2330			374			2.96	
4C3	1	2239	2234	2309	343	309	335	2.91	2.79
	2	2219			281			2.72	
	3	2244			302			2.73	

PSS-SFE-348

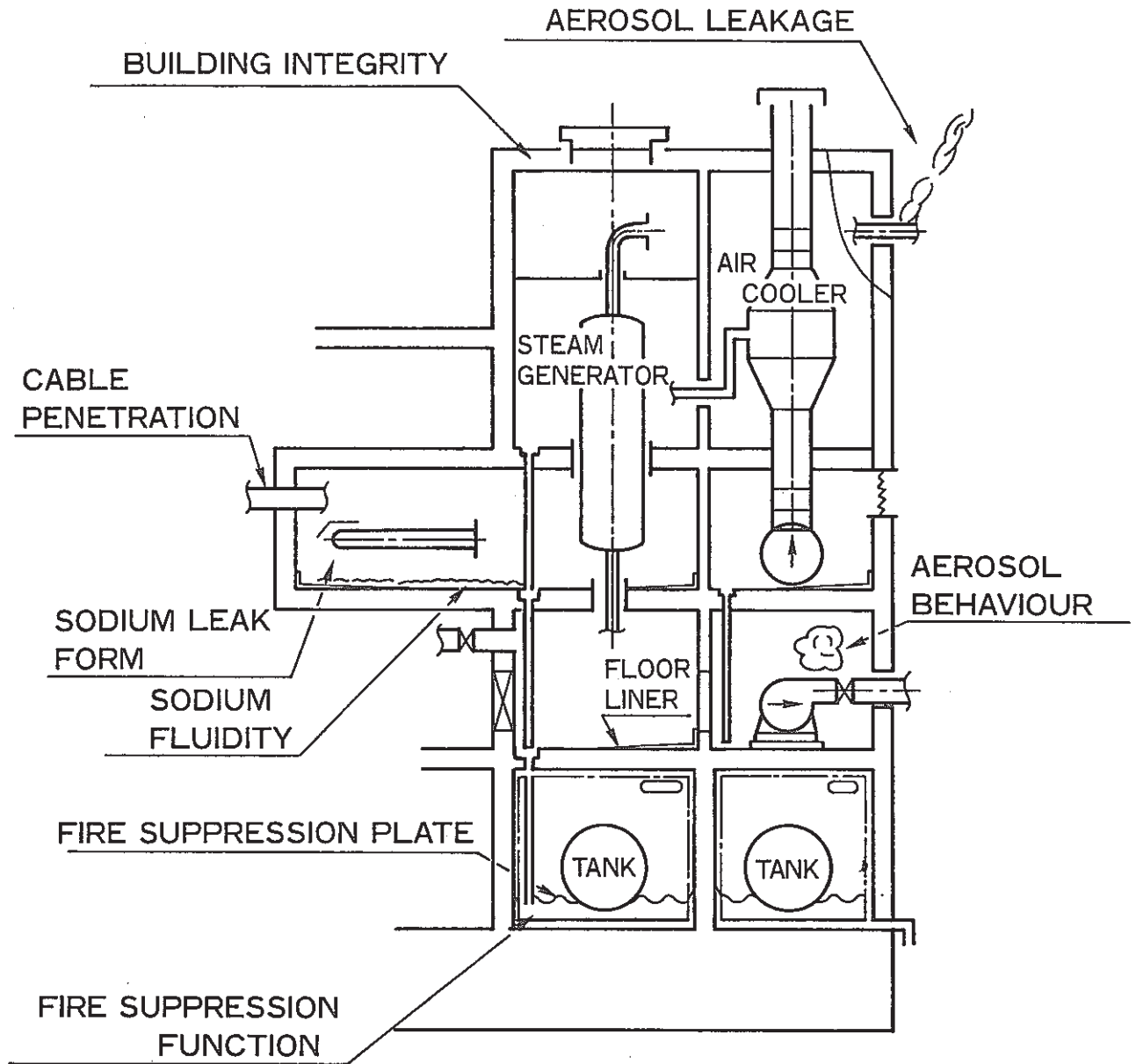


Fig.1 SUBJECT EXAMPLES IN "MONJU" SECONDARY SYSTEM

PSS-SFE-349

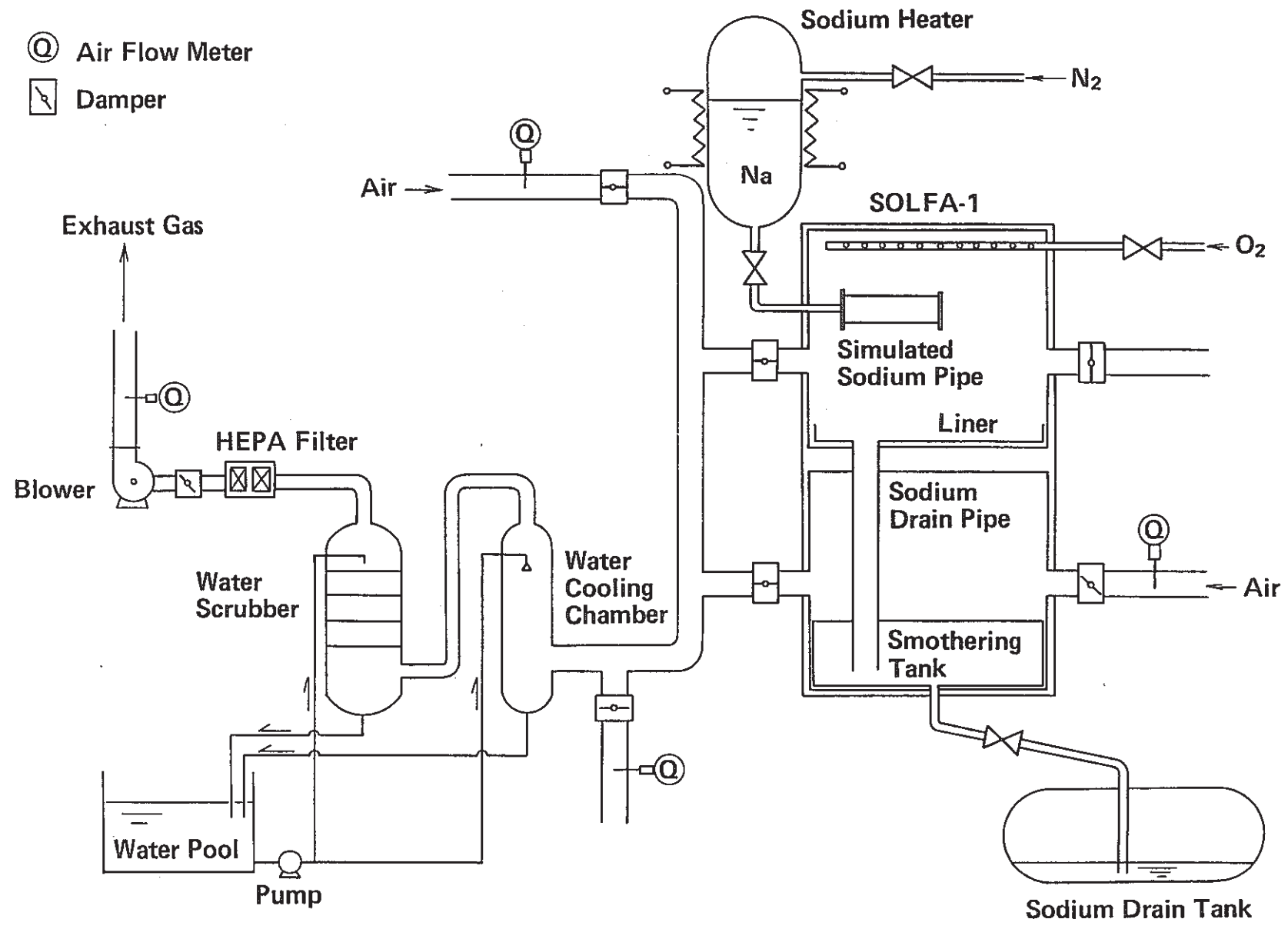


Fig.2 Arrangement of Test Rig for Run-D2

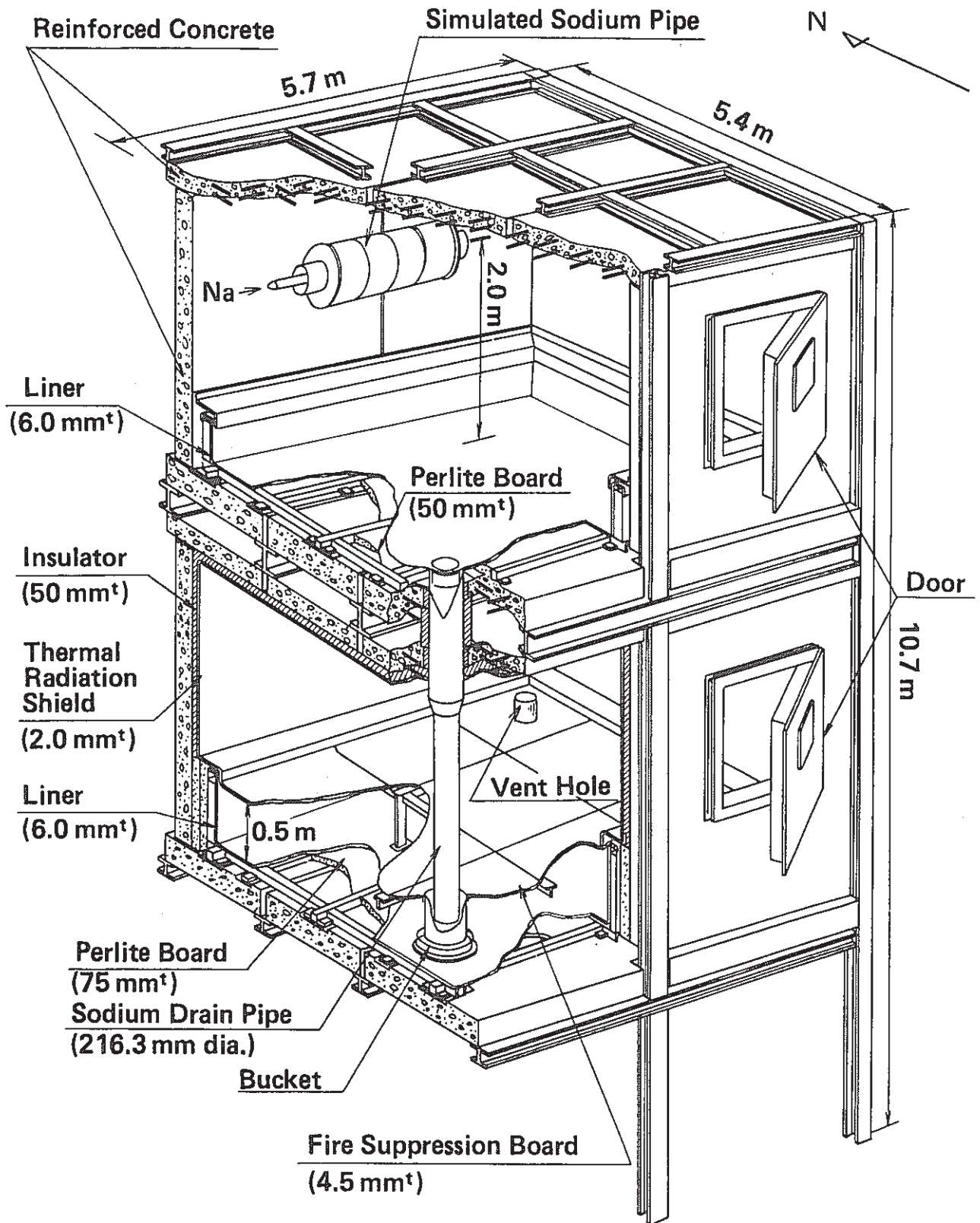



Fig.3 Bird's-eye View of SOLFA-1 for Run-D2

PSS-SFE-35 I

Note for keys

- | | |
|---|--------------------------------|
| (T) Thermocouple | (O ₂) Oxygen meter |
| (P) Pressure gauge | (D) Displacement meter |
| (F) Flow meter | |
| (C) Aerosol concentration meter | |
|  TV Camera | |

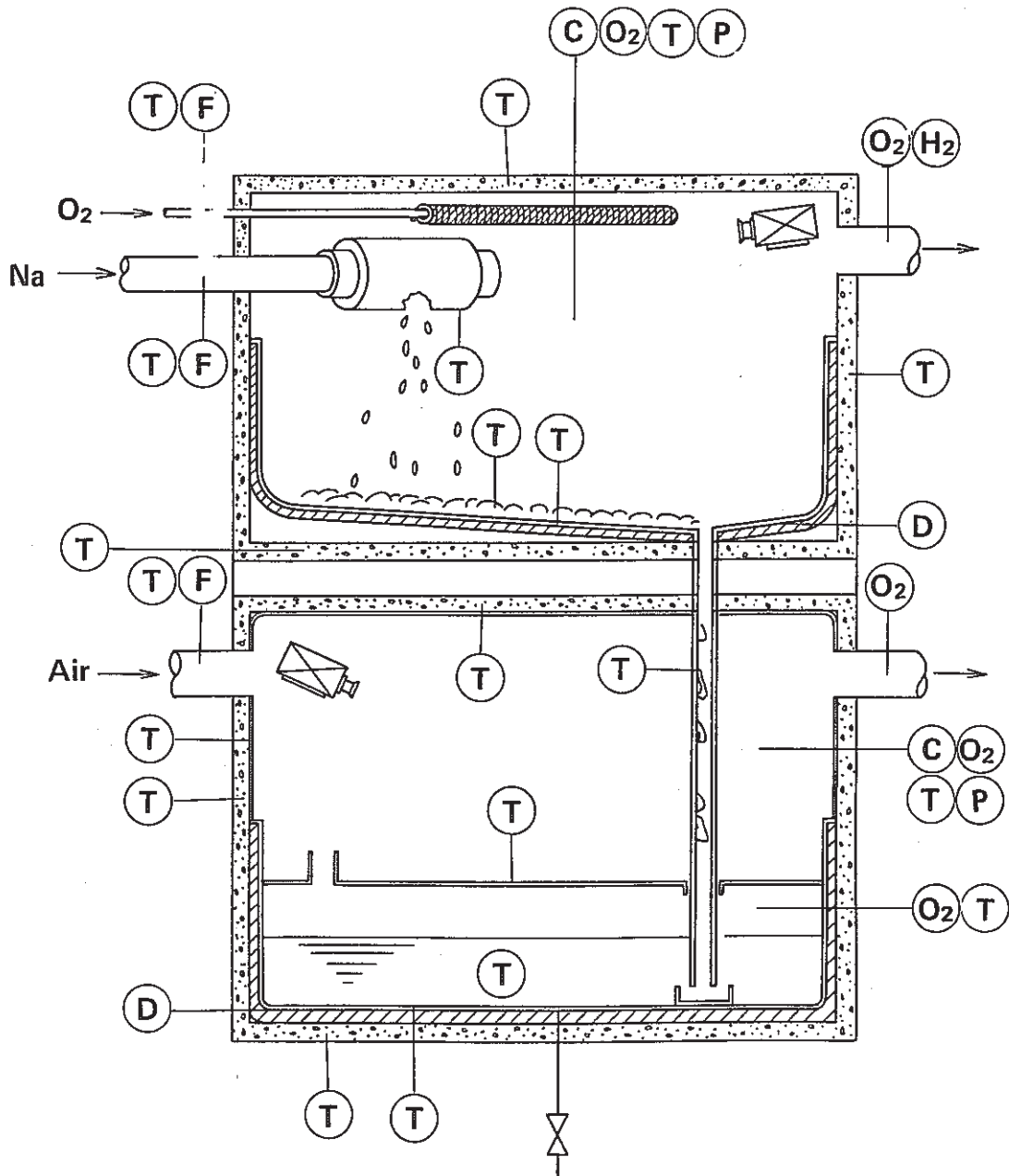


Fig.4 Instrumentations and Sensors Installed in Test Rig for Run-D2

PSS-SFE-528

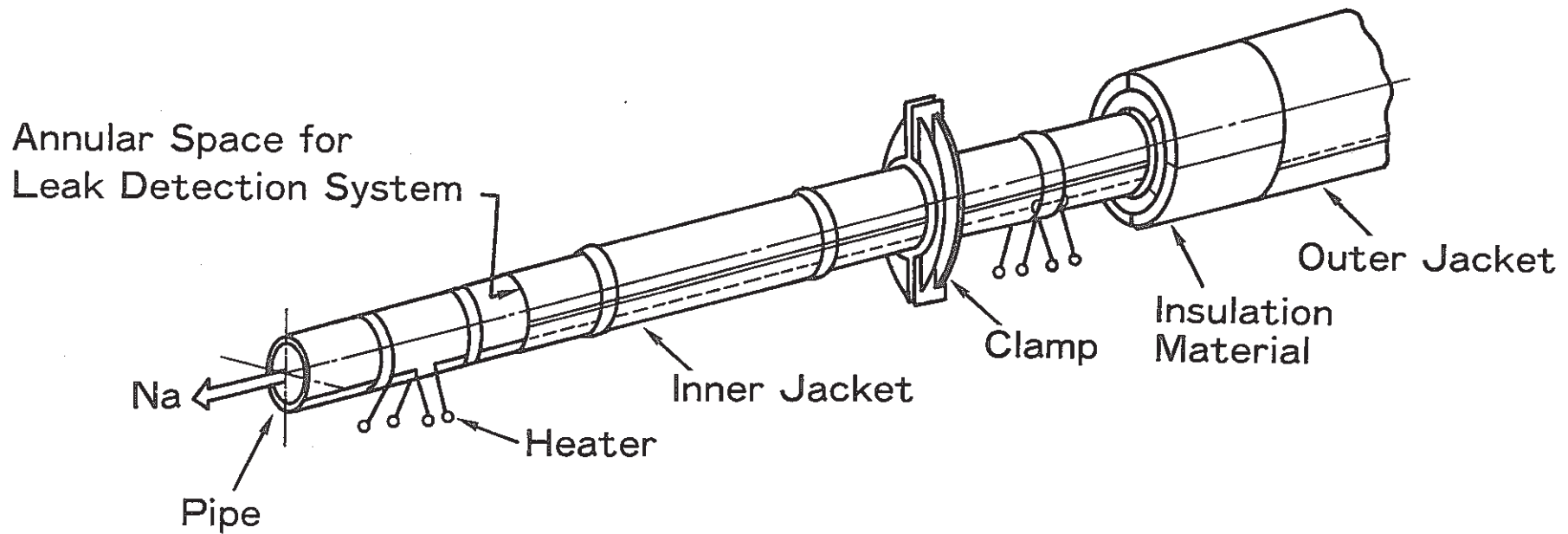


Fig.5 Concept of Monju Secondary Sodium Piping with Thermal Insulation Cover

PSS-SFE-353

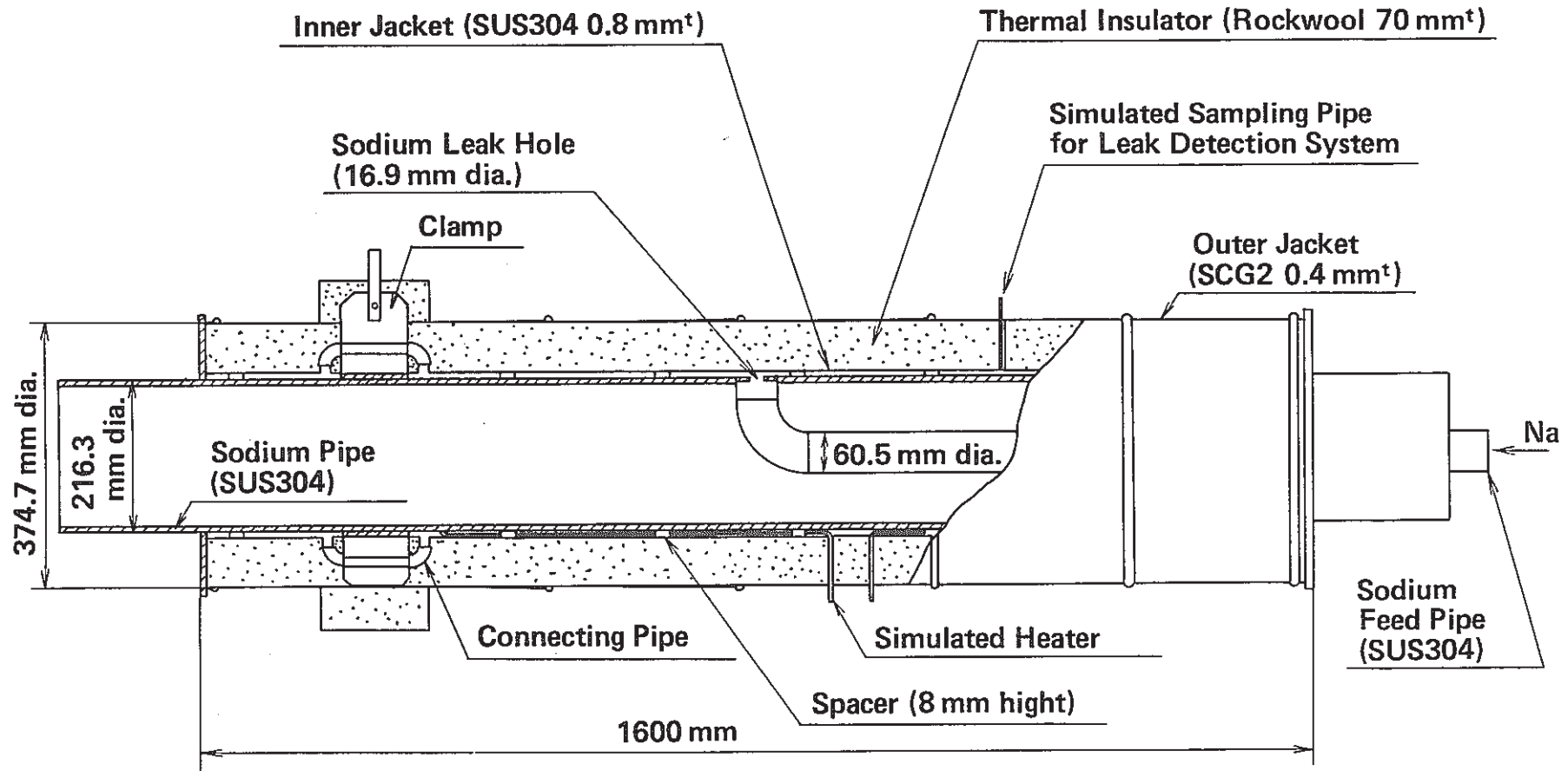


Fig.6 Cut View of Simulated Sodium Pipe for Run-D2

PSS-SFE-354

unit : mm

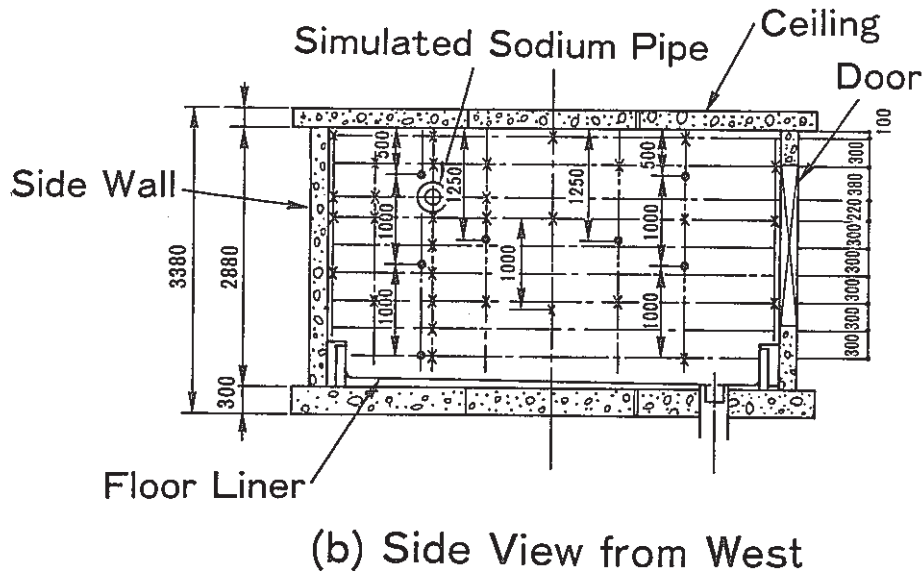
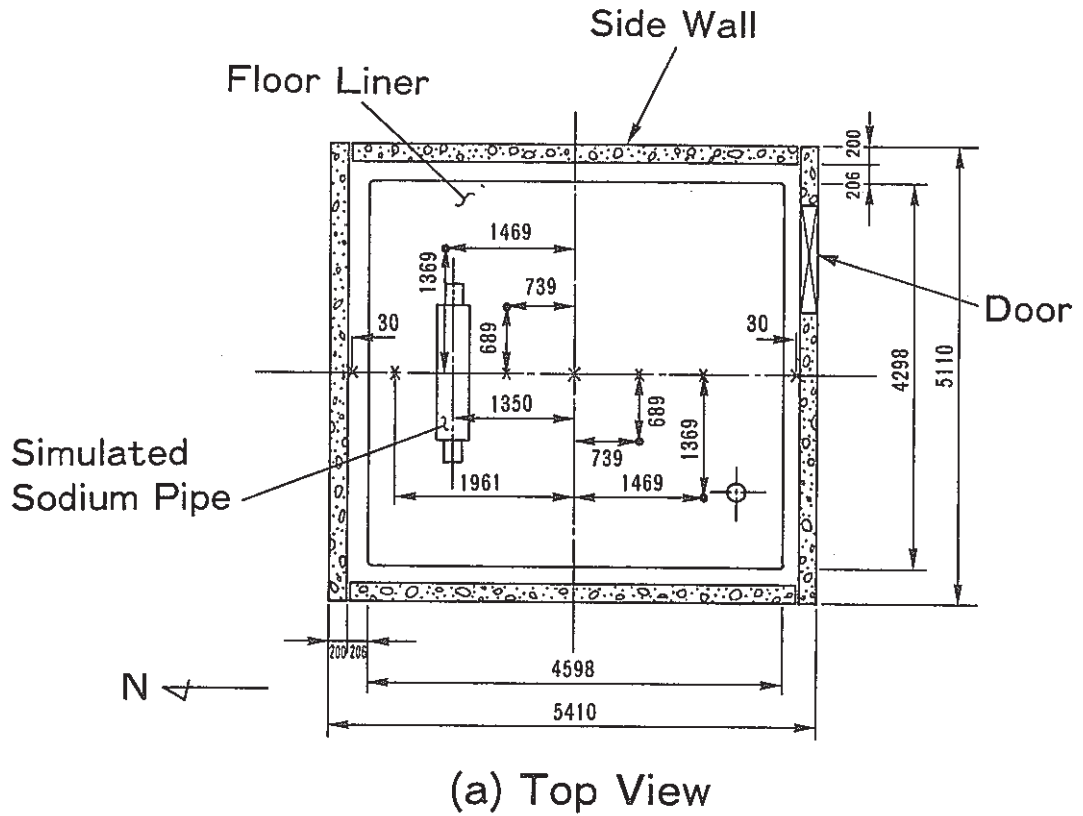


Fig.7 Geometric Configuration of the Upper Cell of SOLFA-1

PSS-SFE-355

unit : mm

× indicates location of thermocouples on upper surface of floor liner

● indicates location of thermocouples on lower surface of floor liner

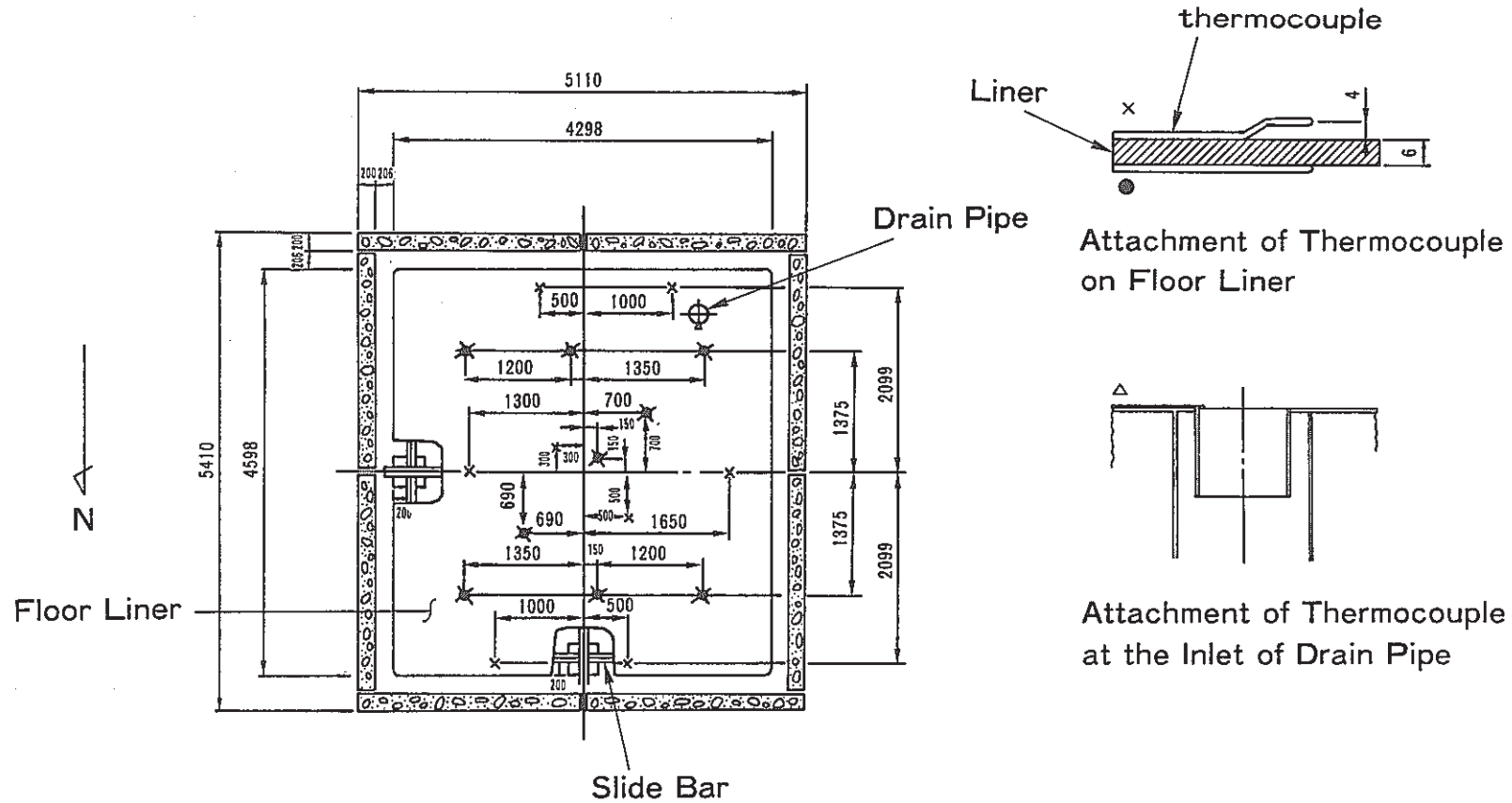
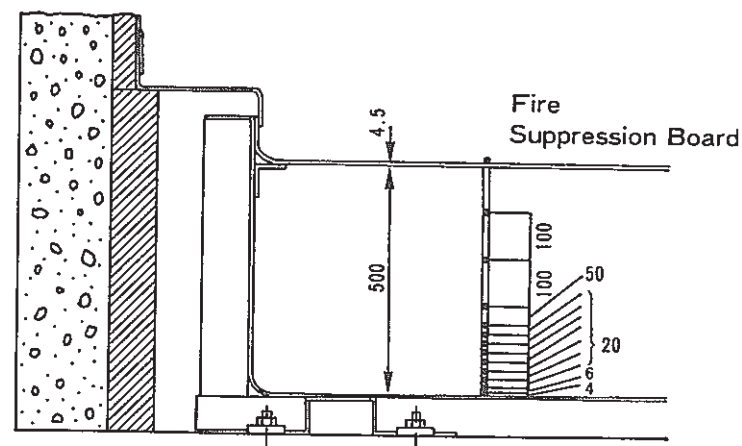
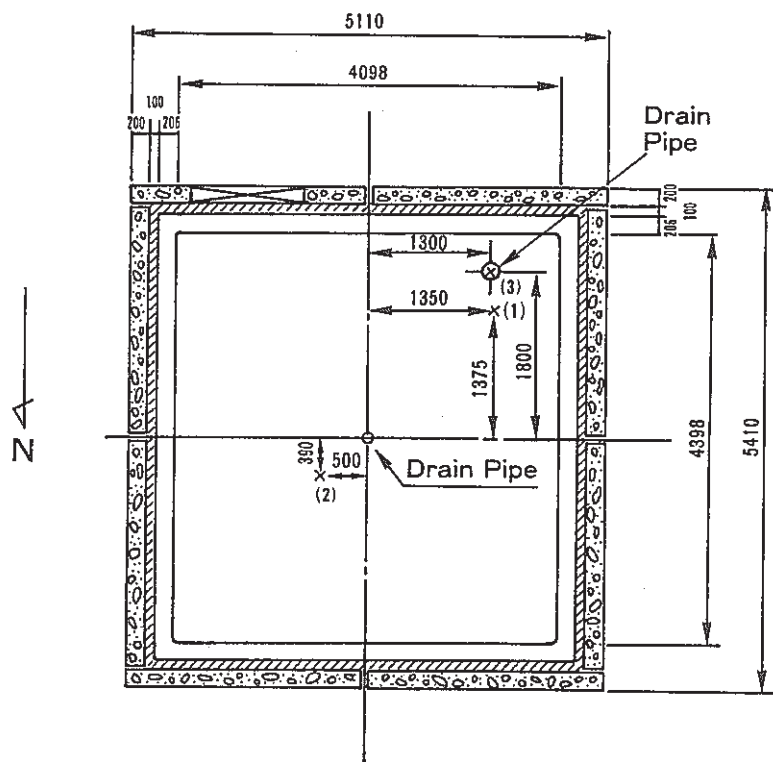
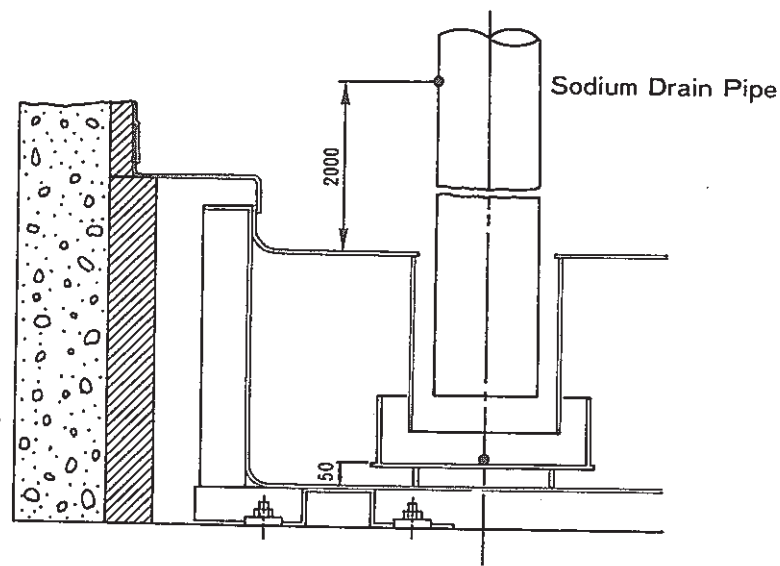


Fig.8 Location of Thermocouples on Floor Liner of the Upper Cell of SOLFA-1

unit : mm



Location (1) and (2)



Location (3)

Fig.9 Location of Thermocouples in the Lower Cell of SOLFA-1

PSS-SFE-357

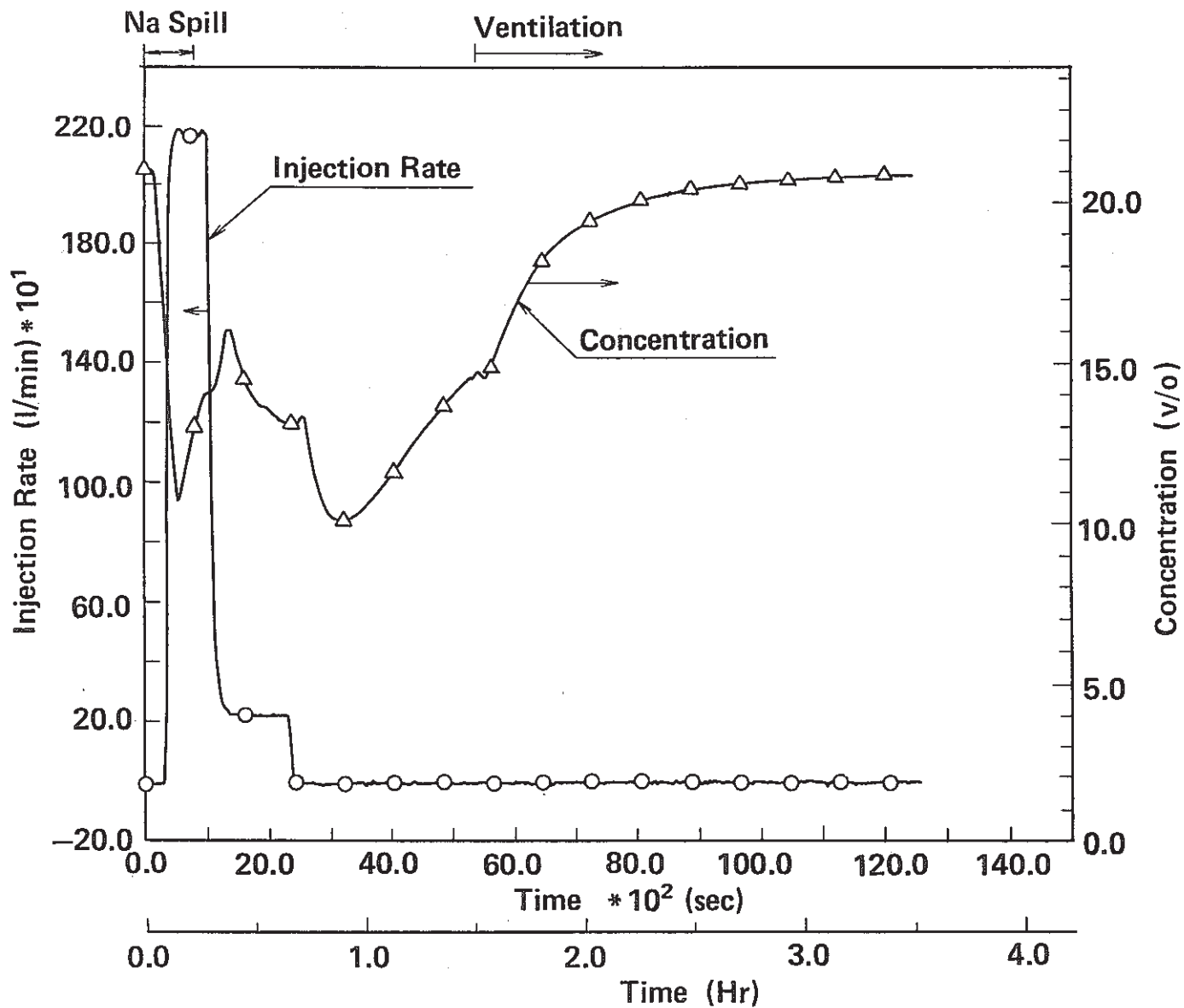


Fig.10 Changes of Oxygen Injection Rate and of Oxygen Concentration during the Test (Upper Cell)

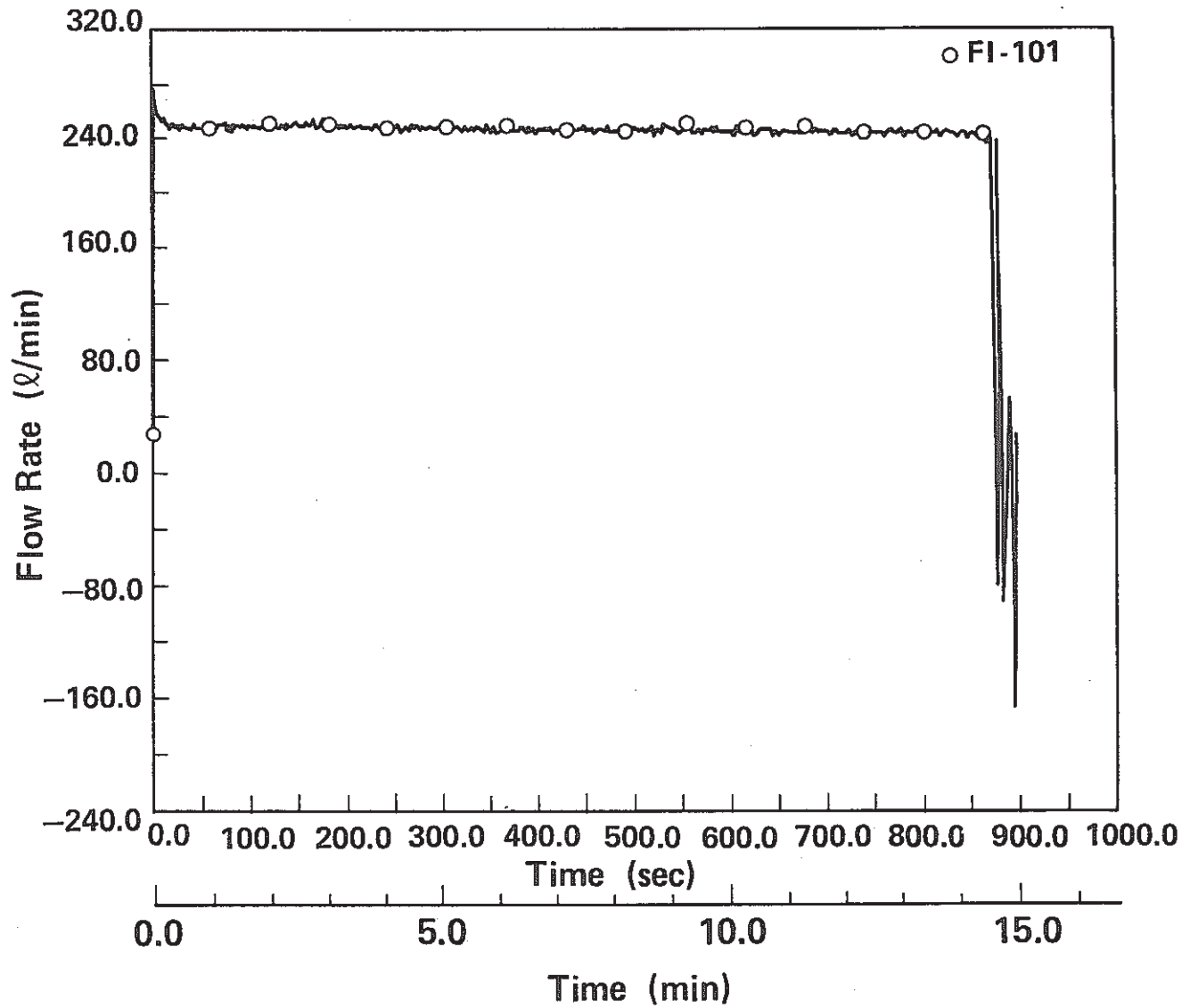


Fig.11 Flow Rate of Feed Sodium into Simulated Sodium Pipe

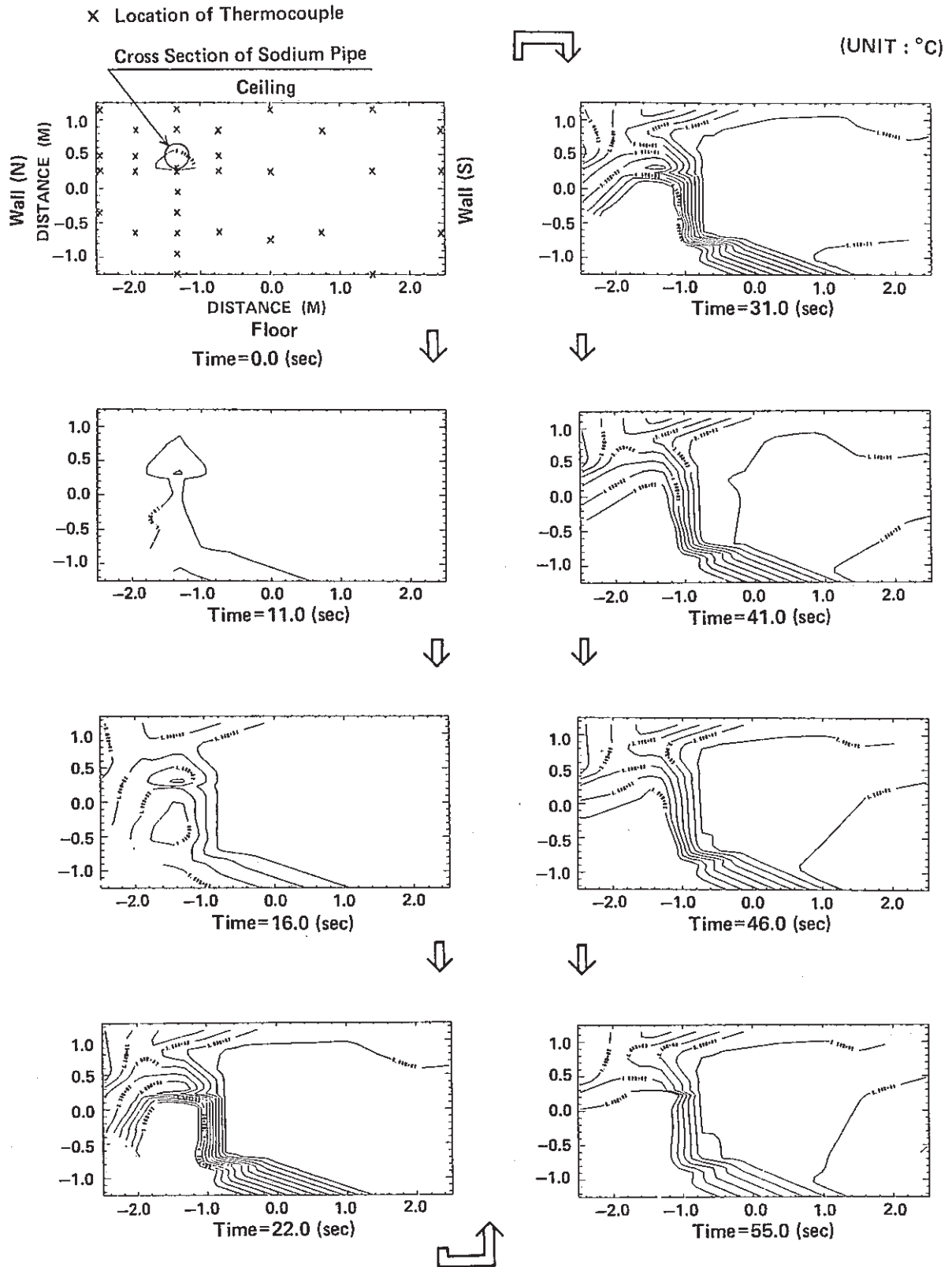


Fig.12 Temperature Distribution Changes in Vertical Cross Section of Upper Cell Atmosphere during Sodium Spill

PSS-SFE-360

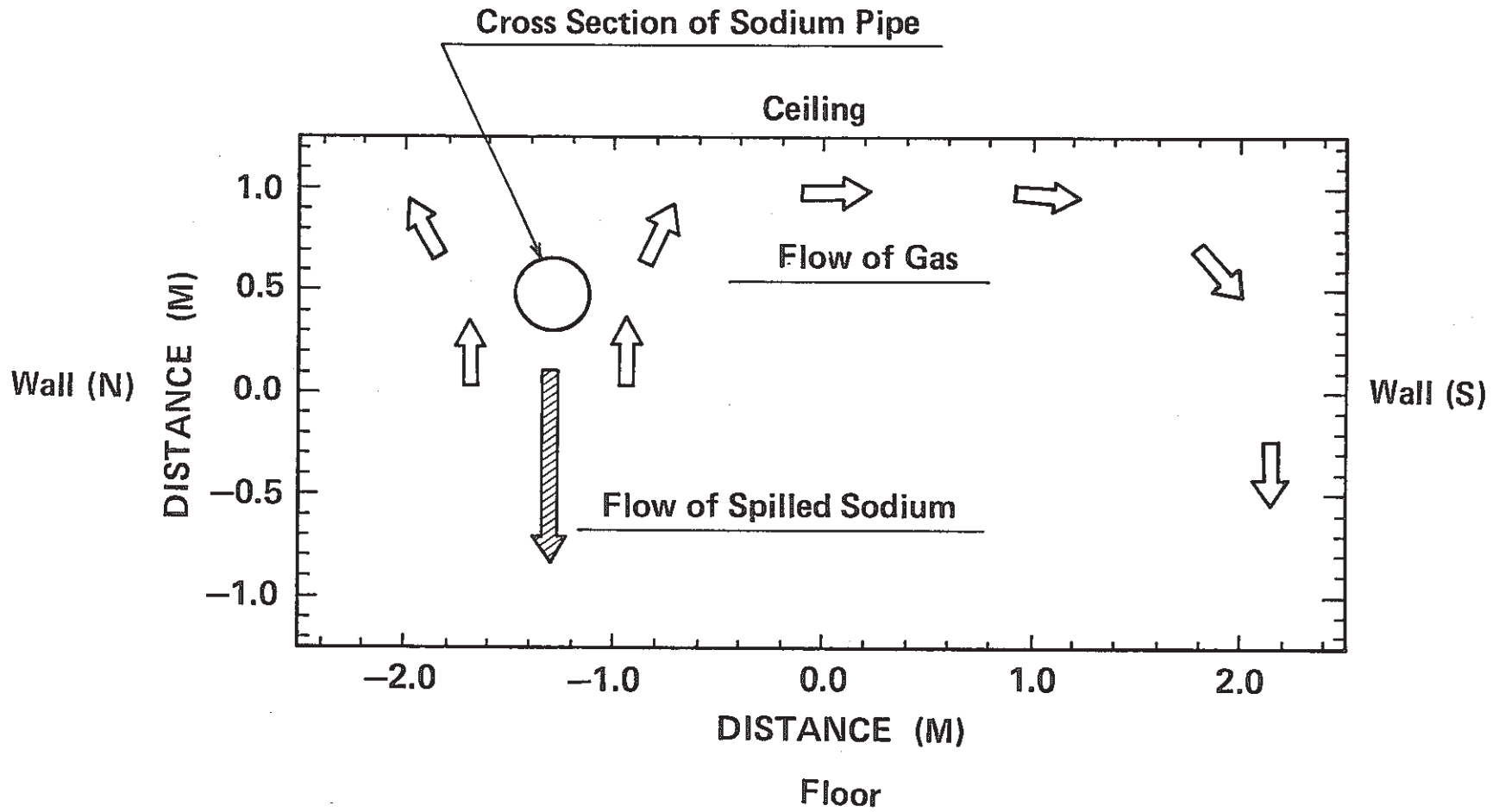


Fig.13 Flow Pattern of Gas and of Spilled Sodium in Vertical Cross Section of Upper Cell Atmosphere during Sodium Spill

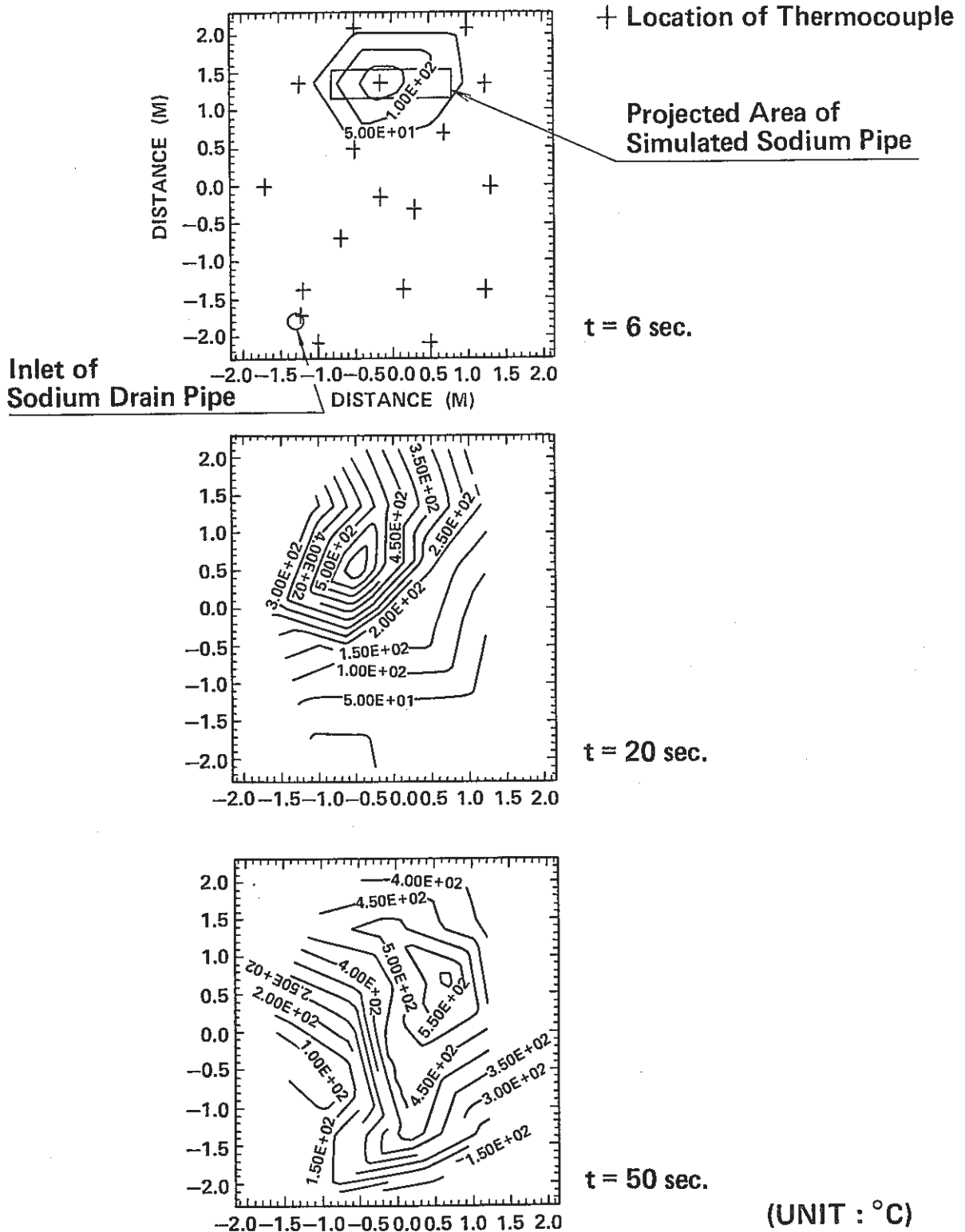


Fig.14 Temperature Distribution of Sodium on Floor Liner and Its Change during Sodium Spill (Top View)

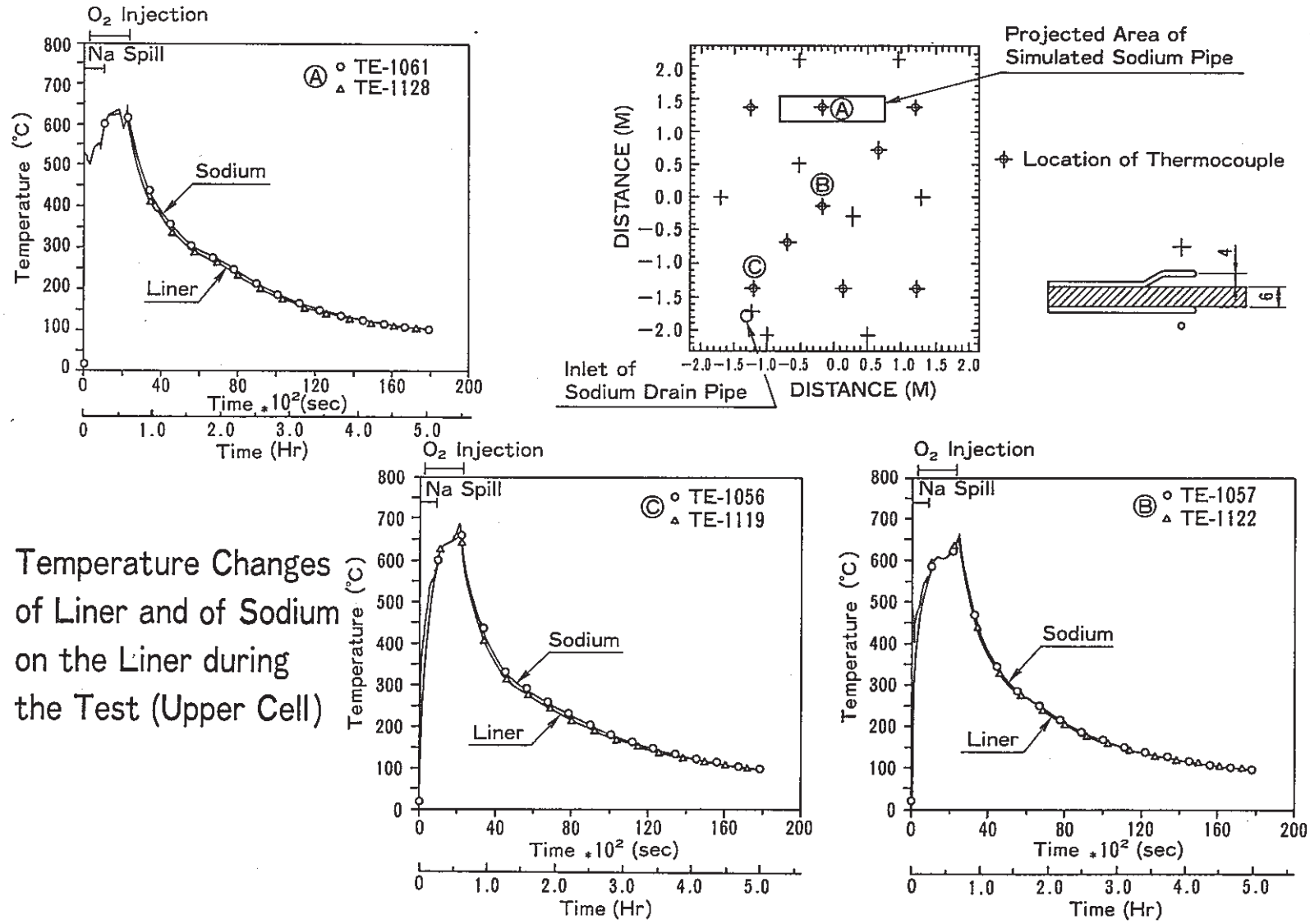


Fig.15 Temperature Changes of Liner and of Sodium on the Liner during the Test (Upper Cell)

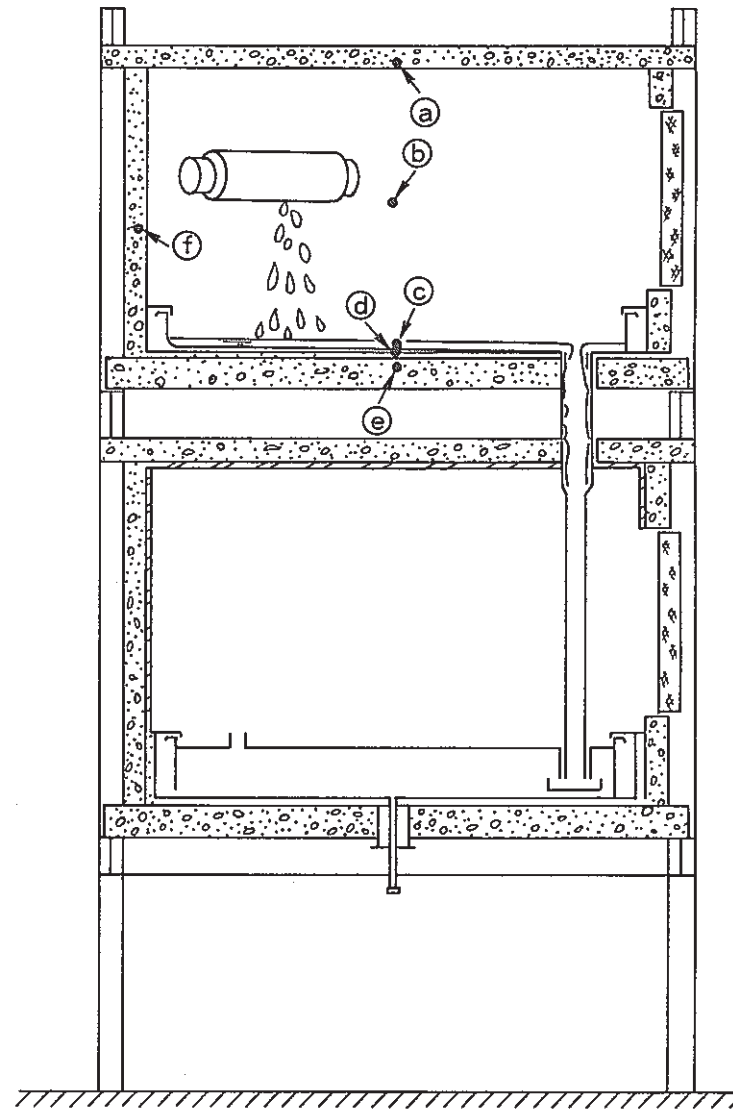
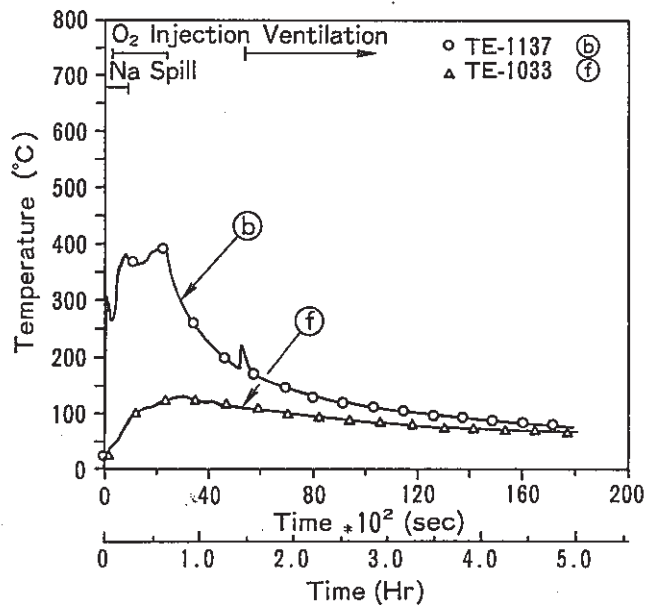
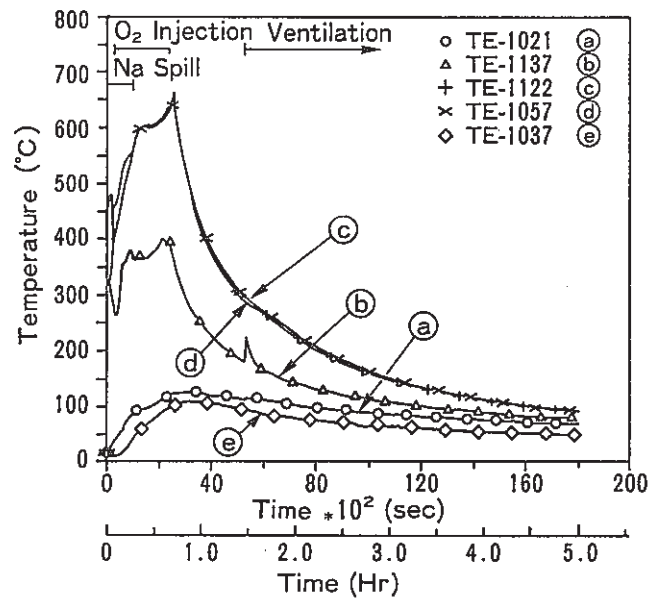


Fig.16 Temperature Distribution Change in the Upper Cell of SOLFA-1 during the Test
PSS-SFE-364

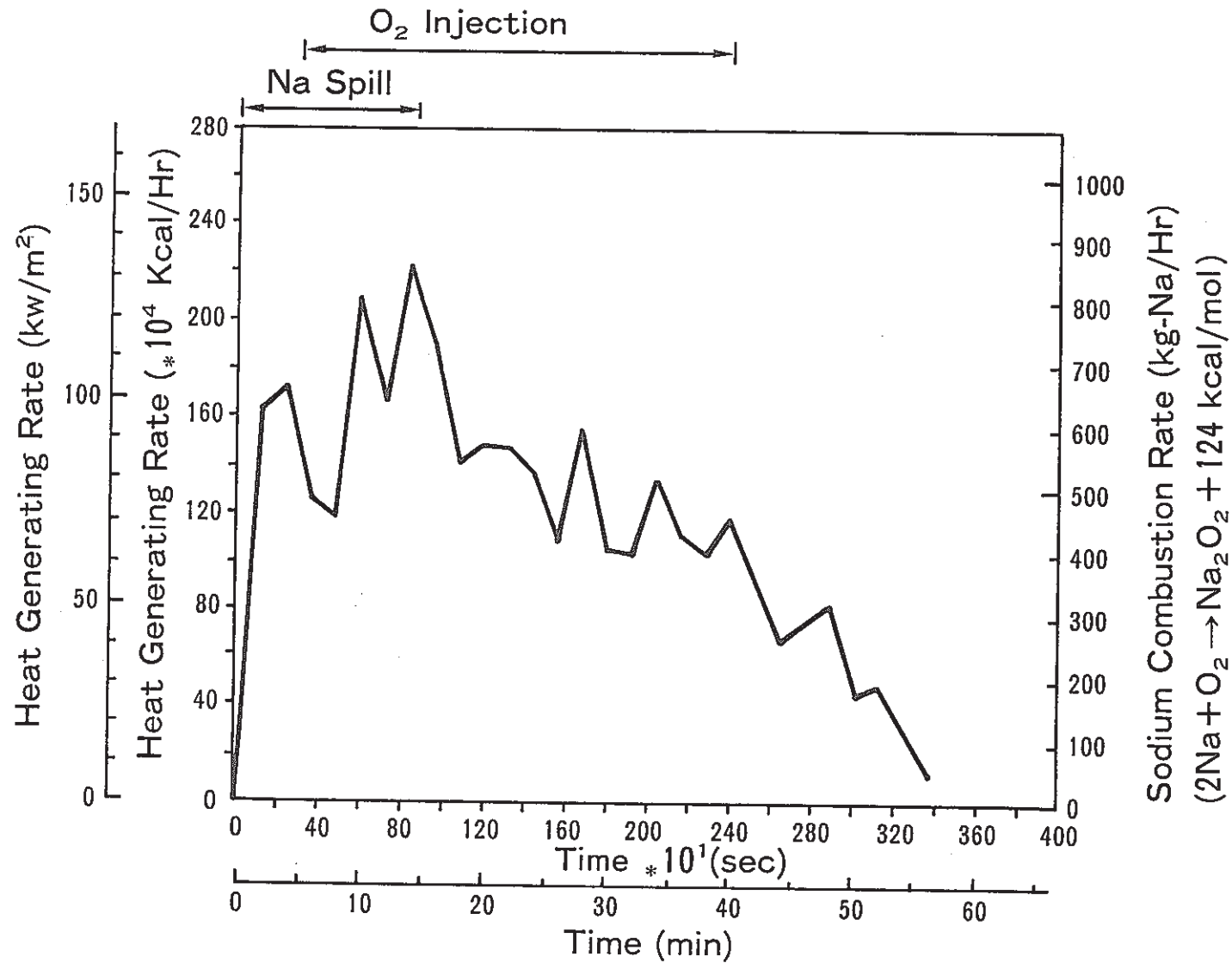


Fig.17 Heat Generating Rate and Sodium Combustion Rate during the Test (Upper Cell)

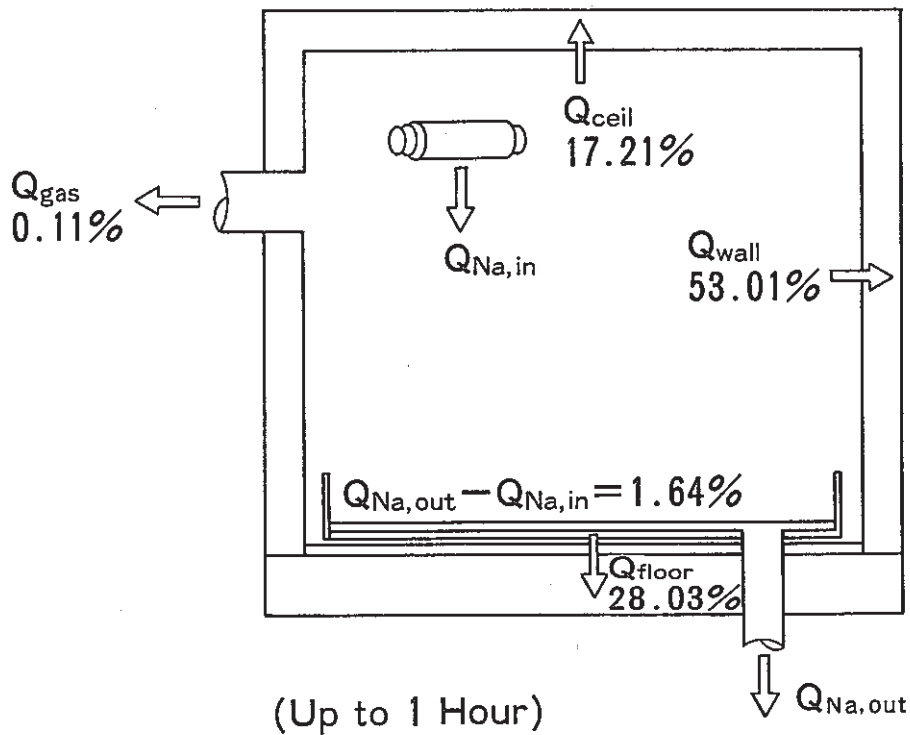
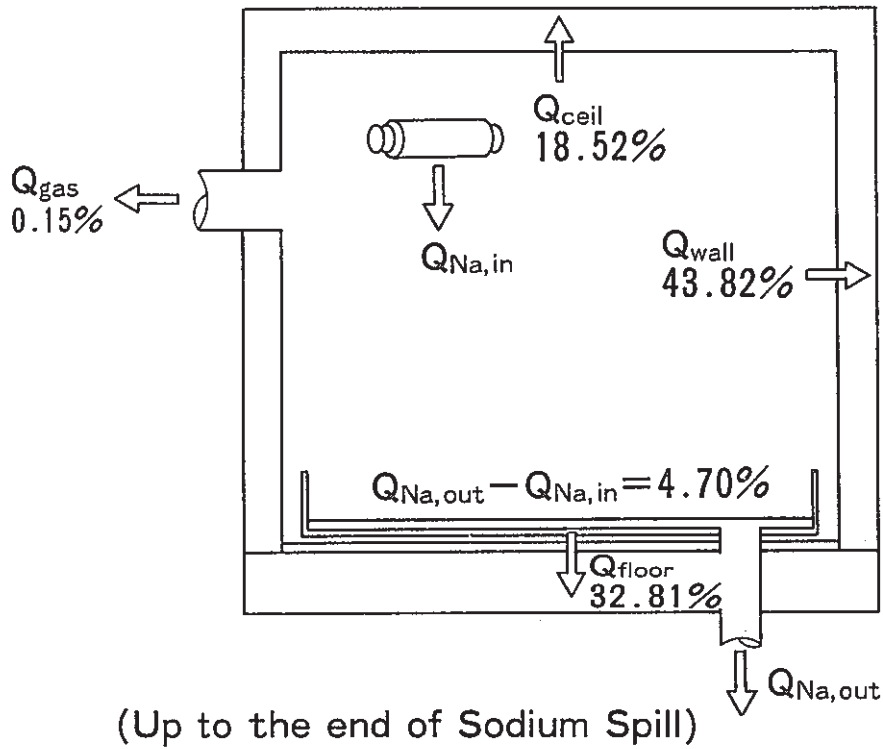


Fig.18 Distribution of Combustion Heat Transferred to the Various Portions of the Upper Cell

PSS-SFE-366

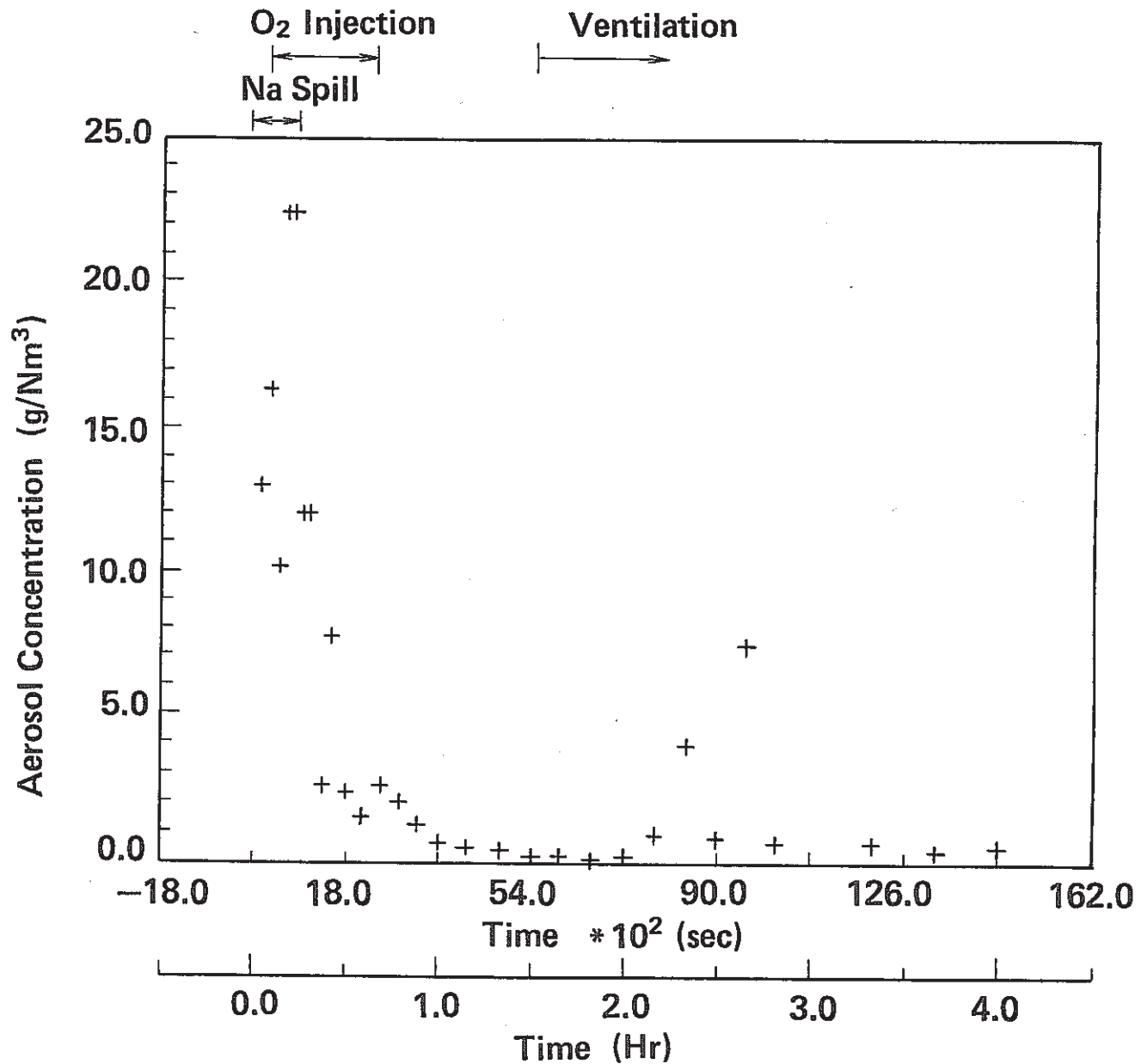


Fig. 19 Concentration Changes of Aerosol during the Test (Upper Cell)

PSS-SFE-529

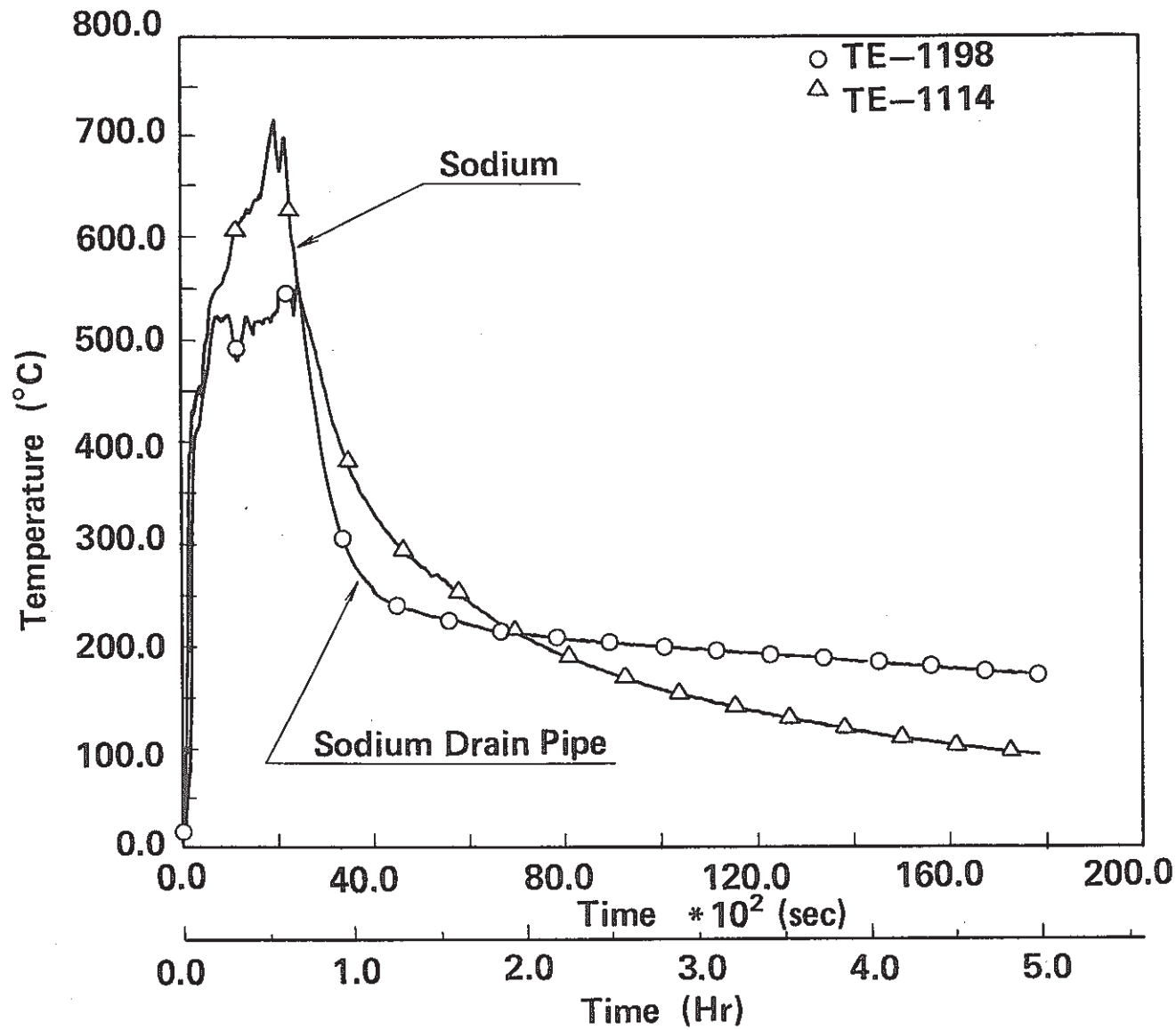


Fig.20 Temperature Changes of Sodium Drain Pipe and of Sodium at Inlet of the Pipe during the Test

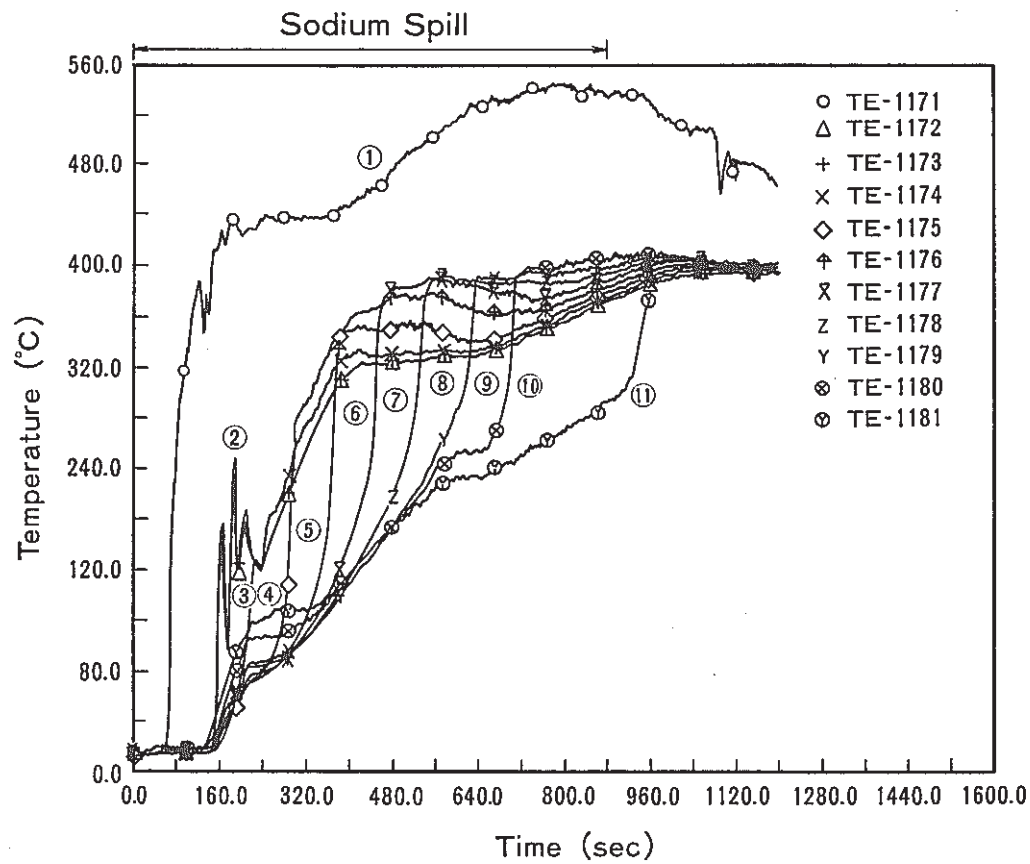
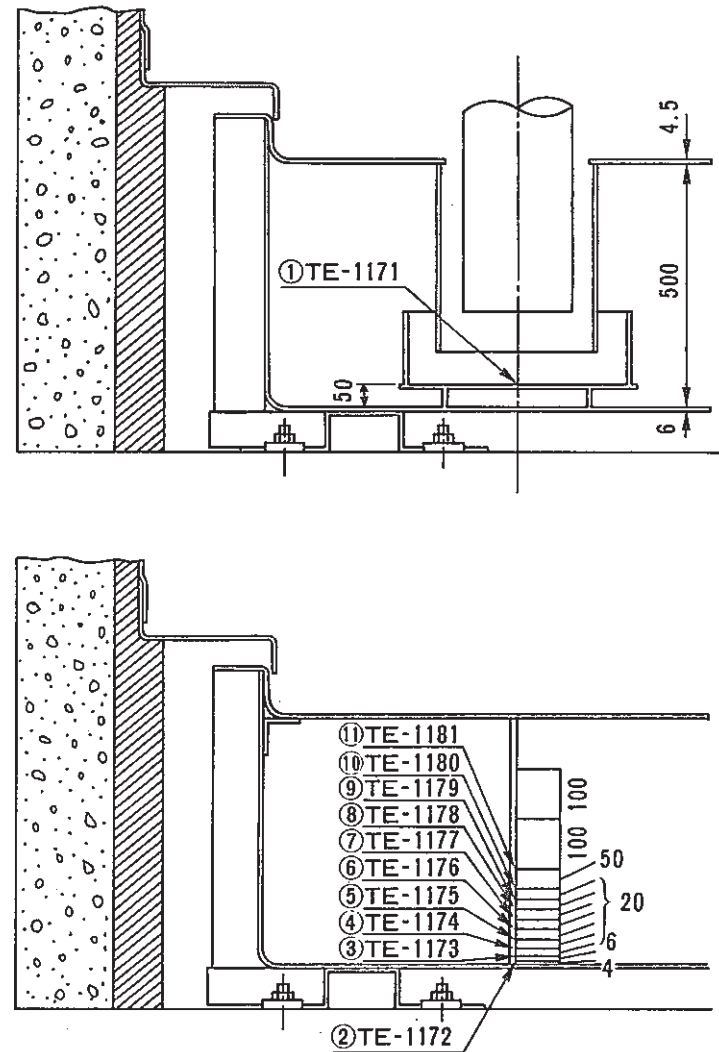


Fig.21 Temperature Change in Bucket and in Smothering Tank during Sodium Spill



PSS-SFE-369

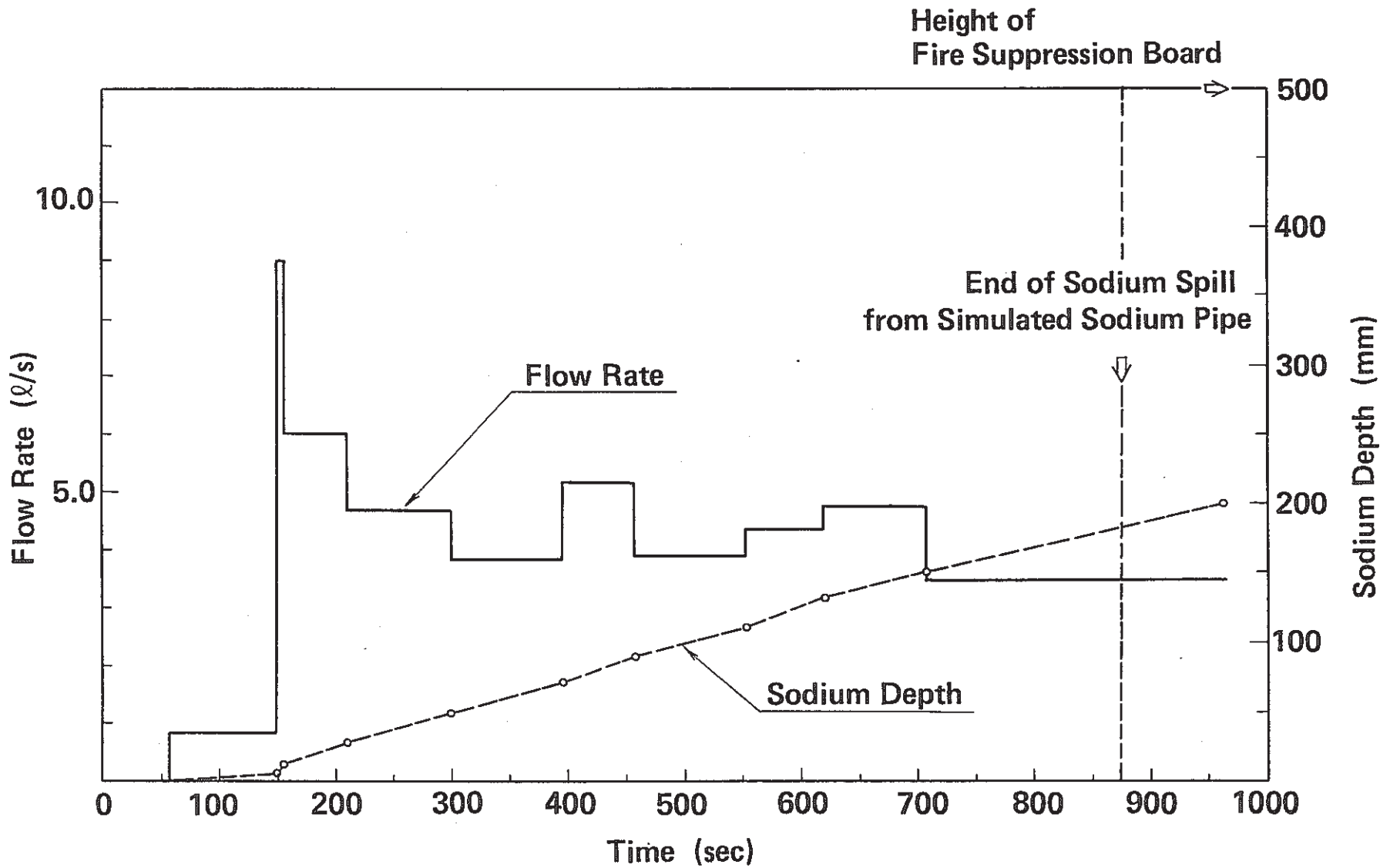


Fig.22 Flow Rate of Drain Sodium into Smothering Tank

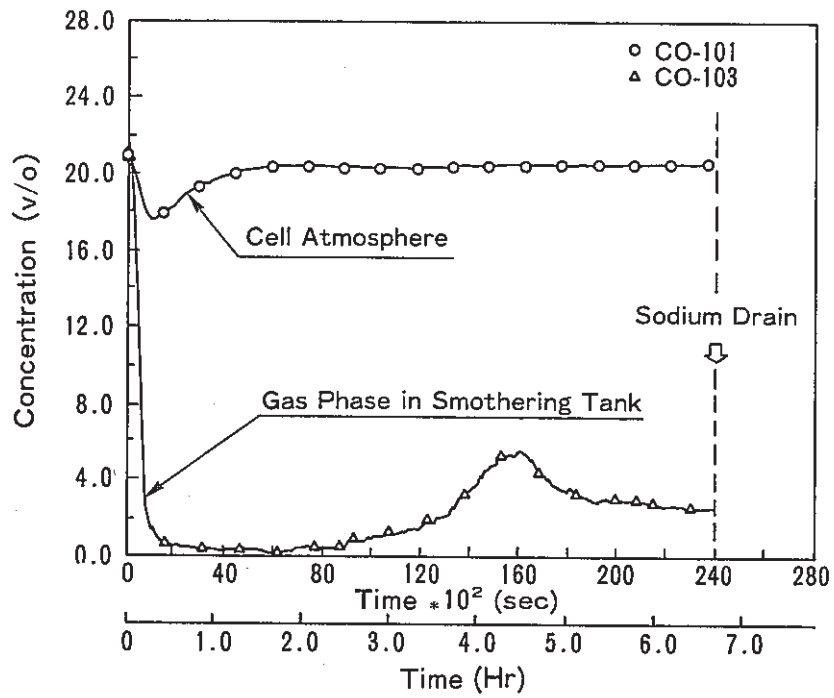


Fig.23 Oxygen Concentration Changes of Cell Atmosphere and of Gas Phase in Smothering Tank during the Test

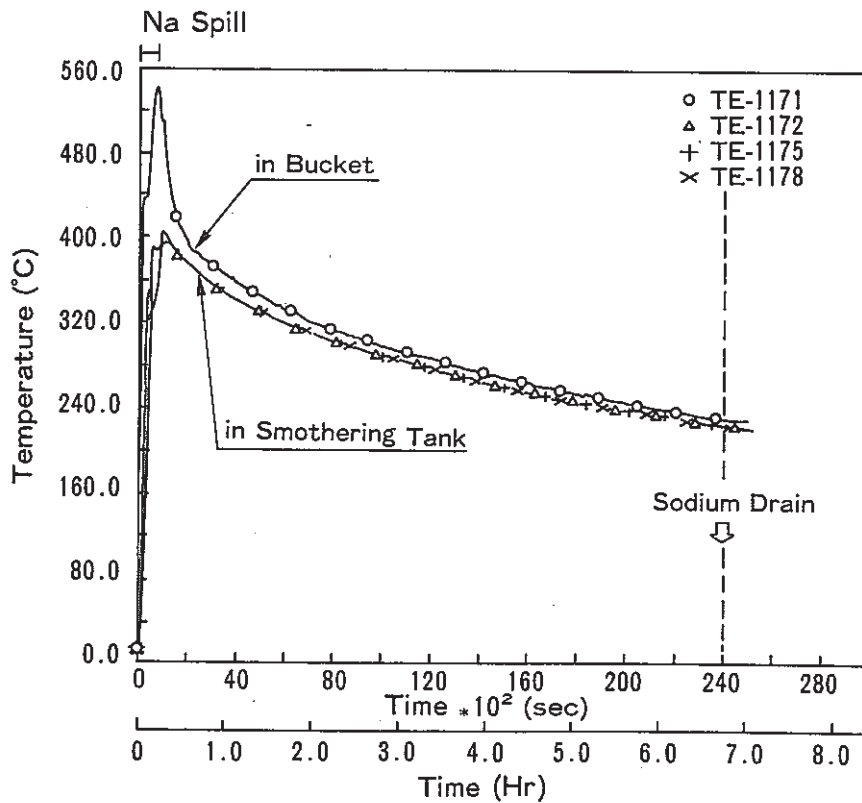


Fig.24 Temperature Changes of Sodium in Bucket and in Smothering Tank during the Test

PSS-SFE-371

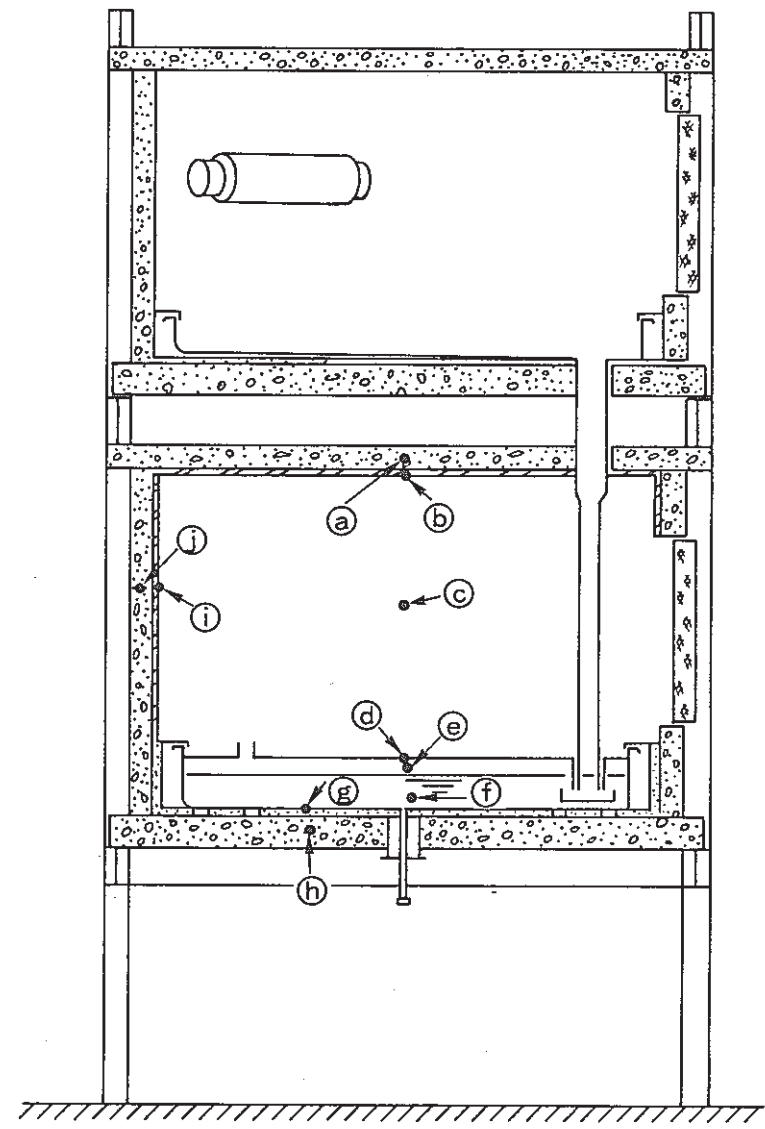
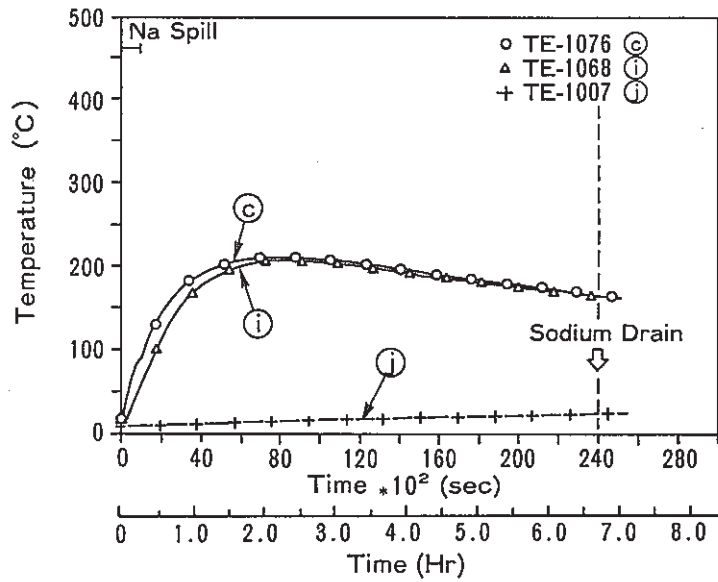
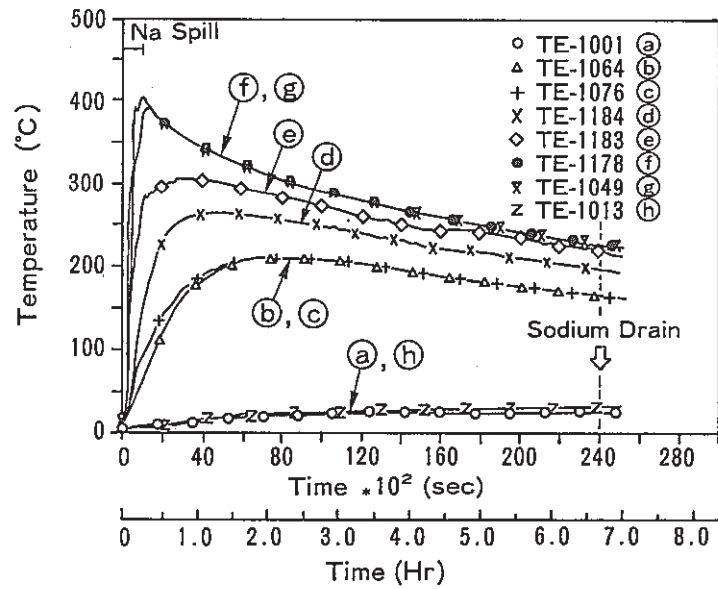


Fig.25 Temperature Distribution Change in the Lower Cell of SOLFA-1 during the Test PSS-SFE-372

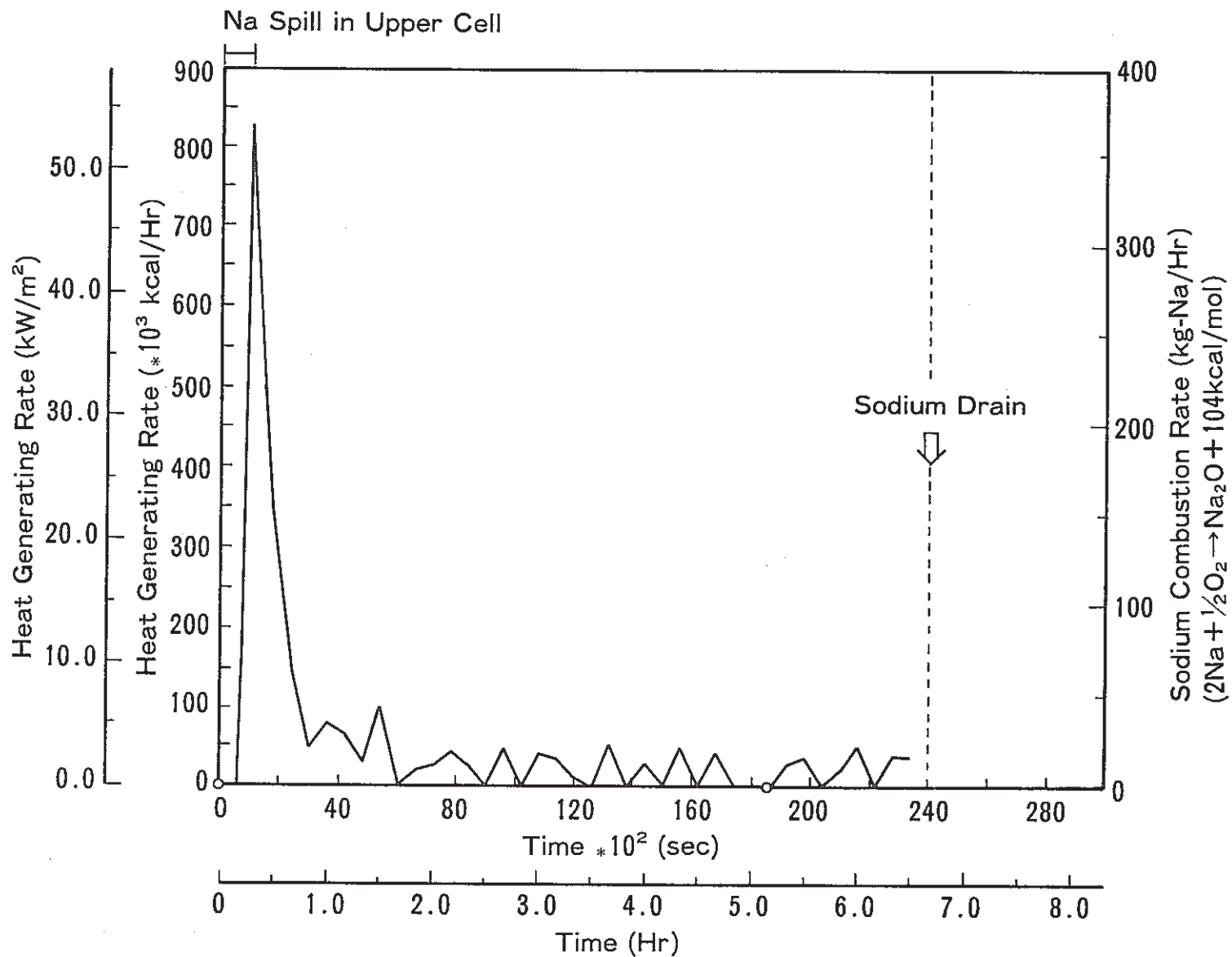


Fig.26 Heat Generating Rate and Sodium Combustion Rate in Smothering Tank during the Test (Lower Cell)

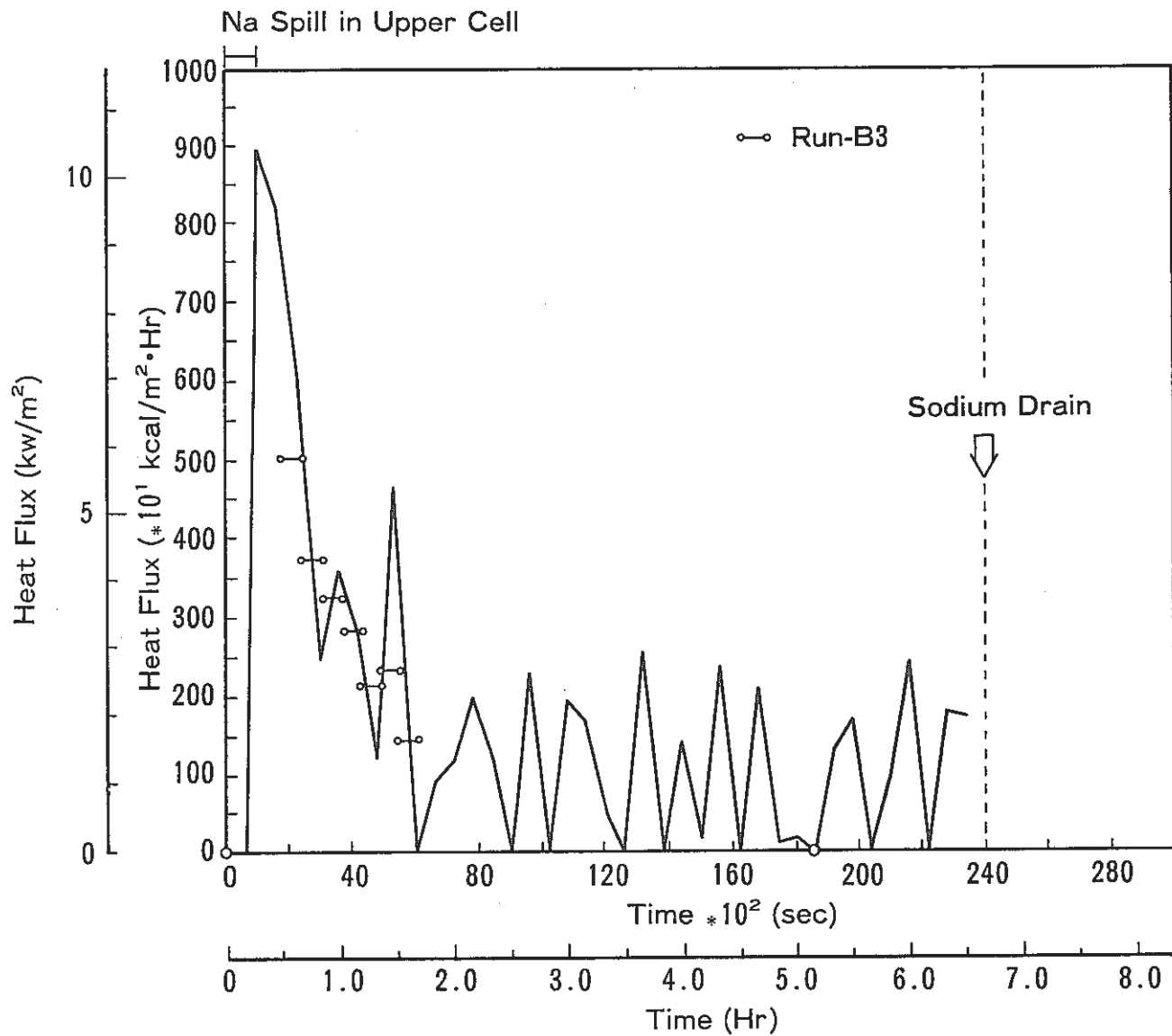


Fig.27 Heat Flux to Floor Concrete in Lower Cell during the Test

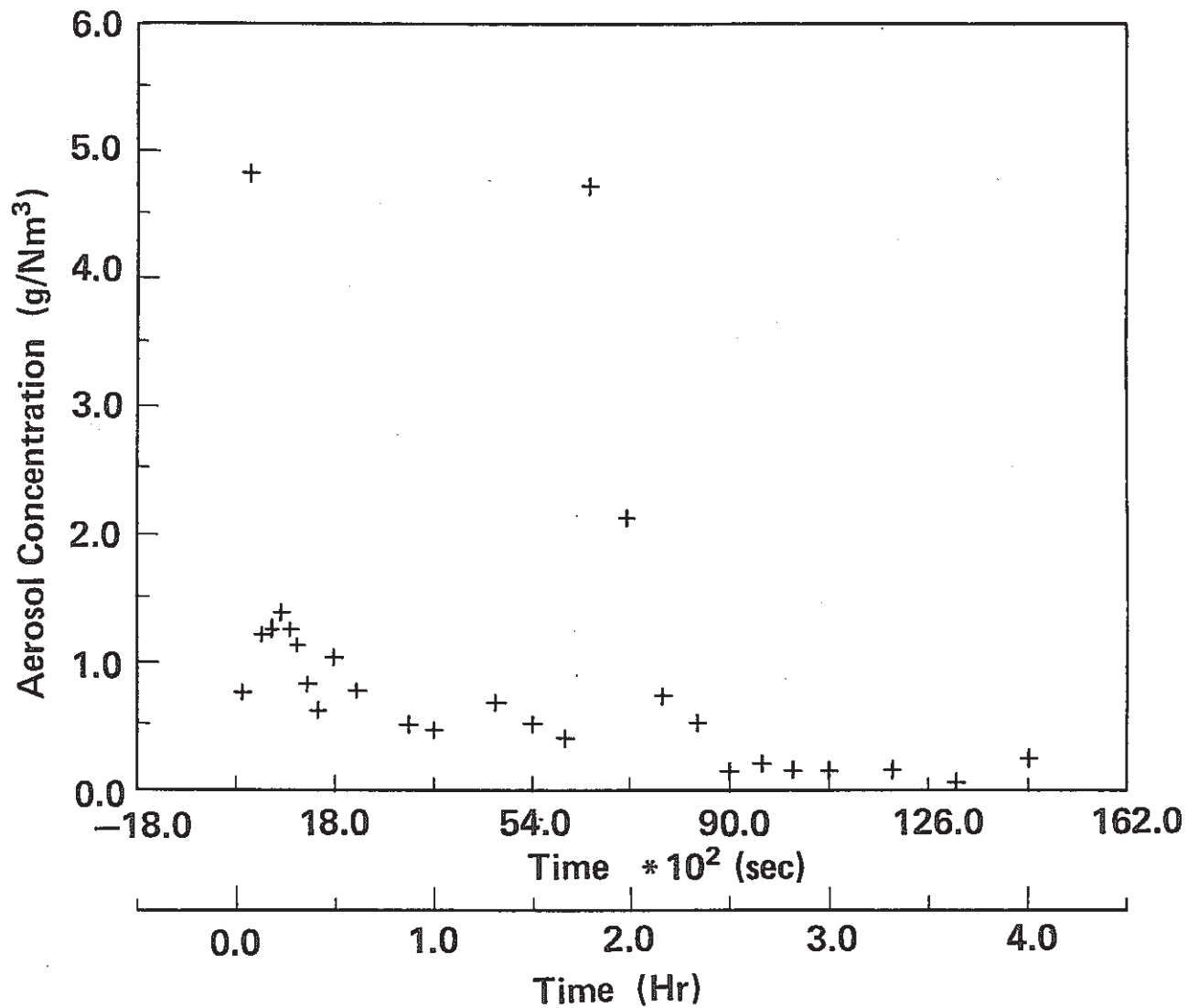


Fig. 28 Concentration Changes of Aerosol during the Test (Lower Cell)

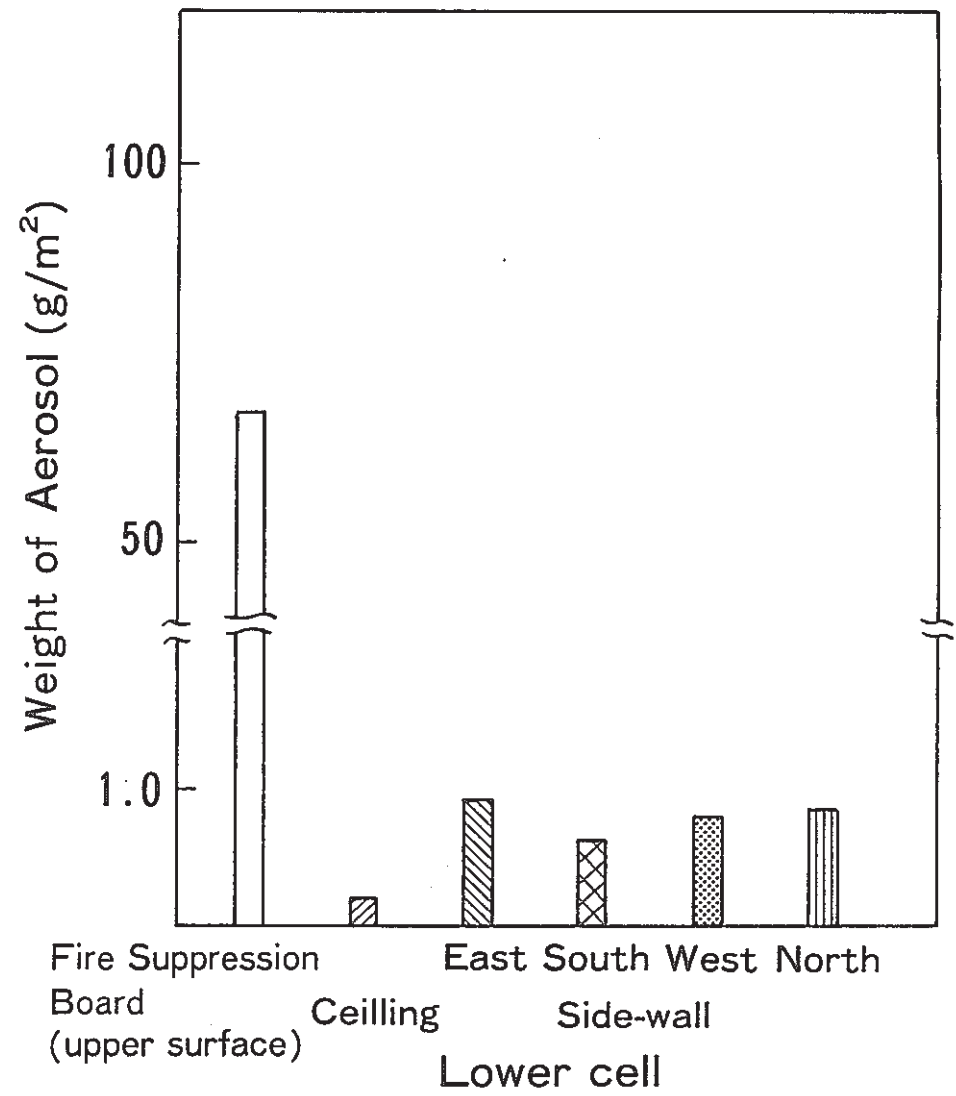
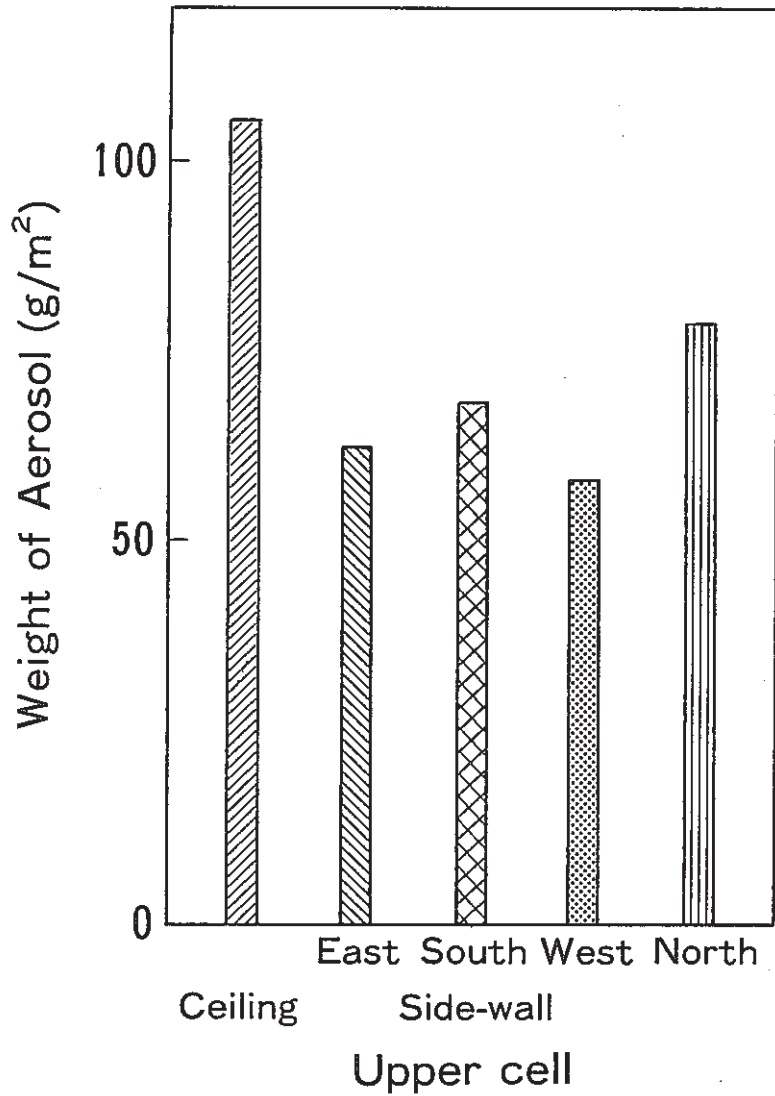


Fig.29 Amount of Aerosol in SOLFA-1 after the Test

- ⊙ Air Flow Meter
- ☒ Damper

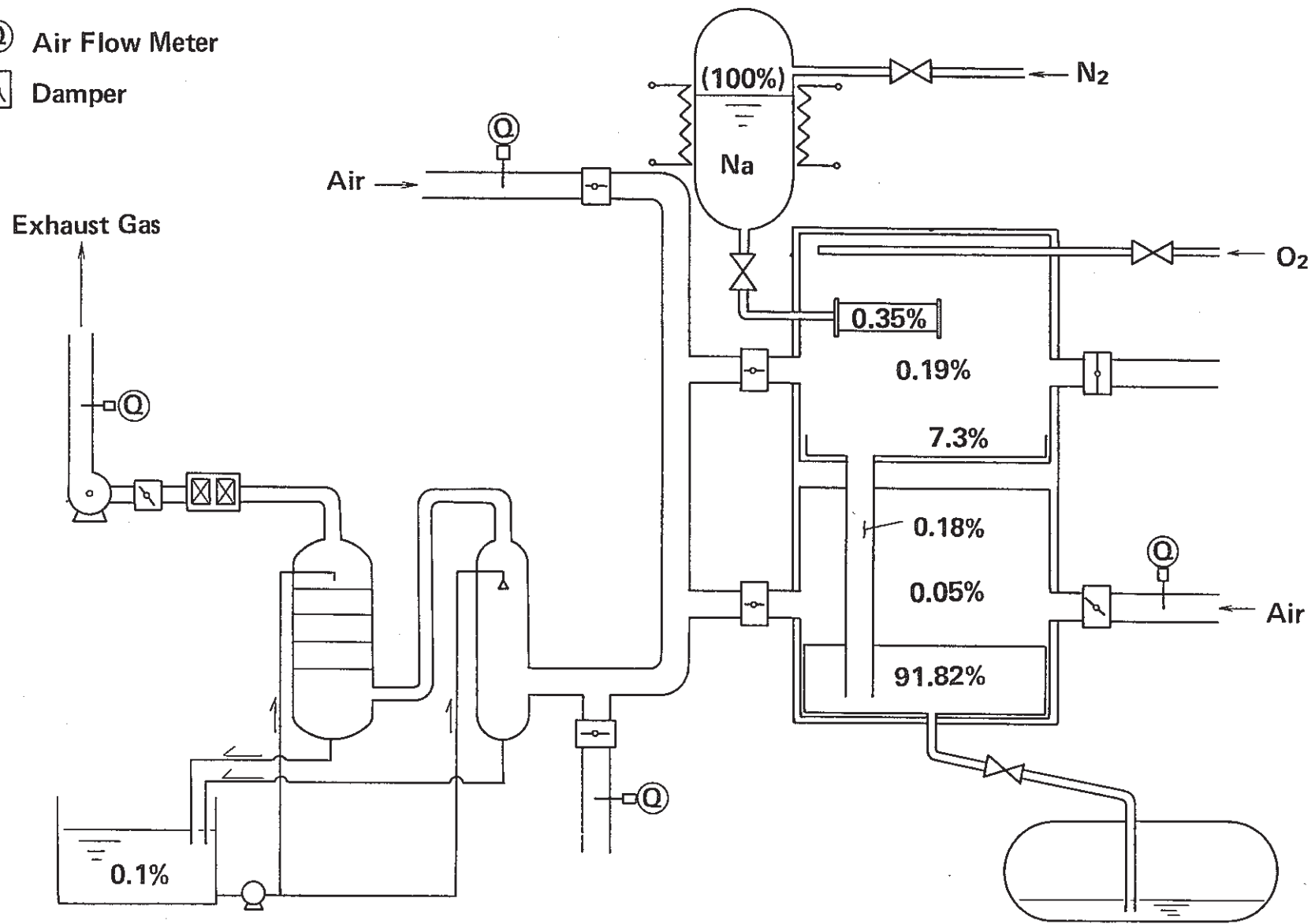


Fig.30 Post-Test Sodium Distribution in Test Rig

PSS-SFE-377

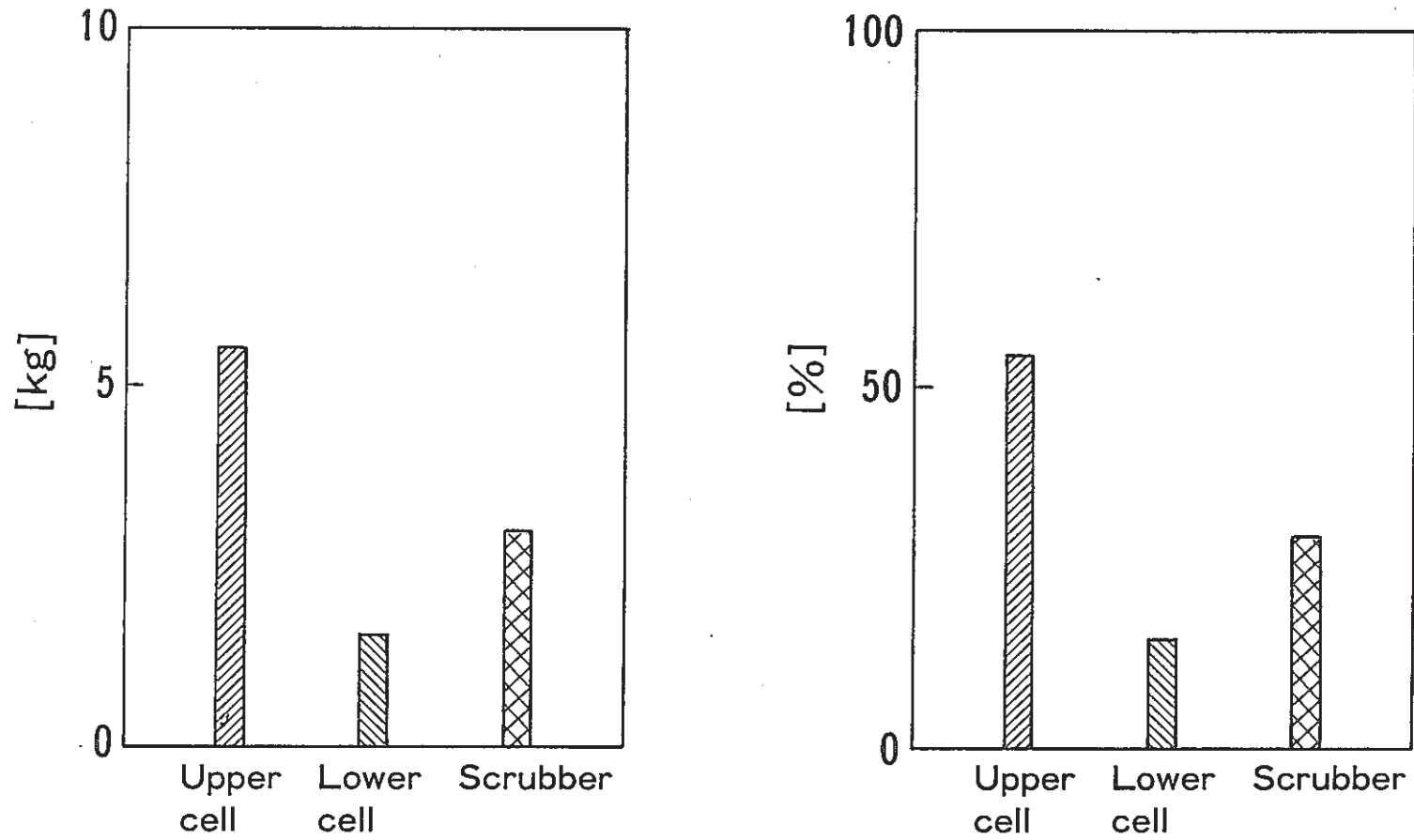


Fig.31 Post-Test Aerosol Distribution in Test Rig

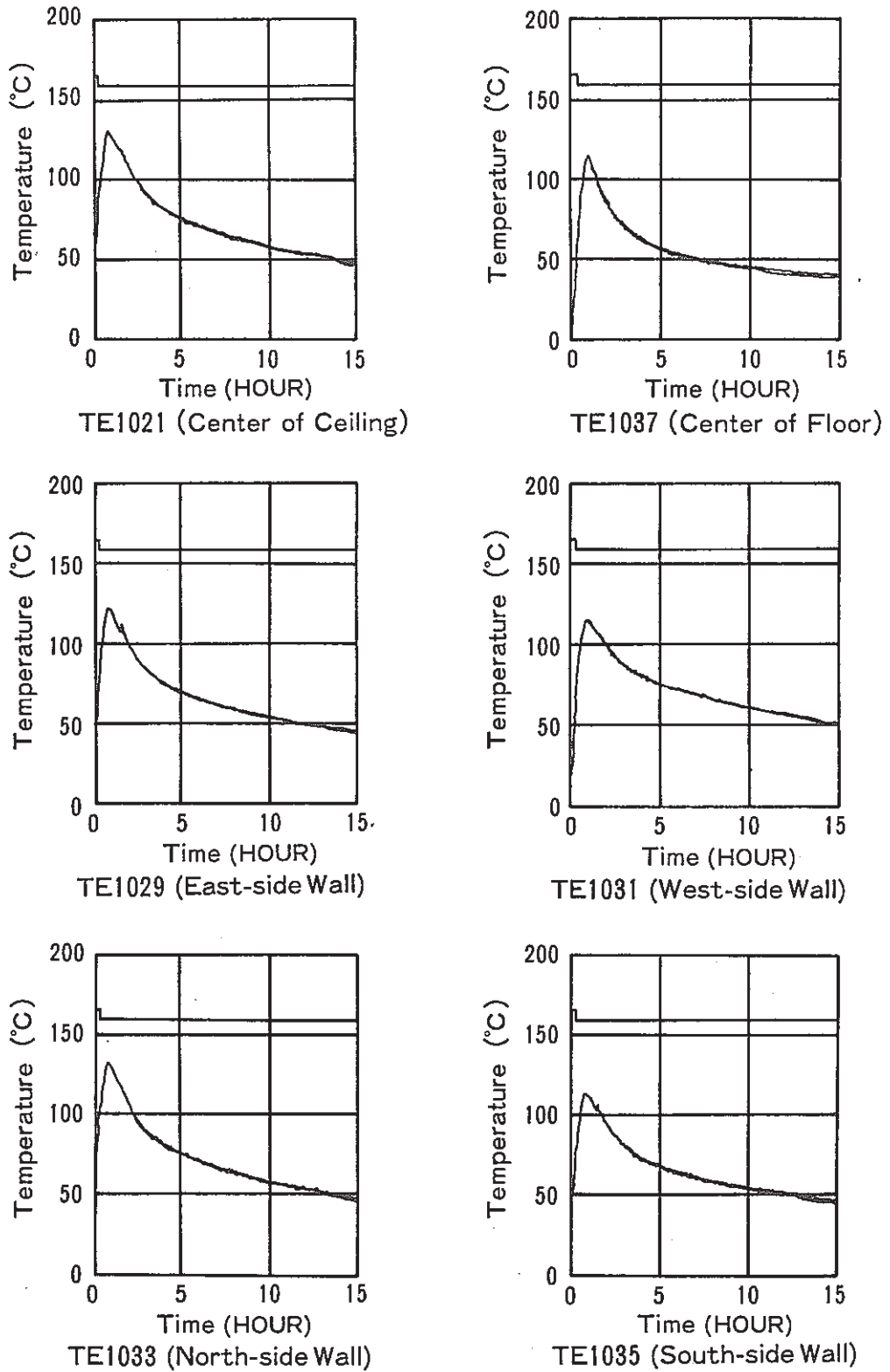


Fig.32 Temperature Changes of Upper Cell
Concrete during the Test
(At the point of 12mm from inner surface)

PSS-SFE-379

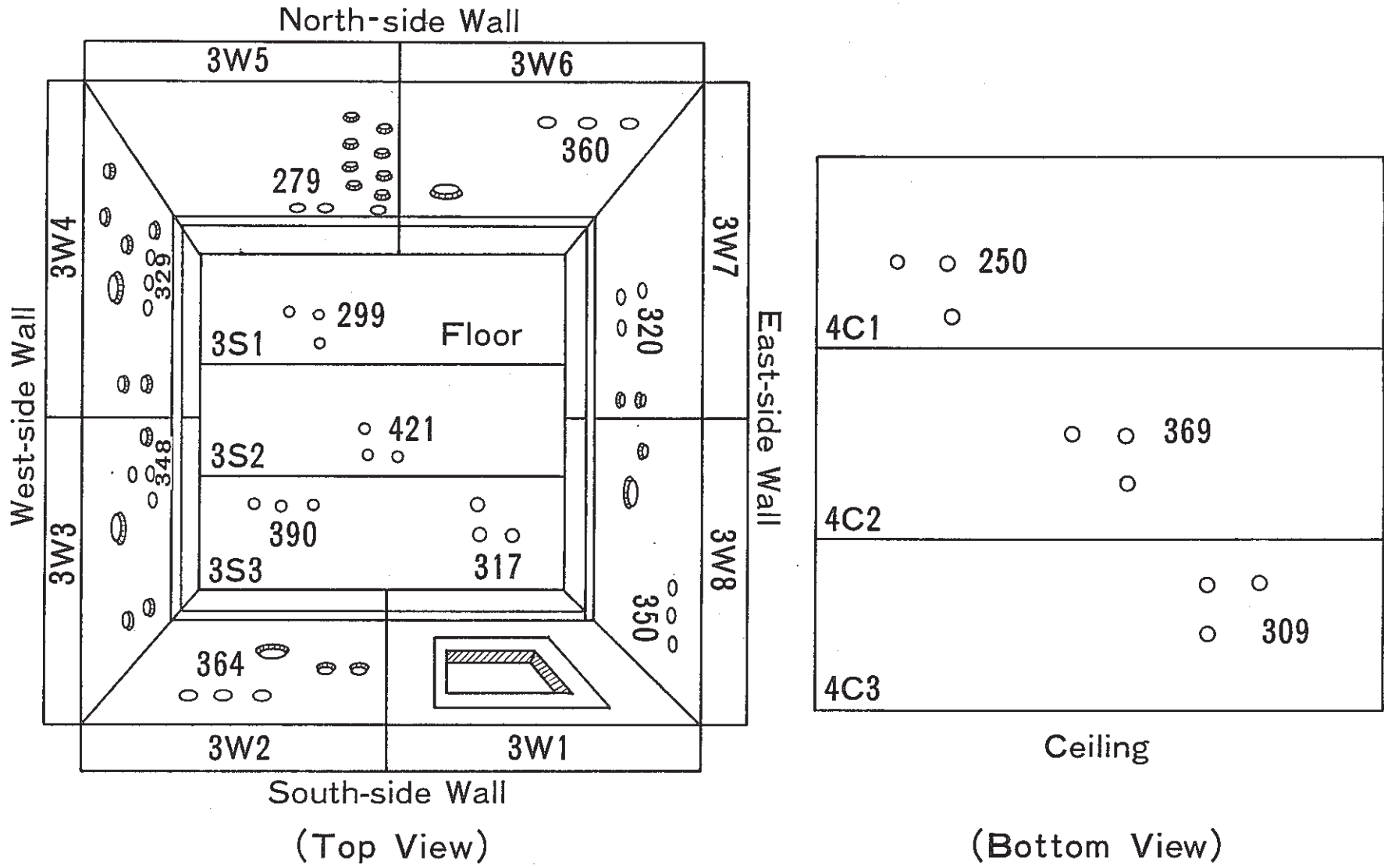


Fig.33 Compressive Strength of the Various Portions in Upper Cell Concrete after the Test

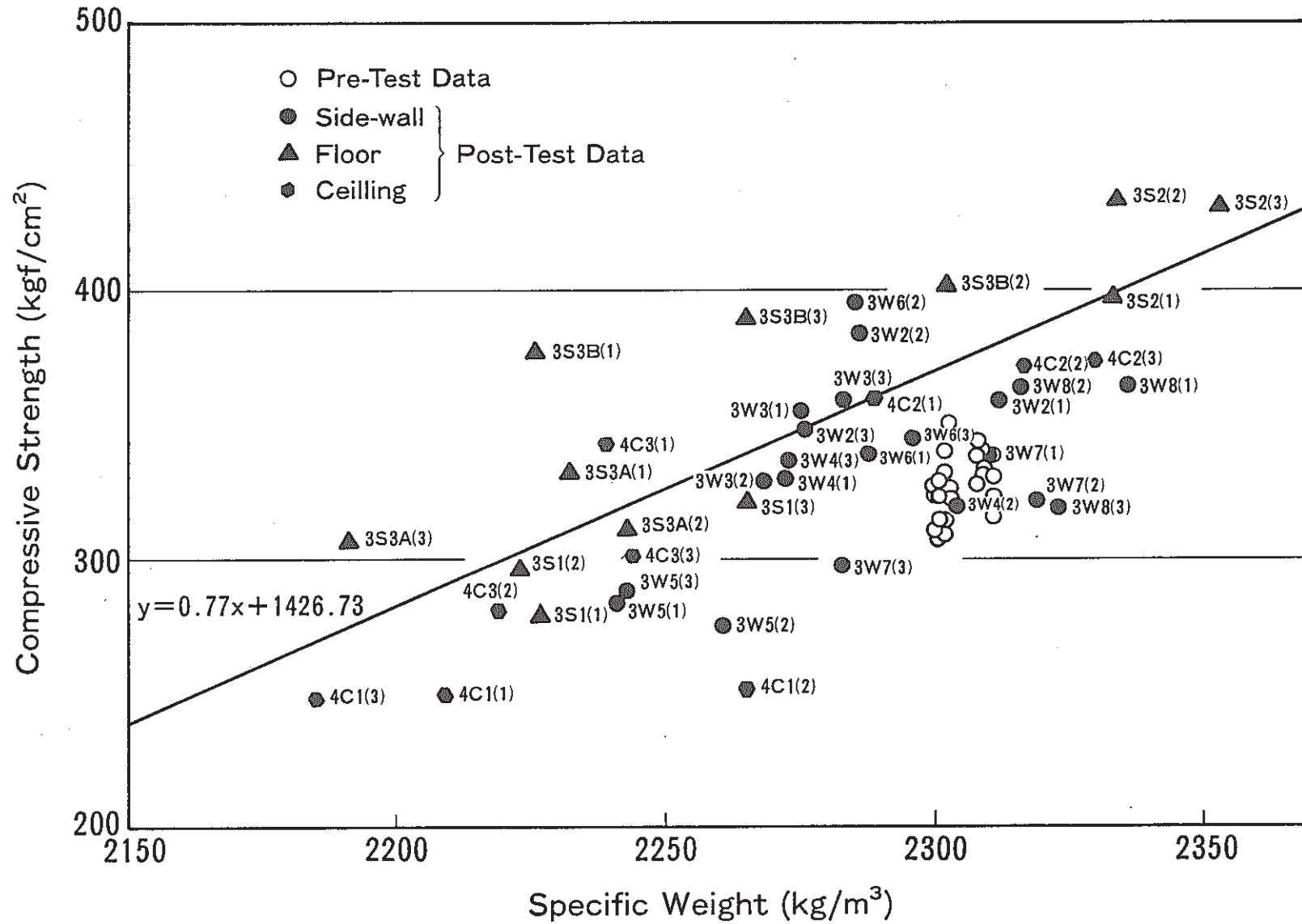


Fig.34 Relation between Specific Weight and Compressive Strength of Upper Cell Concrete

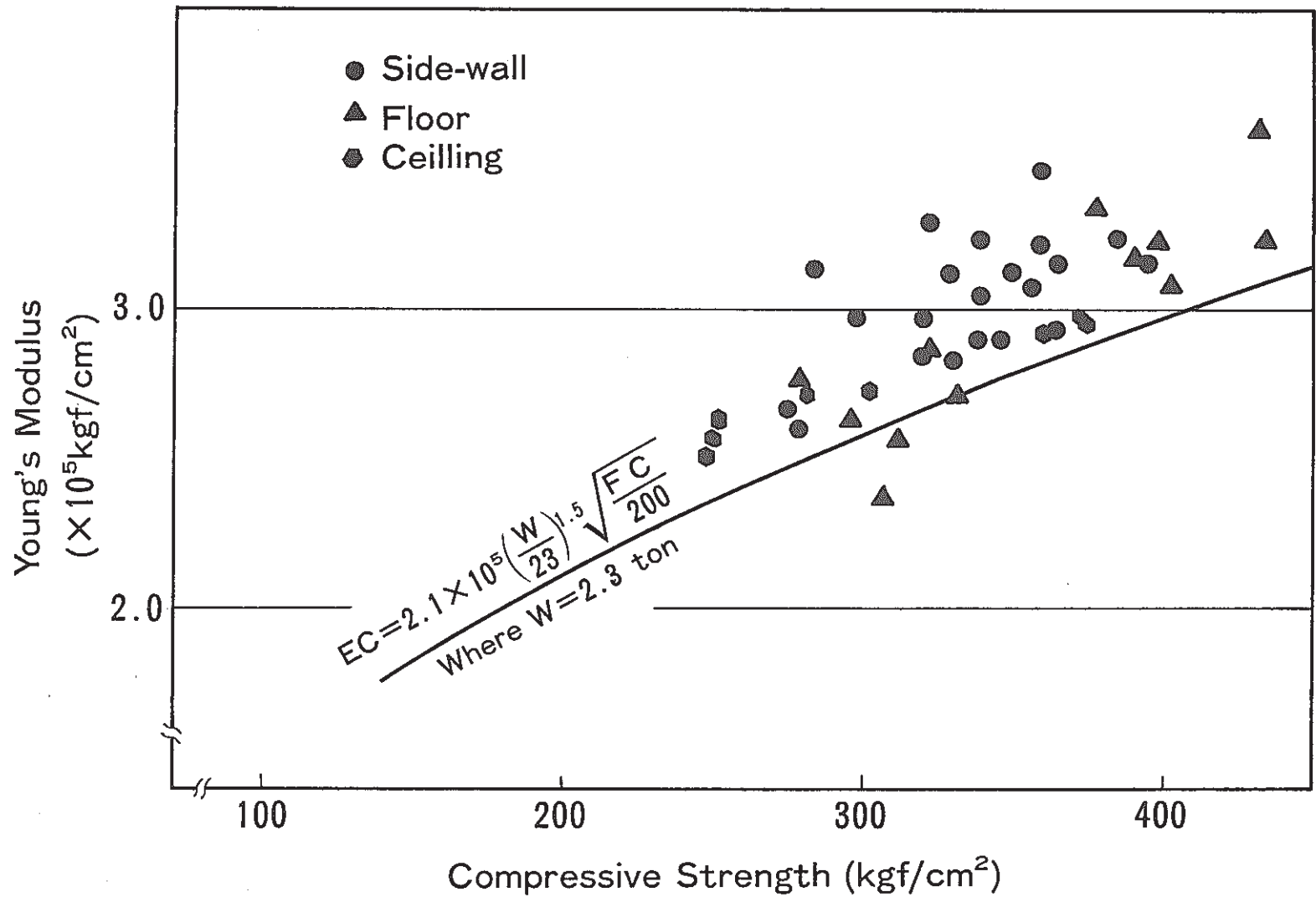


Fig.35 Relation between Compressive Strength and Young's Modulus of Upper Cell Concrete

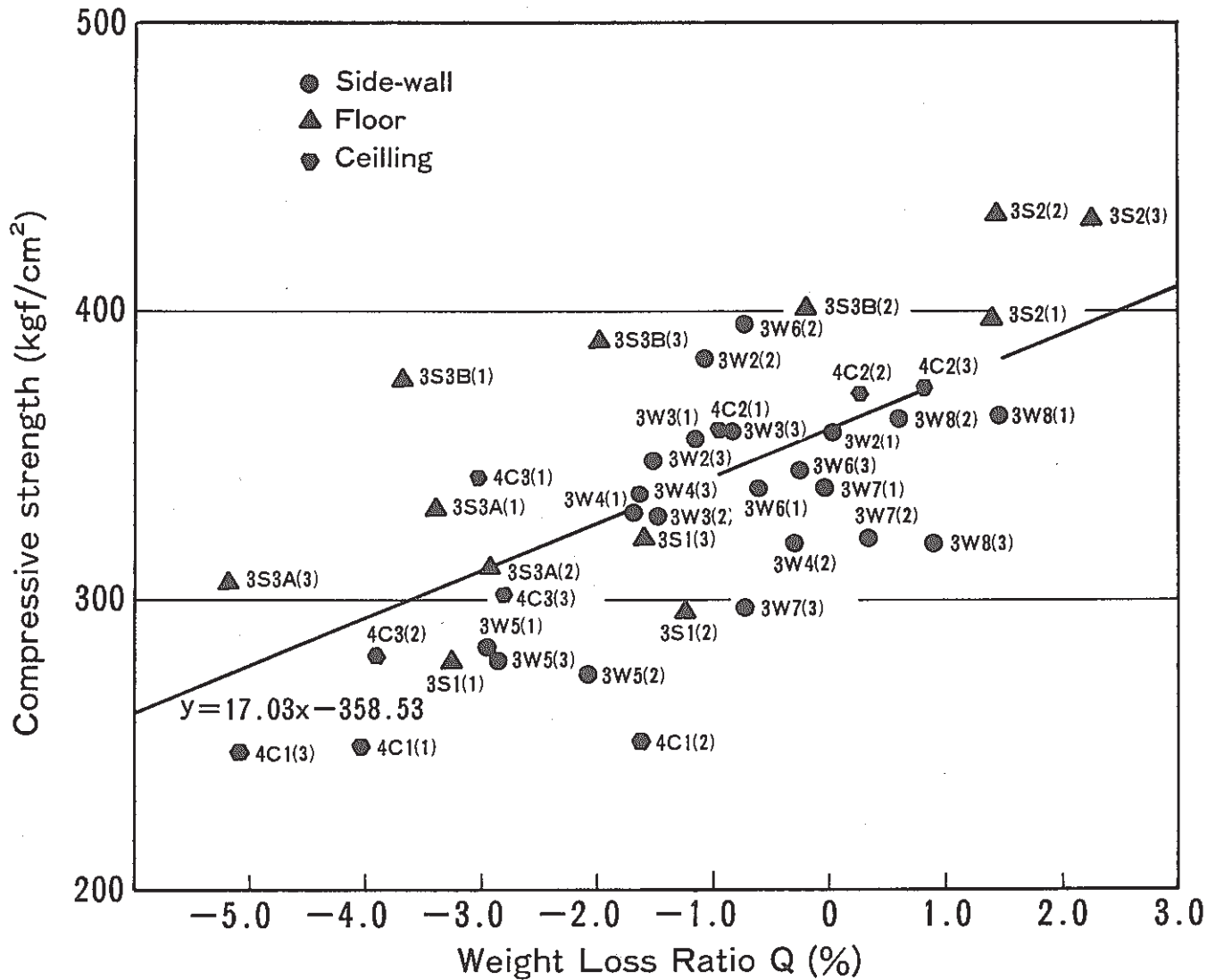


Fig.36 Relation between Weight Loss and Compressive Strength of Upper Cell Concrete

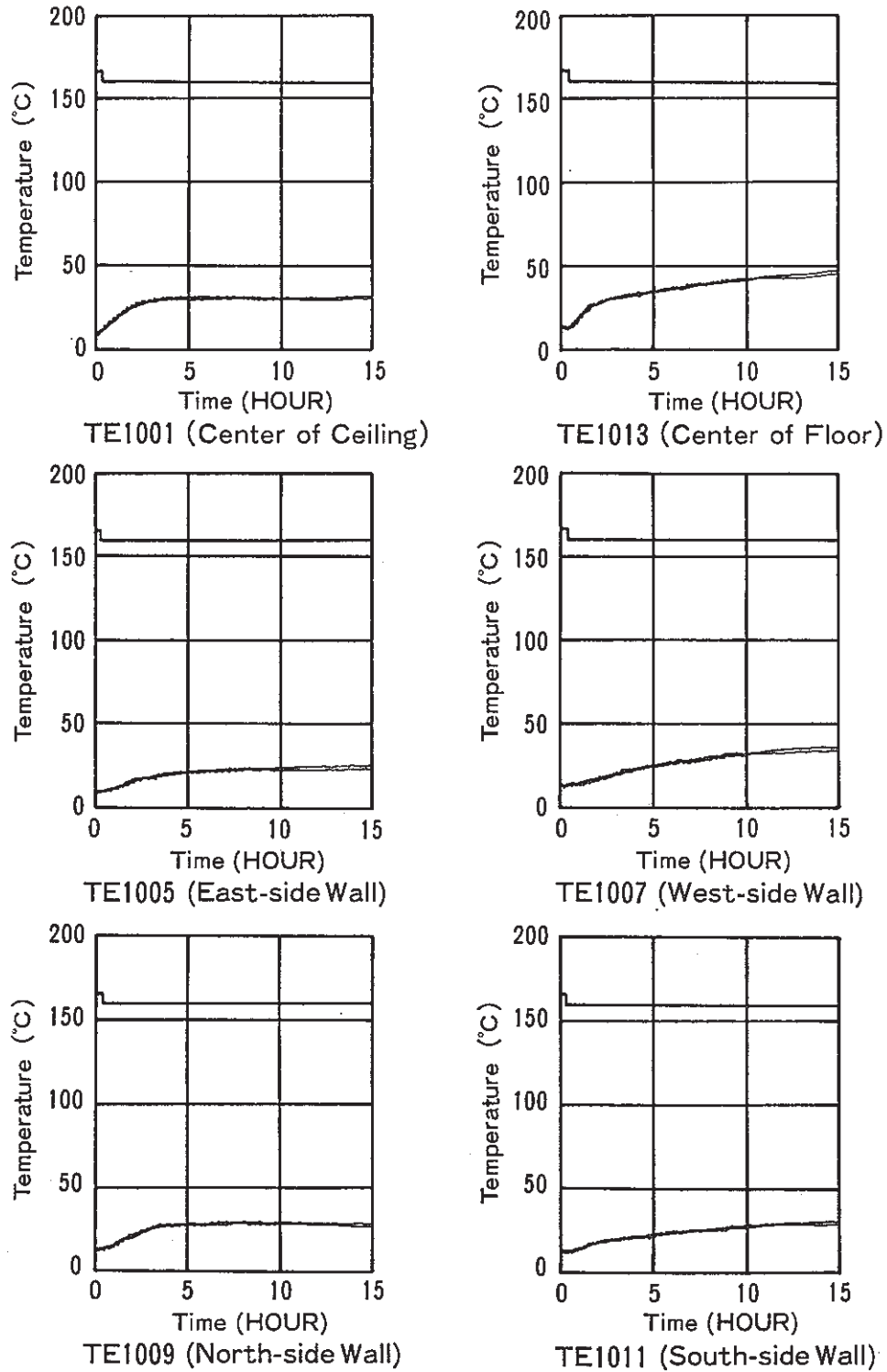


Fig.37 Temperature Changes of Lower Cell Concrete during the Test
(At the point of 12mm from inner surface)

PSS-SFE-384

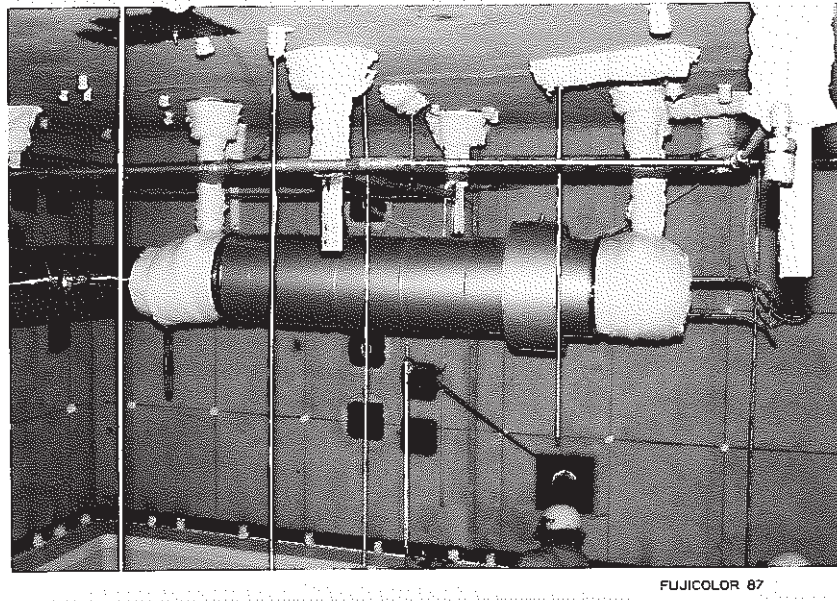


Photo. 1 : Simulated Sodium Pipe installed in the Upper Cell of SOLFA-1 (Pre-Test)

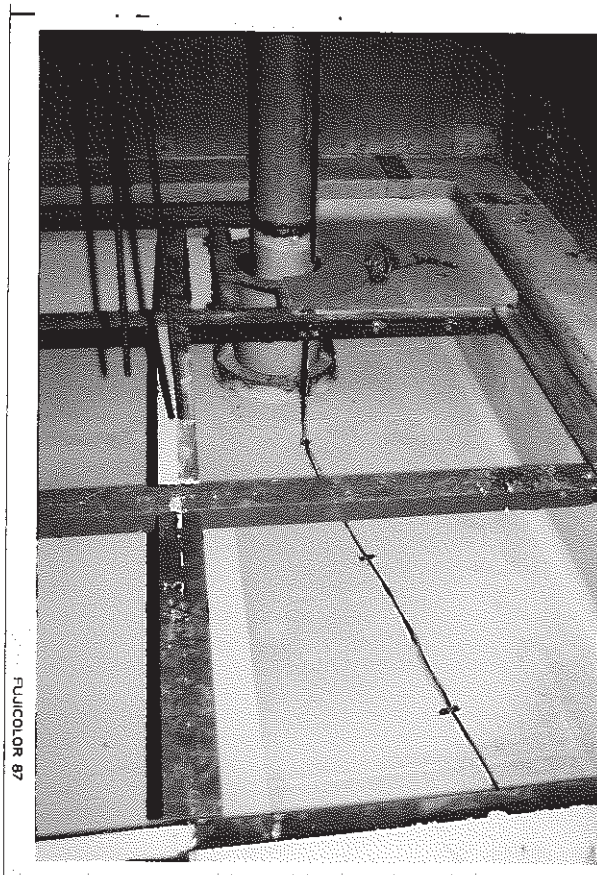


Photo. 2 : Arrangement of Drain Pipe and Smothering Tank

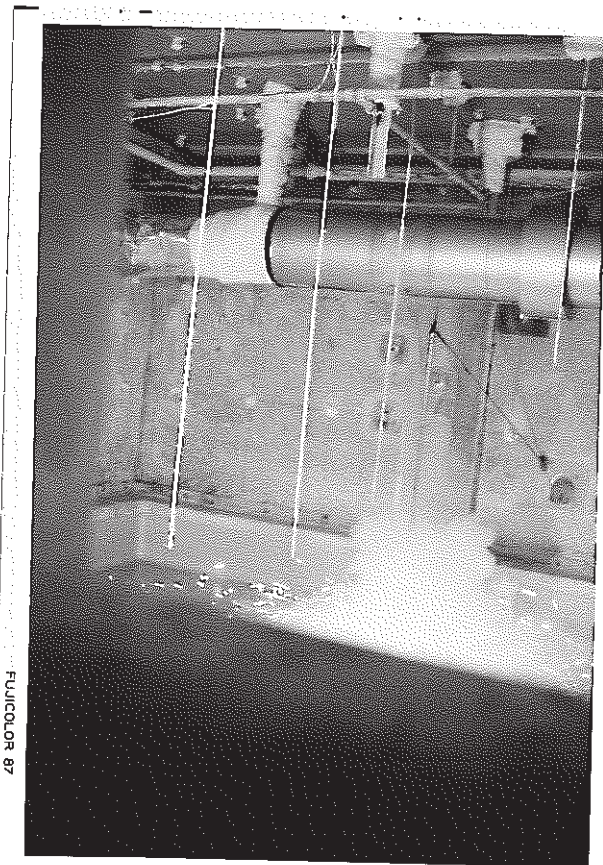


Photo. 3 : Sodium Leak at the
Beginning of the Test

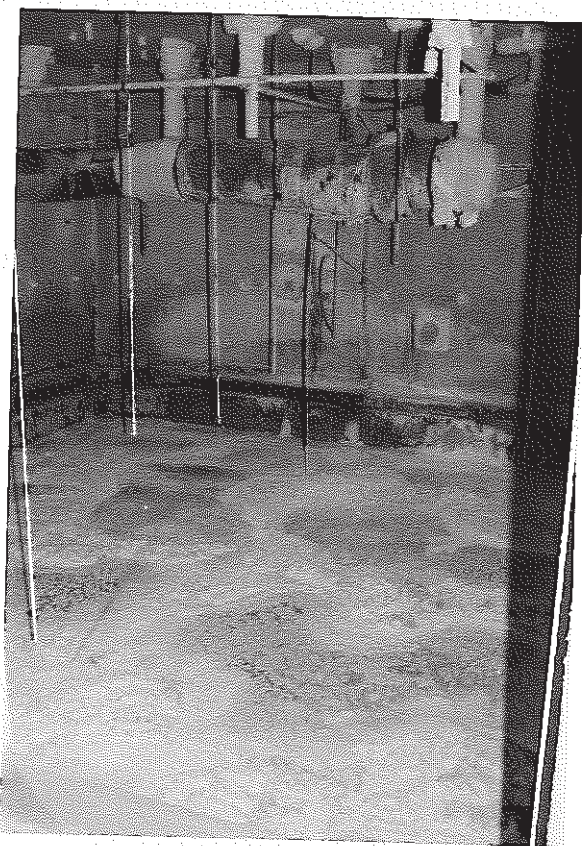


Photo. 4 : Post-Test View of
the Upper Cell of SOLFA 1



Photo. 5 : Post-Test View of Inlet of Drain Pipe



FUJICOLOR 87

Photo. 6 : Post-Test View of Sodium and Its
Reaction Products in Smothering Tank
(A part of fire suppression board is removed
for Visual Inspection)



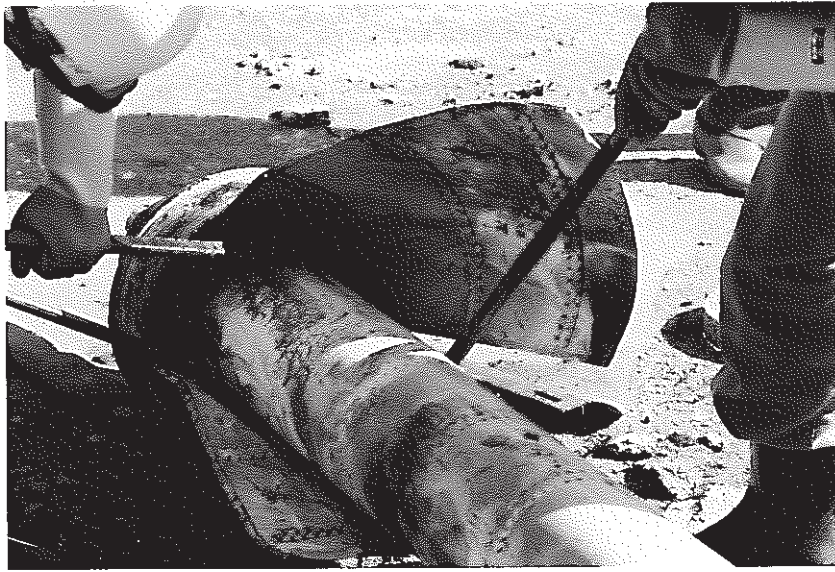
FUJICOLOR 87

Photo. 7 : Post-Test View of wall Concrete
Surface in Upper Cell



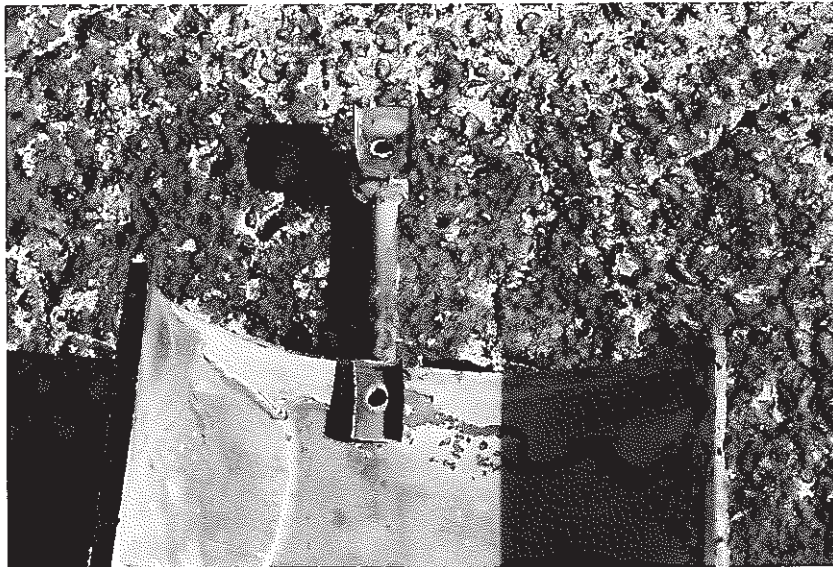
FUJICOLOR 87

Photo. 8 : Post-Test View of Simulated Sodium Pipe



FUJICOLOR 87

Photo. 9 : Disassembling of Simulated Sodium Pipe
after the Test



FUJICOLOR 87

Photo. 10 : Post-Test View of Connecting
Pipe in Simulated Sodium Pipe

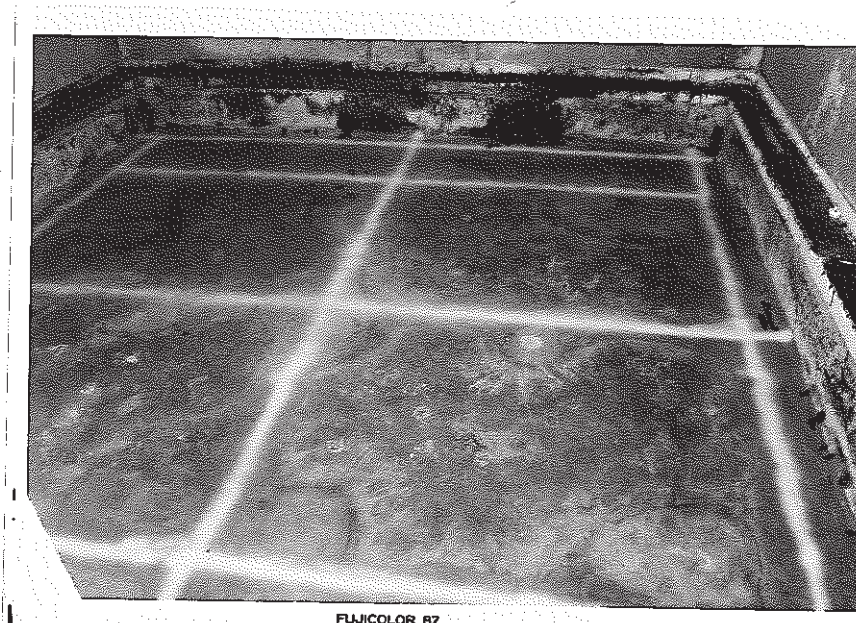


Photo. 1 1 : Non-desructive Inspection of Weld Line
of Liner in Upper Cell after the Test

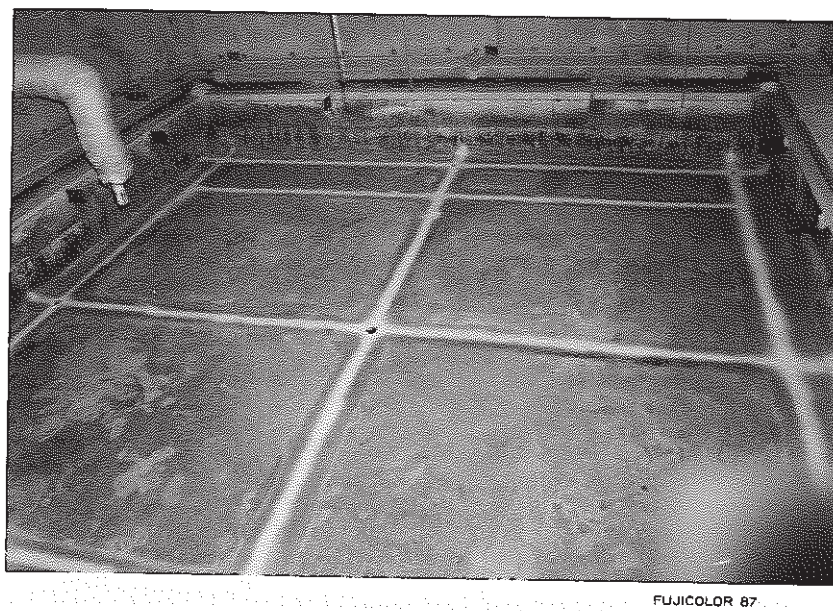


Photo. 1 2 : Non-desructive Inspection of Weld Line
of Liner in Lower Cell after the Test

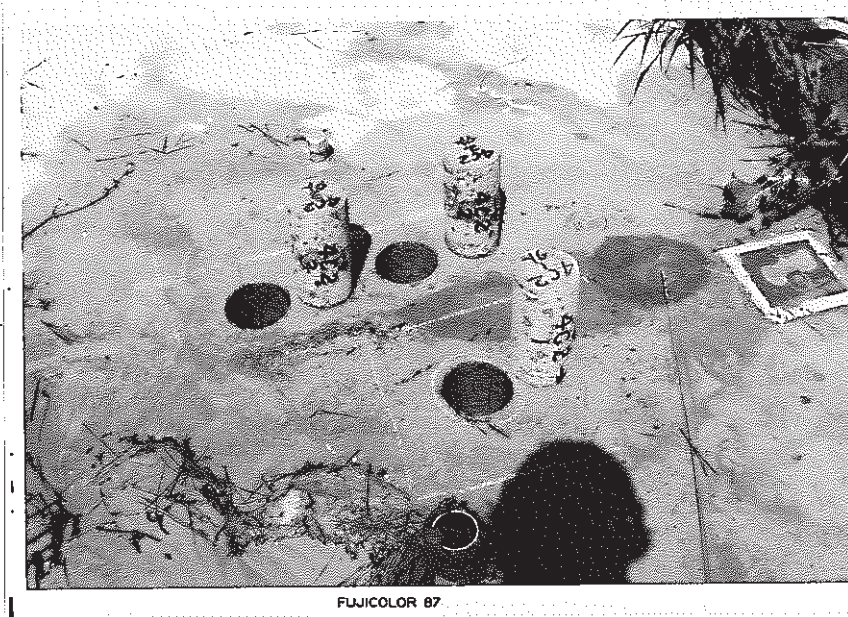


Photo. 1 3 : Concrete Samples for measuring the Compressive Strength and the Young's Modulus